UiT The Arctic University of Norway

Faculty of Health Science

Department of Pharmacy

Electrospinning of nanofibers with chitosan and β-glucan as active wound healing ingredients

Optimization and characterization

Julie Wik Olaussen

Thesis for the degree Master of Pharmacy, May 2020

THESIS FOR THE DEGREE MASTER OF PHARMACY

ELECTROSPINNING OF NANOFIBERS WITH CHITOSAN AND β-GLUCAN AS ACTIVE WOUND HEALING INGREDIENTS OPTIMIZATION AND CHARACTERIZATION

BY

JULIE WIK OLAUSSEN

MAY 2020

SUPERVISORS

Associate Professor Ann Mari Holsæter

and

PhD fellow Laura Schulte Werning

Drug Transport and Delivery Research Group Department of Pharmacy

Faculty of Health Sciences

UiT – The Arctic University of Norway

Acknowledgements

The work presented in this thesis was conducted at Biotec Betaglucans AS research facility in Tromsø and at the Drug Transport and Delivery Research Group at the Department of Pharmacy, University of Tromsø – The artic University of Norway from September 2019 to May 2020.

First of all, I would like to express my deepest gratitude to my academic supervisors associate-professor Ann Mari Holsæter and PhD fellow Laura Schulte Werning. Thank you for your guidance, encouragement and support thorough the extent of this project. A special thanks to Laura for always being available, patient and understanding. This accomplishment would not have been possible without you, and your next master student is lucky to have you.

My sincerest gratitude to Biotec Betaglucans AS for allowing my access to their facilities and for providing the SBG® utilized throughout the project. Many thanks to Thor Nøkland for aiding with the instrumentation of the Nanospider™ and for attributing to improving the conditions required for successful electrospinning.

I would also like to thank to my fellow students at the Department of Pharmacy for several memorable years. A special thanks to Sunniva Brurok and Ida Marie Thomassen for being such good friends and classmates. You have made my years in Tromsø very special.

Finally, I want to thank my family for always supporting and encouraging me through my years of studying and through the process of writing this thesis.

Julie Wik Olaussen, May 2020

Table of contents

List of Figures

List of Tables

Abstract

Wound healing is a complex and highly regulated process, vital for preserving the barrier function of the skin. However, several underlying pathologies have the ability to influence the cascade of events involved in this process, resulting in the development of chronic wounds. The heterogeneous nature of chronic wounds increases the requirements of novel wound dressings. Hence, the development of advanced wound dressings capable of interacting with the wound by stimulating and facilitating regenerative processes, are in high demand. Nanofibers as a novel class of wound dressings, is a relevant example of such an innovation.

The incentive of this thesis was to further develop the nanofibers previously produced in the Drug Transport and Delivery Research Group, containing the patented soluble β-glucan (SBG®) as active ingredient. By incorporating chitosan as a second active ingredient, we introduced an antimicrobial effect in addition to β-glucans immune stimulating effect. Hydroxypropyl methylcellulose and polyethylene oxide were included as co-polymers, and water, ethanol and acetic acid as solvents. The focus of this thesis was thereby the characterization and optimization of this novel nanofibrous formulation.

The nanofibers were produced using the needleless Nanospider™ technology through an attempted optimized electrospinning process. To evaluate the properties of produced nanofibers, suitable methods for characterization of both spinning solutions and final nanofibers were applied. To characterize the polymer solutions, the conductivity, surface tension and rheological properties were examined, while the produced nanofibers were evaluated by determining their tensile properties, morphologies, diameters and absorption capacities. We found that optimization of electrospinning conditions was crucial to obtain homogeneous nanofibers, as relative humidity influenced the nanofiber morphology notably. The conductivity of the polymer solutions was determined to be the primary factor affecting their spinnability. Moreover, solvent volatility was found to affect the morphology of the produced nanofibers by influencing fiber diameter. The tensile properties of the fibers were proven to be limited, due to the influence of polymer composition. Lastly, the nanofibers ability to absorb simulated wound fluid was found to be high, suggesting that they would be suitable for treatment of wounds with moderate to high exudate production.

Keywords: Chitosan; Beta-glucan; Nanofiber; Needleless Electrospinning; Nanospider; Wound dressing; Wound healing; Chronic wounds

Sammendrag

Sårheling er en kompleks og velregulert prosess, som er essensiell for bevaringen av hudens barrierefunksjon. Det er imidlertid flere sykdommer som er i stand til å påvirke denne prosessen og som kan forårsake utviklingen av kroniske sår. Den diverse karakteristikken av kroniske sår øker behovet for nye sårprodukter. På grunn av dette, er etterspørselen etter utvikling av avanserte sårprodukter, i stand til å interagere med såret ved å stimulere og fremme regenerative prosesser, høy. Et relevant eksempel på en slik innovasjon er nanofibre som en ny klasse av sårprodukter.

Formålet med denne avhandlingen var å videreutvikle nanofibrene tidligere produsert i forskningsgruppen, hvor patentert vannløselig β-glukan (SBG®) ble benyttet som aktiv ingrediens. Ved å inkorporere kitosan som en ytterligere aktiv ingrediens, var vi i stand til å introdusere en antimikrobiell effekt i tillegg til den immunstimulerende effekten til β-glukan. Hydroksypropylmetylcellulose og polyetylenoksid ble benyttet som kopolymerer, og vann, etanol og eddiksyre benyttet som løsemidler. Fokuset for avhandlingen var dermed karakteriseringen og optimaliseringen av denne nye nanofibrøse formuleringen.

Nanofibrene ble produsert ved å benytte Nanospider™ teknologi via en forsøkt optimalisert elektrospinningsprosess. For å vurdere egenskapene til de produserte fibrene, ble egnede metoder for karakterisering av både elektrospinnings løsninger og nanofibre benyttet. For å karakterisere de polymerholdige løsningene ble konduktivitet, overflatespenning og reologiske egenskaper undersøkt, mens nanofibrene ble vurdert ved å fastslå deres mekaniske egenskaper, morfologi, diameter og absorbsjonskapasitet. Optimalisering av elektrospinningsbetingelser ble ansett som essensielt for å oppnå produksjon av homogene nanofibre, ettersom relativ luftfuktighet hadde en betydelig påvirkning på morfologi av fibre. Konduktiviteten til de polymerholdige løsningene ble definert som den faktoren som hadde størst innvirkning på spinnbarheten av løsningene. I tillegg, ble flyktighet av løsemiddel ansett å ha innvirkning på nanofiber-morfologi, ved å påvirke fiberdiameter. Den mekaniske styrken til fibrene ble vurdert til å være begrenset på grunn av polymerkomposisjonens innvirkning. Til slutt, ble fibrenes evne til å absorbere simulert sårvæske ansett som høy, noe som tyder på at de vil være egnet til bruk i behandling av sår med produksjon av moderate til store mengder sårvæske.

Nøkkelord: Kitosan; Beta-glukan; Nanofiber; Elektrospinning; Nanospider; Sårprodukt; Sårheling; Kroniske sår

List of Abbreviations

ADP	Adenosine diphosphate
βG	β-glucan (beta-1,3/1,6-glucan)
CS	Chitosan
DA	Degree of acetylation
DD	Degree of deacetylation
ECM	Extracellular matrix
EGF	Epidermal growth factor
EM	Elastic modulus
EtOH	Ethanol
FE-SEM	Field Emission Scanning Electron Microscopy
FGF	Fibroblast growth factor
GlcNAc	N-acetyl-d-glucosamine
HMW	High molecular weight
HPMC	Hydroxypropyl methylcellulose
IGF	Insulin-like growth factor
IL-1	Interleukin 1
IL-6	Interleukin 6
IL-8	Interleukin 8
IL-12	Interleukin 12
IL-1α	Interleukin 1 alfa
IL-1β	Interleukin 1 beta
KGF	Keratinocyte growth factor
LMW	Low molecular weight
MIP-1α	Macrophage inflammatory protein 1 alpha

MIP-1β	Macrophage inflammatory protein 1 beta
MMP	Matrix metallic proteinase
MMP-8	Neutrophil collagenase
MMW	Medium molecular weight
MW	Molecular weight
PDGF	Platelet-derived growth factor
PDGF AB	Platelet-derived growth factor AB
PDGF BB	Platelet-derived growth factor BB
PEB	Percent elongation at break
PEO	Polyethylene oxide
ROS	Reactive oxygen species
SBG®	Soluble β-glucan
SD	Standard deviation
TGF-α	Transforming growth factor alpha
TGF-β	Transforming growth factor beta
TGF-β1	Transforming growth factor beta 1
TGF-β2	Transforming growth factor beta 2
TGF-β3	Transforming growth factor beta 3
TNF-α	Tumor necrosis factor alpha
TS	Tensile strength
VEGF	Vascular endothelial growth factor

1 Introduction

1.1 The skin

The skin is classified as the largest organ of the body, fulfilling many functions. The primary function is to act as a barrier, protecting the underlying tissues from environmental hazards caused by foreign pathogens, chemical- and physical exposures. The skin is divided into two main layers; the outer *epidermis* and inner *dermis*, in addition to a subcutaneous tissue beneath, which attaches it to underlying muscle or bone (Sherwood, 2013).

1.1.1 Epidermis

The epidermis is the protective outermost layer of the skin, composed of four or five layers, depending on the region of skin being considered. These layers are, in descending order; *stratum corneum*, *stratum lucidum*, *stratum granulosum*, *stratum spinosum* and *stratum basale* (Sherwood, 2013) (**Figure 1**).

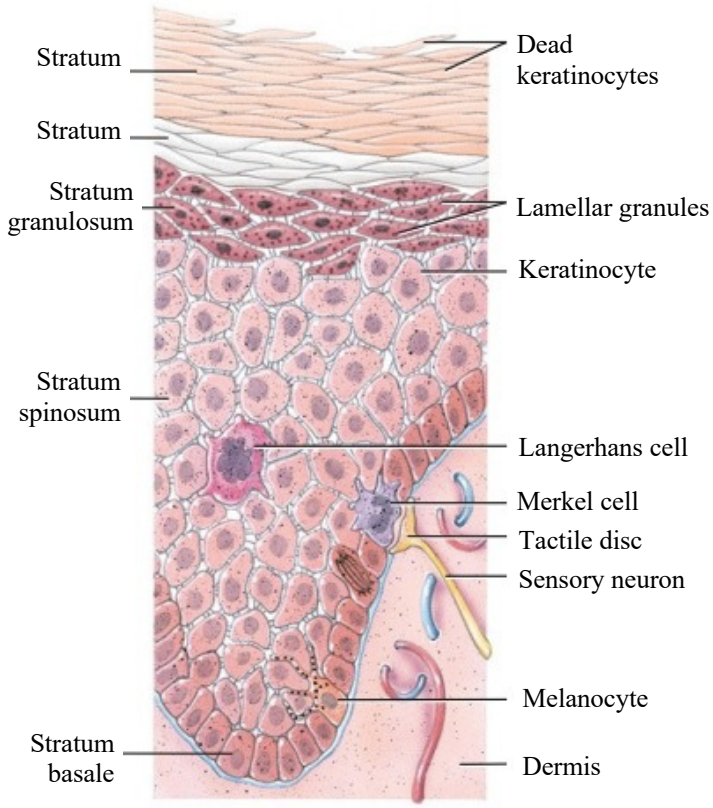

Figure 1: The epidermal structure, including epidermal layers and location of the principal epidermal cell-types (Tortora and Derrickson, 2014). With permission from Wiley, Copyright© John Wiley & Sons, Inc.

The barrier function of the skin is established by a layer of dead and flattened cells called corneocytes, which are embedded in a lipid matrix, forming the upper layer of the epidermis; *the stratum corneum*. This keratinized layer is established as a result of a continuous differentiation process, originating at the basal layer of the epidermis (Wickett and Visscher, 2006). The inner epidermal layers are composed of cube-shaped cells called keratinocytes. As the epidermis has no intrinsic blood supply, the keratinocytes are dependent on nutrition through diffusion from a rich vascular network found in the underlying dermis (Sherwood, 2013). Keratinocytes in the stratum basale will rapidly divide and begin to migrate toward the surface of the skin. The newly forming cells will thus claim the space of older cells by pushing them closer to the surface and farther away from the dermal nutrient source. This process, in combination with the continuous subjection of the outer skin layers to pressure, causes death and flattening of the older cells, transforming them into corneocytes once they reach the stratum corneum (Baroni et al., 2012; Sherwood, 2013). This process is continuous, as corneocytes are continually eliminated from the stratum corneum through desquamation and continually created through differentiation of keratinocytes. The thickness of the keratinized layer varies in different regions of the body, depending on the degree to which the area is exposed to pressure (Sherwood, 2013). The keratinized layer provides a barrier preventing most foreign material from penetrating into the body and regulates the amount of water and other vital constituents released from the body. In addition to keratinocytes and corneocytes, the epidermis also contains melanocytes involved in pigmentation, Langerhans cells exhibiting vital immunologic functions and Merkel cells functioning as nervous cells (Baroni et al., 2012) (**Figure 1**).

1.1.2 Dermis

The dermis is located beneath the basement membrane of the epidermis and is composed of dense irregular connective tissue containing collagen and elastic fibers. This woven network of fibers gives the skin the ability to stretch and recoil easily. Blood vessels, nerves and cutaneous appendages, such as sweat glands, sebaceous glands and hair follicles are embedded in the dermal layer. The main function of the dermis is to support and protect the skin, and to assist in sensation and thermoregulation (Baroni et al., 2012; Marks and Miller, 2019).

Based on its tissue structure, the dermis is generally subdivided into a papillary layer and a reticular layer (Tortora and Derrickson, 2014) (**Figure 2**).

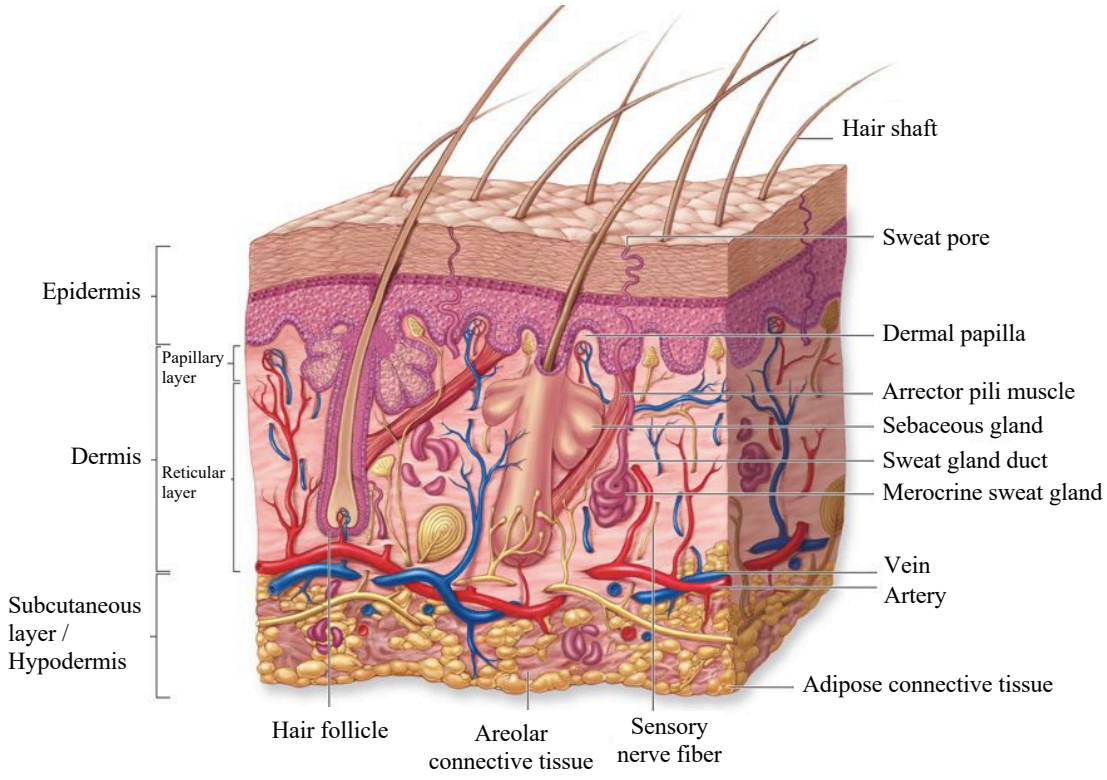

Figure 2: Overview of the skin, illustrating the major layers and dermal appendages, the vasculature and the major sensory receptors (Mescher, 2009). With permission from McGraw Hill, Copyright© The McGraw Hill Companies, Inc.

The papillary dermis presents as the upper layer, located close to the epidermis. It contains thin, loosely arranged collagen and elastin fibers. Collagen fibers help strengthen the skin and connects the dermis to the overlying epidermis, while elastin fibers constitute an important structural element, by providing flexibility and support to the skin (Nafisi and Maibach, 2018). The surface area of the papillary layer is increased by dermal papillae, small structures that protrude into the underside of the epidermis. This increased contact between dermis and epidermis is important for the supply of nutrients to the epidermis, promoting molecular diffusion from the small capillaries in the dermal papillae to the cells of the stratum basale (Tortora and Derrickson, 2014).

The reticular dermis is located lower in the dermis, attached to the subcutaneous layer. It consists of thick collagen fibers, fibroblasts and different migrating cells, such as macrophages. The collagen fibers in this layer are arranged in a higher degree of structural order, compared to fibers in the papillary layer. This regular orientation of thick collagen fibers contributes to

the skins ability to resist stretching. Nerves, blood vessels, sebaceous glands, sweat glands and hair follicles occupy the space between the fibers (Tortora and Derrickson, 2014).

1.1.3 Hypodermis

The dermis rests on a subcutaneous layer, known as the hypodermis, consisting of areolar and adipose tissues (**Figure 2**). Extending fibers from the dermis connects the skin to the hypodermis, which in turn attaches to underlying connective tissue around bones and muscles. The adipose tissue serves as a storage depot for fat and consists of large blood vessels that supplies the skin (Sherwood, 2013; Tortora and Derrickson, 2014).

1.2 Wounds

A wound can be defined as a disruption of normal skin structure and integrity, resulting in a loss of skin function (Lazarus et al., 1994). Wounds can emerge as a result of a disease process or have intentional or accidental etiology. The skin is the one body tissue that is most vulnerable to damage and prone to injury, burns and abrasions caused by trauma. Rapid restoration of physiological conditions is essential for complete tissue repair, as slow and inaccurate repair can provoke further damage such as loss of skin, onset of infection, injuries to the circulatory system and in severe cases tissue necrosis (Boateng and Catanzano, 2015).

Wounds can be defined as acute or chronic, dependent on the healing process. Acute wounds are wounds that heal completely through normal cutaneous wound healing, which occurs in a timely fashion (Clark, 2014). The primary causes of acute wounds include mechanical injuries such as penetrating wounds, abrasions and tears, chemical injuries and burns (Boateng et al., 2008; Enoch and Leaper, 2008). Chronic wounds are wounds developed by a prolonged continuance of the reparative processes involved in cutaneous wound healing. These wounds are often related to underlying pathological disorders that contribute to an impaired healing and will therefore not heal in a timely manner (Clark, 2014). Diabetic ulcers, vascular ulcers and pressure ulcers are examples of chronic wounds facilitated or caused by an underlying condition. Common features shared by these types of wounds include a prolonged inflammatory phase, development of resistant biofilms and continuous infections (Demidova-Rice et al., 2012).

1.3 Wound healing

Normal cutaneous wound healing represents a highly regulated cascade of overlapping processes, established by numerous of cellular activities. The activities involved in this cascade are characterized by the migration of various cell types to the wound site, during different phases of the healing process. These processes are triggered immediately after skin injury and are typically divided into four overlapping phases; hemostasis, inflammation, proliferation, and remodeling (Enoch and Leaper, 2008).

1.3.1 Hemostasis

The wound healing process begins with hemostasis, which forms an immediate response to tissue injury. Hemostasis describes the mechanisms initiated to prevent blood loss at the wound site (Bielefeld et al., 2013). Capillary blood and lymphatic fluid leaks into the wound bed, initiating the coagulation cascade and vasoconstriction. Upon registering a disruption in the endothelial lining, a plasma protein called von Willebrand factor adheres to the exposed collagen in the connective tissue. Platelets attach to binding sites on the protein, creating a layer of platelets at the wound site. Collagen activates these platelets, which promotes their adhesion to collagen and other platelets. Activated platelets also release important chemicals from their storage granules, such as adenosine diphosphate (ADP) and thromboxane A_2, which further stimulates platelet aggregation forming a platelet plug (Sherwood, 2013). The plug releases chemicals to enhance blood coagulation, where fibrinogen is converted to fibrin. Fibrin molecules adhere to the damaged surface of the vessel, forming a clot (**Figure 3**). The clot serves as a temporary barrier protecting the exposed wound tissue and provides a provisional matrix for cell migration in both the hemostatic and inflammatory phase (Enoch and Leaper, 2008; Velnar et al., 2009). The clot also functions as a reservoir for cytokines and growth factors that can be released upon degranulation of activated platelets. These platelets contain α-granules filled with growth factors and cytokines, such as transforming growth factor (TGF)-β, platelet derived growth factor (PDGF), epidermal growth factor (EGF) and insulin-like growth factors (IGFs). These are important molecules, functioning as promotors of the wound healing cascade by activating and attracting neutrophils, macrophages, endothelial cells and fibroblasts (Velnar et al., 2009).

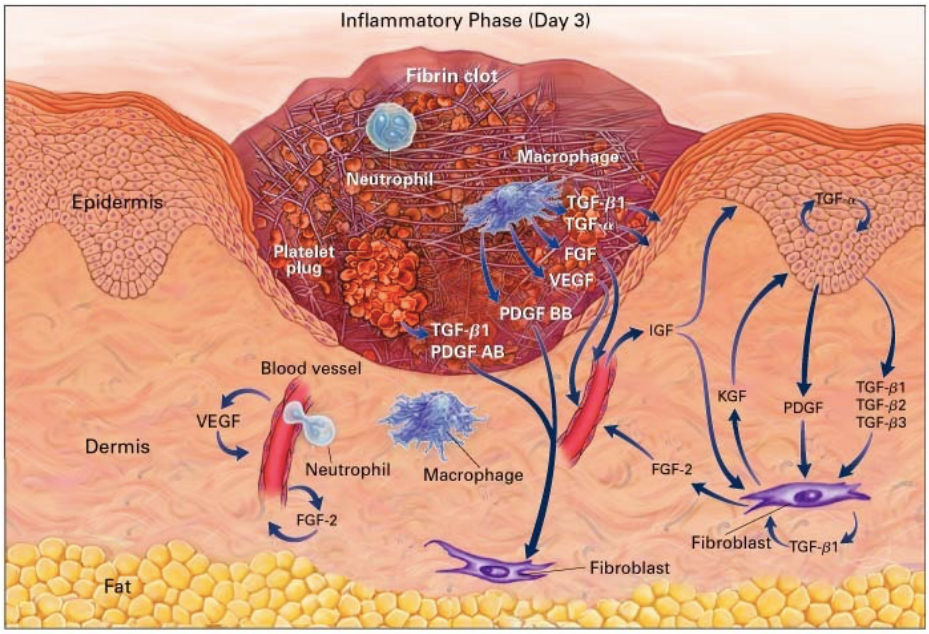

Figure 3: A cutaneous wound three days after injury. Illustrating the inflammatory phase and the growth factors necessary for cell movement into the wound. For abbreviations, see page XIII. Reproduced with permission from (Singer and Clark, 1999), Copyright© Massachusetts Medical Society.

1.3.2 Inflammation

The aim of the inflammatory phase is the formation of an immune barrier against intruding microorganisms (Velnar et al., 2009). Polymorphonuclear cells, namely neutrophils, are the first inflammatory cells to arrive at the wound site. The main function of these cells is to minimize bacterial contamination of the wound. In the wound environment, neutrophils phagocytose foreign material and bacteria, eliminating them by releasing proteolytic enzymes and reactive oxygen species. Furthermore, neutrophils are an important source of proinflammatory cytokines, such as tumor necrosis factor (TNF)-α, IL-6, IL-1α and IL-1β (Baum and Arpey, 2005). The activity of the neutrophils normally ceases after a few days, and redundant cells are cleared from the wound either by extrusion to the wound surface or by uptake by macrophages (Enoch and Leaper, 2008). In addition to neutrophils, monocytes will appear in the wound after 2-3 days, where they are activated and subsequently differentiate into macrophages (**Figure 3**). The activated macrophages will phagocytose remaining pathogenic organisms, particles and dead neutrophils (Goldberg and Diegelmann, 2017). Furthermore, macrophages are the primary producer of growth factors responsible for the activation and proliferation of keratinocytes, fibroblasts and endothelial cells, which are instrumental in reestablishing the extracellular matrix and stimulating angiogenesis (Enoch and Leaper, 2008).

1.3.3 Proliferation

The focus of the proliferative phase is to reestablish the epithelial barrier function, generate new granulation tissue and restore the vascular network (Reinke and Sorg, 2012). During re-epithelialization, epidermal cells originating from skin appendages, eliminate damaged stroma and clotted blood from the wound. Simultaneously, the cells endure phenotypic alterations including abjuration of intracellular tonofilaments and formation of actin filaments, allowing cell movement (Singer and Clark, 1999). Due to dissolution of specific links between the epidermis and the basement membrane, epidermal and dermal cells no longer adhere to each other. This allows for the lateral movement of epidermal cells expressing integrin receptors, enabling interactions with a variety of ECM-proteins. The epidermal cells dissect the wound by separating viable tissue from eschar. Moreover, they are stimulated by local growth factors to proliferate, which eventually re-establishes the stratified epithelium (Enoch and Leaper, 2008; Singer and Clark, 1999).

Three to four days post injury, local fibroblasts immigrate to wound site. Once in the wound, fibroblasts proliferate profusely and synthesize the matrix proteins fibronectin and hyaluronan, proteoglycans and collagen, which represent the basis for the new extracellular matrix (ECM) of granulation tissue (Velnar et al., 2009). Gradually, abundant ECM accumulates, further supporting cell migration. At this stage, fibroblasts differentiate into myofibroblasts which contain thick actin bundles beneath the plasma membrane. These cells actively extend and attaches to fibronectin and collagen in the ECM. As these cell extensions retract, contraction of the wound is initiated. Redundant fibroblasts are eliminated by apoptosis after completing this action (Robson et al., 2001; Velnar et al., 2009).

Angiogenesis, formation of new blood vessels, is required to sustain the newly formed granulation tissue (Li et al., 2007). This process is initiated by the binding of growth factors to receptors on endothelial cells of existing blood vessels, resulting in the activation of intracellular signaling cascades. Activated endothelial cells secrete proteolytic enzymes that dissolves the basal lamina, enabling the cells to proliferate and migrate into the wound, in a process commonly known as ‘sprouting’. The generated sprouts form small canals that interconnects with others forming a microvascular network. The vessels differentiate and form venules and arteries that gradually matures by stabilization of their vessel walls. Finally, the initiation of blood flow completes the angiogenic process (Enoch and Leaper, 2008; Reinke and Sorg, 2012).

1.3.4 Remodeling

Remodeling is the final phase of the wound healing process and promotes the formation of new epithelium and scar tissue (Velnar et al., 2009). During maturation of the wound, the ECM is remodeled in a process involving continued synthesis and catabolism of collagen. The type III collagen, synthesized by fibroblasts in granulation tissue, is consequently replaced by the more robust type I collagen, thereby increasing the tensile strength of the tissue (Li et al., 2007). This degradation of collagen is facilitated through specific matrix metalloproteinases, produced by fibroblasts, neutrophils and macrophages at the wound site. The catalytic activity of the metalloproteinases is partially controlled by a family of tissue inhibitors, which is crucial in establishing a balance in the process of remodeling (Enoch and Leaper, 2008; Li et al., 2007).

Organization of the collagen matrix is achieved in the final stages of the remodeling phase, through wound contraction facilitated by fibroblasts. During this process the connective tissue shrinks, which brings the wound margins closer together and decreases the surface of the developing scar (Velnar et al., 2009). Moreover, the growth of capillaries stops, blood flow to the wound site and metabolic activity decreases, and the abundance of macrophages and fibroblasts is reduced by apoptosis. The result is the formation of a fully matured scar, exhibiting decreased tensile strength compared to intact skin (Reinke and Sorg, 2012).

1.4 Impaired wound healing

Chronic wounds were previously described as wounds that have failed to progress through the normal stages of the healing process, resulting in a continuous state of pathologic inflammation. In normal cutaneous wound healing, the inflammatory phase is initiated to prepare the wound bed by removing debris, necrotic tissue and bacterial contaminates, in addition to recruiting and activating fibroblasts (Menke et al., 2007). Inflammation is thereby under normal conditions a self-limiting process. In chronic wounds, however, a prolonged inflammation period facilitates further injury. Excessive neutrophil infiltration throughout the healing process, appears to be critical to uphold the cycle of chronic inflammation characteristic for chronic wounds. The abundance of neutrophils causes accumulation of reactive oxygen species (ROS), inflicting direct damage to the ECM and cell membrane. Neutrophils also release large amounts of matrix metallic proteinases (MMP) such as neutrophil collagenase (MMP-8), and serine proteases such as elastase. MMP-8 inactivates and degrades components of the ECM, while elastase degrade important growth factors such as TGF-β and PDGF (Zhao et al., 2016). The abundance of

inflammatory cells in the wound bed also affect the cytokine profile. Both neutrophils and activated macrophages produce pro-inflammatory cytokines such as TNF-α and IL-1β. These cytokines increase the production of MMPs and reduce the number of inhibitors of MMPs (Menke et al., 2007). This imbalance between degradative and protective factors creates a wound environment favoring degradation.

There are several factors contributing to impaired wound healing, which affects the probability of developing chronic wounds. Local factors such as infection, oxygenation, neuropathy, necrotic tissue and repetitive trauma are directly influencing the wound itself. There are also systemic factors such as age, gender, nutritional status, alcohol consumption, smoking, obesity, medications, diabetes and vascular disease, affecting the condition of the person and their ability to heal (Guo and Dipietro, 2010). Chronic non-healing wounds present a substantial economic burden to the healthcare system. In the United States alone, chronic wounds affect an estimated ~2% of the total population, with an annual total cost of 20 billion US dollars (Järbrink et al., 2017). They cause a significant reduction in quality of life for those affected, as pain, loss of function and infections are characteristic and often result in amputations or sepsis. This problem is also likely to grow with an increasing population of elderly and an increasing prevalence of chronic diseases such as diabetes and obesity (Järbrink et al., 2017; Mustoe et al., 2006).

1.5 Wound dressings

A wound dressing is a medical device that is applied to the wound site to establish optimal healing conditions, while protecting the wound from additional trauma and invasion of bacteria (Hayes and Su, 2011). Traditional wound dressings, such as bandages, plasters, cotton wool and gauze, were utilized mainly with the intention of protecting the wound (Alberti et al., 2017). However, the concept of wound dressings has evolved. The modern wound dressing should be able to provide an ideal healing environment by: protecting the wound from microorganisms and foreign material, preventing loss of heat and fluid, absorbing wound exudate, being nonadherent to prevent disruption of the wound upon removal, and most importantly creating a moist occluded environment to promote epithelialization (Alberti et al., 2017; Lionelli and Lawrence, 2003). No single wound dressing can fulfill all of these functions optimally, and not all functions are required for all wound types. This means that the attributes of different wound

dressings would have to align with the specific wound on which it is to be applied (Lionelli and Lawrence, 2003).

1.5.1 The concept of occlusion

Comprehending the concept of occlusion has been pivotal for the advancement of modern wound dressings and has initiated a critical shift in the treatment of wounds (Lionelli and Lawrence, 2003). The ability to retain and create a moist wound environment is often viewed as modern wound dressings most essential characteristic, as it has been associated with substantially increased healing rates (Jones et al., 2006).

Firstly, occlusive dressings regulate the transference of water vapor, gasses and fluids from the wound site to the environment (Lionelli and Lawrence, 2003). This contributes to establishing a moist wound environment, enabling the dressings to sustain a relatively low oxygen tension and a mildly acidic pH on the surface of the wound. These described characteristics mimic the early wound environment, stimulating angiogenesis and providing favorable conditions for fibroblast proliferation and formation of granulation tissue. These processes are further encouraged by cytokines, which are often present in an moist wound environment (Han and Ceilley, 2017; Lionelli and Lawrence, 2003). Furthermore, a moist wound environment promotes healing due to decreased desiccation, inflammation and eschar formation, in addition to accumulation of exudate rich on growth factors contributing to epithelialization. However, it is important to establish a balance in moisture levels, as excess wound fluid could contribute to an increase in bacterial growth (Rivera and Spencer, 2007). Moreover, exudate produced by chronic wounds have proven to be damaging to tissues, due to elevated and uncontrolled levels of proteases such as neutrophil elastase, matrix metalloproteases and pro-inflammatory cytokines. The combined presence of these destructive components could result in damage of the wound bed and wound margin (Ousey et al., 2016).

1.5.2 Choice of wound dressing

As previously described, there is no single wound dressing that can possess all the features necessary to create an optimal wound healing environment in all wounds. The needs of each individual wound would therefore have to be evaluated to find the most suitable dressing (Lionelli and Lawrence, 2003). Factors to consider when choosing a dressing could for example

be the size, severity, location and exudate production of the wound (Memic et al., 2019). Wound dressings can be classified into four main categories, namely passive, interactive, advanced and bioactive (Abrigo et al., 2014).

1.5.2.1 Passive wound dressings

Passive wound dressings are mainly designed to cover the wound, protecting it from mechanical trauma and bacterial infiltration. These dressings are generally dry, rendering them unable to control the moisture balance in the wound bed. As a result, they often adhere to the wound causing pain and potential trauma at removal. The use of low adherent materials in formulation of such dressings are thus preferred, allowing wound exudate to permeate, maintaining moisture while minimizing adherence. Passive dressings are suitable for treatment of minor wounds (Jones et al., 2006; Memic et al., 2019).

1.5.2.2 Interactive wound dressings

Interactive wound dressings are semi-occlusive or occlusive, and thus able to establish a moist wound environment. These dressings generally have high flexibilities, making them suitable for wounds located in areas of the body subjected to excessive stretching and bending (Memic et al., 2019). There are several types of interactive dressings on the market, such as foams, films and hydrogels (Dhivya et al., 2015). Foam dressings are absorbent, nonadherent, and able to expand and conform to the wound structure. However, they provide minimal protection from bacterial contamination, and they need to be replaced frequently to suit the reducing size of the wound (Lionelli and Lawrence, 2003).

Film dressings are water-resistant, but permeable to transmission of water vapor, oxygen and carbon dioxide. They are thin and flexible, and their transparency make visualization of the wound state easy. However, film dressings might not be applicable for wounds producing moderate amounts of exudate, as they are non-absorptive. Another criterion for the use of film dressings is that the skin needs to be intact in the area surrounding the wound, for required film adherence, making them less suitable for the treatment of burns (Lionelli and Lawrence, 2003). Hydrogels are composed of large amounts of water, combined with polymers and a supportive mesh or film. The formulations mainly function as rehydrating agents for dry wounds, creating an occlusive environment with application. In addition, they are nonadherent and cool the surface of the wound, potentially contributing to pain reduction. However, due to their large

water content, hydrogels are only able to absorb restricted amounts of exudate, thus they are mainly used for wounds producing light to moderate amounts of exudate. Furthermore, hydrogels have low mechanical strength, which could make them challenging to handle, potentially affecting influencing compliance (Boateng et al., 2008; Memic et al., 2019).

1.5.2.3 Advanced wound dressings

Advanced wound dressings include hydrocolloids and alginates, facilitating wound healing by establishing and maintaining a moist wound environment (Memic et al., 2019). Hydrocolloids are dressings containing a hydrocolloid matrix that efficiently absorbs water and swells on contact with wound exudate, liquidizing into a moist gel. The absorbency of these dressings makes them suitable for wounds producing light to moderate amounts or exudate, such as chronic wounds or burns. Furthermore, hydrocolloid dressings are impermeable to bacteria and allows for limited gas and moisture transmission (Lionelli and Lawrence, 2003). Disadvantages of this dressing option is the occurrence of leakage or maceration with accumulation of excess exudate, in addition to an unfortunate odor associated with the gels (Rivera and Spencer, 2007).

Alginates are wound dressings consisting of polysaccharides, derived from the calcium salt of alginic acid. Alginates have the ability to form hydrophilic gels upon contact with wound exudates, giving them a high absorbency, limiting wound secretion and bacterial contamination (Boateng et al., 2008). The gel also establishes an occlusive environment, promoting wound healing. Another valuable property of such dressings is their hemostatic ability, promoting the clotting cascade (Rivera and Spencer, 2007). Alginate dressings are mainly utilized for moderate to heavily exuding wounds, such as chronic ulcerations. The main disadvantage of alginate dressings is that their use is limited to wet wounds, as they require moisture to function properly (Lionelli and Lawrence, 2003).

1.5.2.4 Bioactive wound dressings

Bioactive wound dressings are made from biomaterials that actively takes part in the wound healing process. Biomaterials have the advantage of being biocompatible, biodegradable and non-toxic, as they are derived from natural sources. These formulations often combine different polymers such as collagen, elastin, hyaluronic acid and chitosan. In some cases, they could also be incorporated with active compounds such as antimicrobials and growth factors to enhance wound healing process (Boateng et al., 2008; Dhivya et al., 2015).

By combining various polymers, bioactive wound dressings with multitargeting abilities can be obtained. This has been attempted in this project, by combining chitosan (CS) and β-glucan (βG) to create nanofibrous wound dressings with both antimicrobial- and immunostimulant effect.

1.6 Nanofibers as wound dressings

Nanofibers has recently emerged as a novel class of wound dressings, offering distinct advantages due to favorable inherent properties (Doostmohammadi et al., 2020). Nanofibrous dressings is comprised of numerous intersecting nanofibers, which is solid polymer fibers with diameters ranging from a few micrometers to a few hundred nanometers (Liu et al., 2019). These ultrathin fibers have several favorable intrinsic properties, which makes them appealing in the design of novel wound dressings. Due to their alignment and nanometer size, nanofibrous dressings are capable of mimicking the structure and function of the natural ECM, encouraging cell adhesion, proliferation and maturation. Furthermore, the formulations can be tailored to exhibit favorable porosity, gas permeability, mechanical integrity and high surface area to volume ratio, supporting their utility in wound healing (Abrigo et al., 2014; Mohiti-Asli and Loboa, 2016)

As a result of the reduced fiber diameter and increased specific surface area, nanofibers exhibit several advantages over conventional wound dressings. Firstly, nanofibrous wound dressings are able to promote hemostasis, due to their reduced pore size and large specific surface area, thereby strengthening the natural wound healing process of the body. Their large surface area to volume ratio also facilitates an elevated water absorption capacity, potentially contributing to an increased efficiency in absorbing wound exudates. The porous structure of the fibers is advantageous for cellular respiration, preventing desiccation of the wound. Moreover, reduced pore size facilitates high gas permeation and prevents infiltration of microorganisms from the external environment (Abrigo et al., 2014; Andreu et al., 2015). Nanofibrous dressings also have a high degree of conformability, due to the thin nature of the fibers, delivering improved protection and coverage of the wound site. In addition, the dressings allow efficient incorporation of therapeutic agents, enabling the establishment of multi-functional drug delivery systems. This ability is a result of their expansive surface area and short diffusion

distance, facilitating efficient and sustained drug delivery (Hayes and Su, 2011; Zahedi et al., 2010; Zhang et al., 2005b).

The correlation between fiber diameter and specific surface area is presented in **Figure 4.** Important to recognize is the similarity in size of nanofibers to other biological structures, such as the natural ECM.

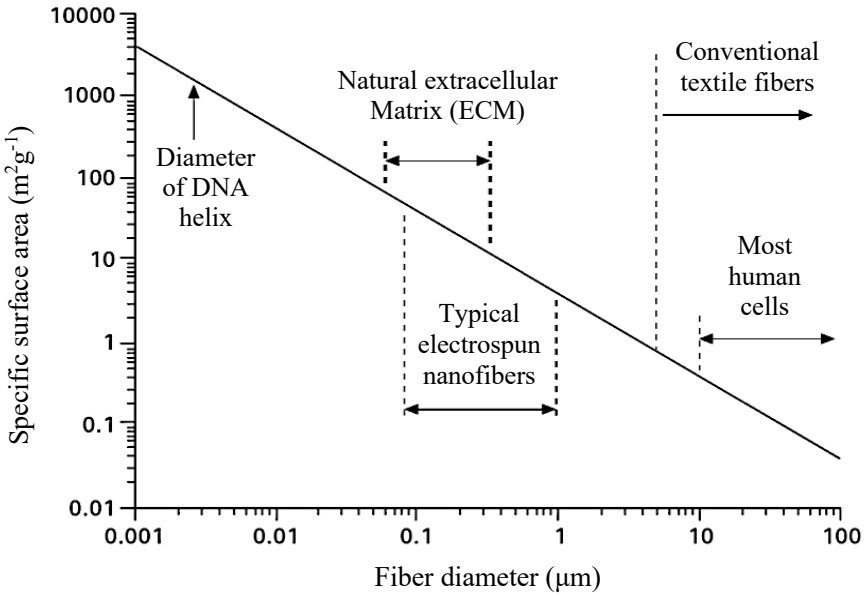

Figure 4: Graphical example presenting the correlation between fiber diameter and specific surface area of fibrous materials (Hayes and Su, 2011). With permission from Elsevier, Copyright© Woodhead Publishing Limited.

A large part of the appeal of nanofibers in tissue engineering is their structural similarity to the ECM. The ECM consists of both nano and micro sized fibers and pores that provides structural support to cells and establishes optimal conditions for cell adhesion, proliferation and maturation (Rošic et al., 2013). Specifically designed polymeric nanofibers exhibiting the ability to mimic both the fibrillar microarchitecture and the complex function of the ECM, is thus a promising approach for the treatment of wounds. These abilities are evoked by nanofibers alignment, nanometer size and mechanical properties, enabling cells to recognize the structure and facilitate cellular adhesion, proliferation, migration, and differentiation, favoring re-epithelialization (Beachley and Wen, 2010; Gunn and Zhang, 2010; Zahedi et al., 2010).

1.7 Production of nanofibers

Several nanofiber manufacturing techniques have been introduced in later years, as a result of increasing interest in the generation of nanofibers for different applications. The most common being phase separation, self-assembly and electrospinning (Mohiti-Asli and Loboa, 2016). Among these techniques, electrospinning has attracted attention in wound healing, because of its ability to produce continuous, biomimetic nanofibers using polymers of both natural and synthetic origin. Furthermore, there are several advantages of electrospinning, such as its simplicity, cost-effectiveness and potential for large scale production for industrial applications (Agarwal et al., 2008; Doostmohammadi et al., 2020).

In this project we have applied electrospinning for the formation of novel nanofibrous wound dressings. This manufacturing method will therefore be described in further detail.

1.7.1 Electrospinning

Electrospinning is an electrostatically driven manufacturing technique, that utilizes high voltage to produce nanofibers from a polymer solution or melt (Fujihara et al., 2005). The main components of the standard electrospinning setup includes a syringe fitted with a metal needle, a syringe pump, a high voltage power supply and a grounded collector (Kenry and Lim, 2017). The standard electrospinning setup is depicted in **Figure 5**.

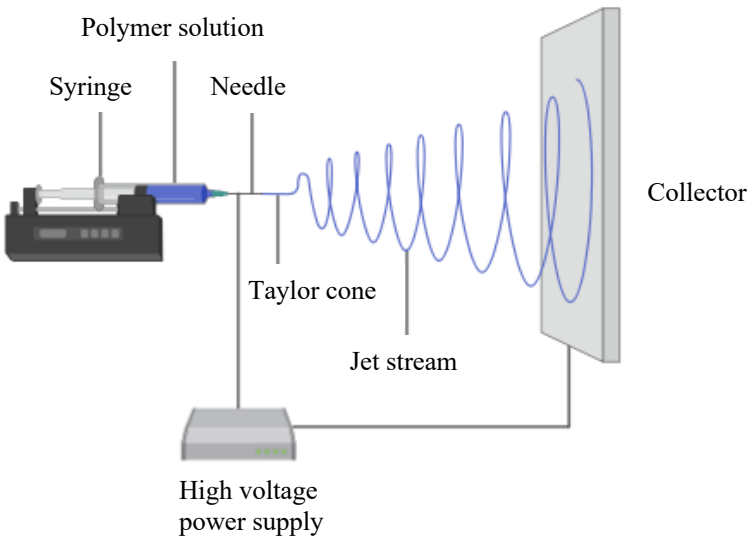

Figure 5: Standard single needle electrospinning setup. Created with Biorender.com.

The syringe, filled with electrospinning solution or melt, is attached to a pump that maintains a constant flow of spinning liquid. A high voltage power supply is connected to the tip of the metal needle, generating a large electric field between the needle and the collector and mutual electrical repulsive forces within the polymer solution. Nanofibers are generated as the polymer solution or melt is fed through the needle and into the region of high electric field. As the liquid is ejected, the droplet at the tip of the needle deforms into a conical shape known as the Taylor cone (Pelipenko et al., 2015). This phenomenon occurs as a result of the competing interaction between the electrostatic force and the surface tension of the liquid. When the applied voltage is sufficiently high for the electrostatic force to overcome the surface tension, a charged jet stream is drawn from the Taylor cone and accelerated towards the grounded collector. Instabilities in this jet causes whipping and stretching motions, resulting in an elongation and thinning of the jet stream. This process enables the evaporation of solvent or cooling of melt, producing uniform fibers as the filaments are deposited on the collector and solidifies (Alghoraibi and Alomari, 2018).

1.7.1.1 Needleless electrospinning

The standard single needle electrospinning technique does however have some limitations, such as low productivity and occasional needle clogging due to precipitation of polymer, which have led to the development of several new techniques in later years (Yu et al., 2017). One of these new techniques is needleless electrospinning. The needleless spinning process is based on the principle that waves of an electrically conductive liquid will organize on a mesoscopic scale, and form jets when the intensity of the electric field is exceeding a critical value (Alghoraibi and Alomari, 2018). One of the main advantages of needleless electrospinning systems is their improved productivity, as a result of the formation of numerous polymeric jets (Alghoraibi and Alomari, 2018; Yan et al., 2019).

The Nanospider™ technology represents a needleless electrospinning technique. Unlike standard needle electrospinning, the Nanospider™ system uses a wire electrode coated with polymer solution. In this system there is a stationary wire electrode onto which a spinning solution is continuously deposited by a closed carriage with a calibrated orifice (Yan et al., 2019) (**Figure 6**).

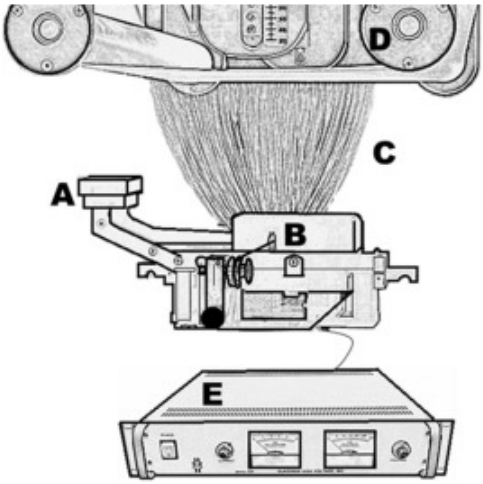

Figure 6: The Nanospider™ Lab. (A) closed solution carriage, (B) wire electrode, (C) spinning area, (D) take-up cylinder connected to substrate material, (E) high voltage supply (Yalcinkaya, 2019). With permission from Elsevier.

As a result of the movement of this carriage along the metal wire, a thin layer of polymer solution will cover the surface of the wire electrode. In the upper part of the instrument there is a second electrode; the collecting electrode, which is grounded. When applying the electric field, an electric force will fight to overcome the surface tension of the polymer solution. If successful, this results in the creation of several Taylor cones on the surface of the metal wire, and initiation of jet formation. Thin streams of polymer solution will travel from the wire electrode to the collecting electrode at the top of the instrument. In this process solvent evaporates and nanofibers are created and deposited onto the substrate material that runs adjacent to the collecting electrode (Yalcinkaya, 2019).

1.7.1.2 Parameters affecting electrospinning

The prosperity of the electrospinning process and the morphology of the generated nanofibers is contingent on various individual, but interrelated, parameters (Rošic et al., 2012b). Parameters affecting electrospinning can be broadly classified into solution-, process- and ambient parameters. The most influential solution parameters include solution viscosity, conductivity and surface tension. Furthermore, the most decisive process parameters are the applied electric field, distance to the collector and the flow rate of solution. Finally, ambient parameters encompass the temperature and humidity of the surroundings (Haider et al., 2018; Pelipenko et al., 2015).

The influence of individual process and solution parameters has been thoroughly investigated, establishing correlations. However, morphology of generated nanofibers often differs from predictions, indicating a complex interplay of both known and unknown parameters (Pelipenko et al., 2013). The interdependence of various electrospinning parameters is therefore an established challenge of nanofiber design, as minor adjustments of single parameters could influence the morphology, arrangement and structure of generated fibers. A complete understanding of the influence and interaction of different parameters is thus pivotal for the production of nanofibers with desired properties.

Nanofibers have so far been successfully prepared from a large selection of both natural and synthetic polymers. However, the applicability of electrospinning is not easily transferable between different polymer solutions. This means that for each new combination of polymer, solvent and excipients, the parameters have to be determined individually (Rošic et al., 2012b).

Solution parameters

Solution viscosity, controlled by the polymer concentration, has shown to be one of the greatest determinants of fiber size and morphology when spinning fibers from polymer solutions (Pham et al., 2006). As earlier described, the electrospinning process relies on the uniaxial stretching of a charged jet. This stretching process is notably affected by the concentration of the polymeric solution. With polymeric solutions of low concentration, the applied electric field and surface tension elicit fragmentation of the entangled polymer chains before they reach the collector, which results in formation of beaded nanofibers. An increase in polymer concentration will increase the viscosity of the solution, which in turn increases the polymer chain entanglement. Improved chain entanglement prompts the polymer solution to overcome the surface tension resulting in the formation of uniform, beadless nanofibers. However, at polymer concentrations over a certain limit, the viscosity of the solution becomes exceedingly high, obstructing the flow of solution. This ultimately results in defective or beaded nanofibers (Haider et al., 2018).

The morphologies of beaded nanofibers portray an alteration in shape contingent on the viscosity of the solution. Low-viscosity solutions typically form round droplet shaped beads, while solutions of sufficient viscosities forms elongated or stretched droplet shaped beads, or smooth nanofibers without the presence of beads (Fong et al., 1999; Haider et al., 2018; Zargham et al., 2012) (**Figure 7**).

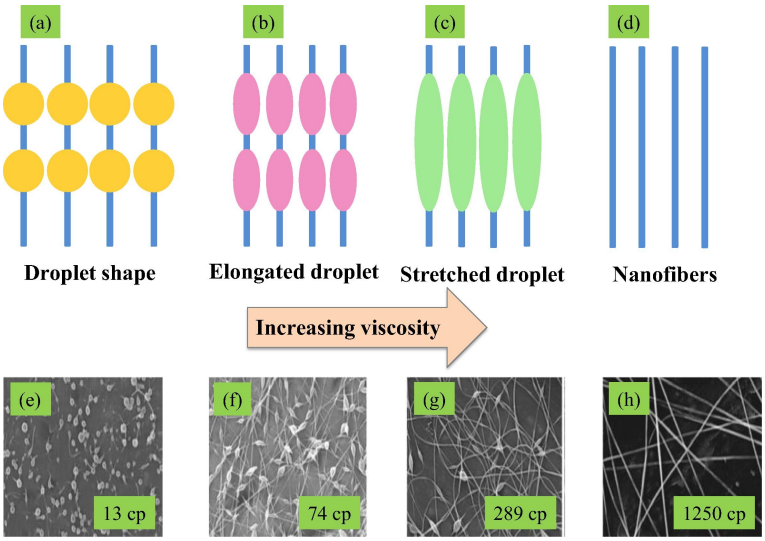

Figure 7: Variation in morphology of electrospun nanofibers of PEO with increasing viscosity: (a–d) schematic illustration and (e–h) corresponding SEM micrographs (Haider et al., 2018). Licensed under a Creative Commons Attribution 4.0 International license.

The surface tension and conductivity of polymer solutions have also been reported in literature as pertinent solution parameters. The conductivity of a polymer solution affects the Taylor cone formation, in addition to the diameter of the nanofibers (Haider et al., 2018). Polymer solutions of lower conductivity cannot be electrospun, due to an insufficient charge at the surface of the fluid preventing formation of the Taylor cone. Increasing the conductivity of the solution to a critical value, will enable Taylor cone formation and elicit a decrease in fiber diameter (Sun et al., 2014). However, increasing the conductivity beyond the critical value, will cause a depleted electric field on the surface of the fluid, preventing formation of the Taylor cone. In general, polymer solutions of higher conductivity generate thinner nanofibers, with reduced formation of beads (Bhardwaj and Kundu, 2010).

Surface tension, likely to be a function of solvent compositions of the solution, plays a central role in the electrospinning process. In general, high surface tension of a solution can inhibit the electrospinning process due to instability of the jet streams and generation of sprayed droplets. Literature indicates that reduction in surface tension could reduce bead formation; however, no decisive correlation between fiber morphology and surface tension has been established thus far (Bhardwaj and Kundu, 2010; Zhang et al., 2005a).

Process parameters

There are several process parameters affecting the electrospinning of nanofibers, and the applied voltage, distance to collector and flow rate of solution have previously been emphasized. However, for the needleless electrospinning process relevant in thesis, flow rate is affected by solution viscosity but cannot be directly controlled, it will therefore not be further discussed.

The effect of the applied electric field on electrospinning has been thoroughly examined in literature. In general, an increase in the applied voltage results in a thinning of the generated nanofibers, due to the increased repulsive electrostatic forces generated in the polymer solution (Bhardwaj and Kundu, 2010). The high voltage could promote formation of beads in the spun nanofibers, potentially due to instability of the Taylor cone (Megelski et al., 2002; Pham et al., 2006).

The distance to the collector is instrumental in determining the morphology of electrospun nanofibers, but varies depending on the polymer solution (Haider et al., 2018). The optimal distance depends on the evaporation rate, deposition time and whipping of the liquid. Hence, a minimal distance needs to be maintained to assure sufficient time for the jet stream to dry before reaching the collector, to form smooth and uniform fibers. A too short distance does not permit solidification of the jet before it is deposited on the collector, which could result in fusion of nanofibers and polymer film formation. Increasing the distance results in the formation of nanofibers of smaller diameters (Bhardwaj and Kundu, 2010).

Ambient parameters

Ambient parameters include the temperature and relative humidity of the environment. The environmental temperature affects the average diameter of the nanofibers by influencing two opposing effects; it causes an increase in the evaporation of the solvent and a decrease in the viscosity. These effects function by different mechanisms, but together they promote a decrease in mean fiber diameter of the produced nanofibers (Haider et al., 2018; Pelipenko et al., 2015).

The effect of relative humidity on the electrospinning process is highly dependent on composition of the polymer solution. For aqueous solutions, the relative humidity can be utilized to manipulate the diameter and mechanical properties of nanofibers. Adjustments of relative humidity and accompanying changes in fiber morphology can be explained by a

combination of two effects; the solvent evaporation rate and breakup of the viscoelastic fluid, resulting in a beads-on-a-string morphology (Pelipenko et al., 2013). At low relative humidity values, fast solvent evaporation causes the polymer solution to solidify shortly after it comes out of the nozzle or is deposited on the wire, in the case of needleless electrospinning. The solution is also subjected to voltage-induced stretching for a more limited time period, which results in formation of thicker fibers. When the relative humidity is higher, the solidification process is slowed and the liquid in the jet stream is exposed to stretching for an extended time. This results in the formation of thinner nanofibers and in the gradual occurrence of the bead-on-a-string morphology (Pelipenko et al., 2015; Pelipenko et al., 2013).

The described electrospinning parameters and their effects on nanofiber morphology are summarized in **Table 1**.

Table 1: A summary of the expected effects of electrospinning process parameters on the resultant fiber morphology (Rošic et al., 2012b). Licensed under a Creative Commons Attribution 4.0 International license.

Solution parameter	**Effect on nanofiber morphology**
Concentration	Increase in concentration causes an increase in fiber diameter.
Viscosity	Increasing viscosity creates thicker nanofibers without beads.
	Too high viscosity results in production of beads.
Conductivity	Increase in conductivity generates thinner nanofibers.
Surface tension	No conclusive association has been established
Volatility of solvent	Increased volatility demands a higher flow rate and causes formation of nanofibers with reduced beads.
Process parameter	
Flow rate	Reduced flow rate generates thinner nanofibers.
	Exceedingly high flow rate causes production of beads.
Applied voltage	Generation of thinner fibers with higher applied voltage.
Collector distance	A minimum distance necessary to produce dry nanofibers.
	Beads are produced with a too large or too small distance.
Ambient parameter	
Humidity	Reduced humidity permits higher flow rate and causes a reduction in the production of beads.
Temperature	Thinner nanofibers are produced with increasing temperature.

1.8 Nanofiber composition

Material selection is of critical importance in the design of nanofibers for biomedical applications. The ideal biomaterial needs to be biodegradable, biocompatible, nontoxic, moderately hydrophilic and possess sufficient mechanical strength (Pelipenko et al., 2015).

1.8.1 Polymers

Nanofibers can be produced from various polymers. However, polymer characteristics should be closely considered in development of nanofibers, as different polymers will generate fibers with varying degradation rates, mechanical properties and cell-material interactions (Beachley and Wen, 2010; Wang et al., 2009). Natural polymers generally exhibit good biocompatibility, antigenicity, and bioactivity promoting cell attachment and proliferation. Furthermore, the structure of nanofibrous dressings produced from natural polymers is distinctly similar to the natural ECM (Memic et al., 2019). These characteristics generally make natural polymers more suitable for biomedical applications, compared to their synthetic counterparts. Nonetheless, natural polymers have exceedingly complex chemical structures and substantial variations in their physiochemical properties, making them challenging to electrospin. In addition, nanofibers generated from natural polymers tend to have poor mechanical properties, which limits their application as wound dressing materials (Elsabee et al., 2012; Mele, 2016). Synthetic polymers generally have simple and controlled chemical structures, which makes them easy to electrospin. Furthermore, they more often hold the required mechanical integrity, in addition to being cost-effective. Disadvantages of synthetic polymers is their poor biological activity and reduced biocompatibility (Nemati et al., 2019).

A combination of polymers can be applied to overcome the limitations of single-component systems. This strategy could potentially produce suitable biomimetic nanofibers that possess optimal mechanical and biological features. In this project, the natural polymers CS and βG were combined with the synthetic polymers polyethylene oxide (PEO) and hydroxypropyl methylcellulose (HPMC) and processed by electrospinning to obtain nanofibers with desired physicochemical properties.

1.8.1.1 Chitosan

CS is a polysaccharide of marine origin, chemically composed of the copolymers glucosamine and N-acetylglucosamine coupled by β-(1→4) glycosidic linkages (Sahariah and Másson, 2017). CS is a derivative of chitin, a natural polysaccharide produced through biosynthesis (**Figure 8**). Chitin can be found in the exoskeleton of most invertebrates and is one of the main constituents of the exoskeleton in crustaceans and insects. It can also be produced extracellularly in the cell walls of fungi and brown algae (Periayah et al., 2016). However, applications of chitin are limited compared to CS, mainly as a result of its chemical inertness. CS is therefore produced from chitin by partial deacetylation evoked by treatment with concentrated alkali solution (Agnihotri et al., 2004). CS is soluble in dilute aqueous acetic, formic, malic, lactic and succinic acids. Another important trait is the polymers polycationic nature at pH < 6, which enables interactions with negatively charged biologic molecules, such as proteins, anionic polysaccharides, phospholipids and fatty acids (Ahmed and Ikram, 2016).

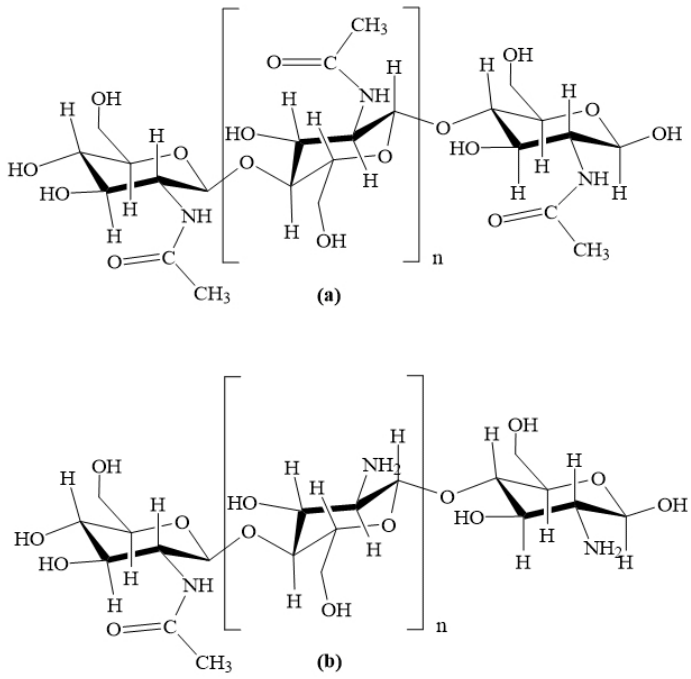

Figure 8: The chemical structure of chitin (a) and chitosan (b). Created with ChemDraw.

Physiochemical properties of chitosan

The physiochemical characteristics of CS are important, as they greatly influence its functional properties. The most important being the molecular weight (MW) and the degree of deacetylation (DD). The degree of acetylation (DA) determines an important feature of CS,

namely its polycationic nature in acidic media, as a result of the ionization of amino groups. Functional properties of CS, such as bioactivity, biodegradation, solubility and swelling ratio are thus influenced by the DA (Matica et al., 2019; Wong, 2009). Furthermore, the molecular weight of CS can influence its biomedical properties. CS is often classified as high molecular weight (HMW), medium molecular weight (MMW), and low molecular weight (LMW). However, the values for each type are not well defined and can vary in literature (Matica et al., 2019).

The nanofibers produced and presented in this thesis consist of medium molecular weight CS, with an average molecular weight of 426 kDa and a degree of deacetylation of 87.4% (Chitinor AS, Tromsø, Norway). Medium weight CS is beneficial for wound healing applications, because the higher degree of deacetylation enhance critical aspects of the natural wound healing process, such as hemostasis and proliferation of cutaneous cells (Howling et al., 2001; Hurler and Škalko-Basnet, 2012; Yang et al., 2008).

Wound healing properties of chitosan

The interest and use of CS for medical and pharmaceutical applications has grown rapidly in the last years. CS is considered an interesting polymer for wound healing applications, due to its favorable biopharmaceutical properties such as biocompatibility, biodegradability, non-toxicity, antibacterial- and hemostatic effect (Bano et al., 2017; Matica et al., 2019). Some of CS's favorable properties in wound healing, could be attributed to the activation and modulation of inflammatory cells such as neutrophils, macrophages and fibroblasts. This promotes a faster and more efficient inflammatory phase, which facilitates an earlier transition to the next stage of the healing process (Matica et al., 2019).

CS accelerates the migration of neutrophils to the wound area and enhances their function as chemical mediators and phagocytizing agents. This is depicted through the activated immune cells increased secretion of inflammatory mediators such as TNF-α, IL-1, IL-8, IL-12, macrophage inflammatory protein (MIP)-1α and 1β, and increased phagocytic activity (Park et al., 2009). Furthermore, CS is composed of N-acetyl-d-glucosamine (GlcNAc), which is an important trait for the activation of macrophages, as they express the receptors for GlcNAc-glycoproteins on their surface. The binding of GlcNAc to these specific receptors is thought to be pivotal for enhancing the activation of macrophages, which plays a central role in the inflammatory process through their release of inflammatory mediators and phagocytosis of

foreign material (Ueno et al., 2001). Lastly, CS accelerates fibroblast proliferation, which promotes the reformation of connective tissue. This process happens indirectly through activation of macrophages and the excretion of stimulating cytokines and growth factors (Park et al., 2009; Ueno et al., 2001). Fibroblast proliferation is beneficial because the cells contribute in ordered collagen deposition and stimulate to increased synthesis of natural hyaluronic acid at the wound site, resulting in rapid wound healing and prevention of scar tissue formation (Bano et al., 2017).

In addition, CS is attributed both hemostatic and analgesic effects, which is due to the polymers ability to promote natural blood clotting and generate a wound environment promoting pain reduction. The hemostatic effect of CS appears to be charge dependent, as its cationic charge determines the degree of interaction with the negatively charged membranes of red blood cells (Bano et al., 2017). The mechanism behind the analgesic effect of CS is not fully explored, but its absorption of bradykinin is thought to be central. Absorption of proton ions released in the inflamed wound area and a subsequent reduction of pH, is also assumed to contribute to the analgesic effect (Ahmed and Ikram, 2016).

CS also has intrinsic antimicrobial effect against bacteria and fungi, which is a beneficial property in wound healing as wounds are vulnerable to infection after trauma (Matica et al., 2019). For chronic wounds, wound infection is one of the main causes of delayed healing. Chronic wounds generally display a complex microbial environment, involving the colonization of diverse populations of both aerobic and anaerobic bacteria, which exacerbates the inflammatory state of the wound (Leaper et al., 2015).

Treatment of chronic wound infections is largely empirical and based on the use of various antimicrobial agents, which mainly includes antibiotics and antiseptics. The indication for antibiotic therapy along with an optimal treatment strategy is thus often poorly defined, which has led to extensive inappropriate use of topical and systemic antibiotics (Leaper et al., 2015). In recent years, reports of chronic wounds becoming infected with healthcare-associated pathogens expressing extensive resistance, such as MRSA, pseudomonads and vancomycin-resistant enterococci, have increased (Siddiqui and Bernstein, 2010). Thus, impeded healing of chronic wounds due to infection is further complicated by rapidly increasing antibiotic resistance and the absence of novel antibiotics in research. To address this issue, alternative or complementary adjuncts to antibiotic therapy have to be considered (Leaper et al., 2015).

Natural polymers exhibiting intrinsic antimicrobial effect present a promising alternative in the treatment of chronic wound infections. Hence, CS represents an optimal active ingredient in novel antimicrobial formulations to treat infection and promote healing of chronic wounds (Santos et al., 2016). However, the exact mechanism of its antimicrobial action is not fully established. It is assumed that the cationic nature of CS enables interactions with negatively charged molecules of the bacterial cell wall, disrupting the structure and eventually entering the cell. In addition, CS is believed to disrupt the transport of nutrients across the bacterial cell wall, facilitating the death of the microorganism (Matica et al., 2019).

1.8.1.2 β-glucans

β-gulcans is the common term for a group of heterogeneous polysaccharides, made up of D-glucose monomers linked by β-glycosidic bonds. These glucose polymers can be found in a variety of natural sources, such as yeast, fungi, cereals, seaweed, algae and bacteria, where they are involved in cell wall structure amongst other biological functions (Du et al., 2014). The structure of β-glucans, deriving from different sources, often vary when it comes to size and branching pattern. In general, the structure of β-glucans originating from microorganisms forms a linear backbone consisting of β-(1→3) linked glucose moieties, where the branching chains is coupled to the linear structure by β-(1→6) linkages. β-glucans stemming from plants, however, typically organize in a structure with β-(1→3) and β-(1→4) linked glucose moieties, devoid of branching (Zhu et al., 2016) (**Figure 9**).

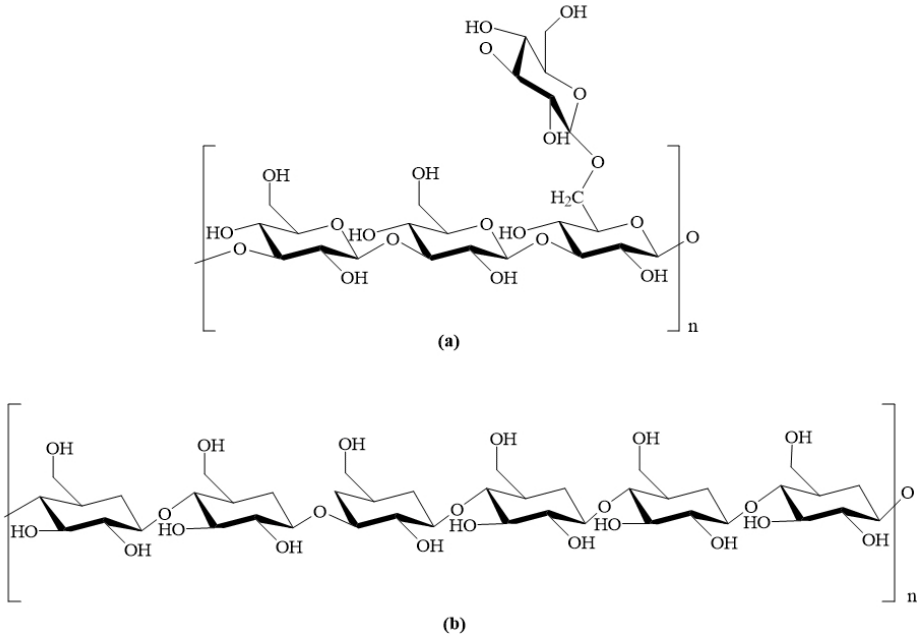

Figure 9: The chemical structures of β-glucans. (a) (1→3) β-glucans with β-(1→6) linkages. (b) (1→3) β-glucans with β-(1→4) linkages. Created with ChemDraw.

β-glucans in wound healing

β-glucans are known to enhance immune functions, displaying anti-infective, antitumor and immunomodulatory activity (Du et al., 2014; Majtan and Jesenak, 2018). These properties are mediated through several pattern recognition receptors located on specific target cells. These target cells are predominantly immune cells, such as macrophages, monocytes, neutrophils, dendritic cells, but also cutaneous cells such as keratinocytes and fibroblasts possess these receptors. β-glucans are able to activate immune reaction mechanisms through binding to these receptors (Majtan and Jesenak, 2018).

A promising pharmaceutical utilization of β-glucans is in wound care, as they have shown to enhance wound healing and reduce associated pain (Seo et al., 2019). However, the molecular mechanisms behind this effect are not fully explored. β-glucans are thought to be able to participate in the wound healing process by activating both immune cells and other cells to stimulate more efficient wound repair. For instance, β-glucans can activate dermal fibroblasts stimulating increased proliferation and secretion of IL-6, which is beneficial for resurrection of the ECM (Kim et al., 2012). β-glucans can also induce production of cytokines and release of reactive oxygen species (ROS) by dendritic cells and macrophages, which in turn would promote neutrophil infiltration and angiogenesis, securing more efficient wound healing.

Moreover, β-glucans are able to influence the process of re-epithelialization by inducing both migration and proliferation of keratinocytes, which is beneficial for accelerating wound closure (Van den Berg et al., 2014).

Soluble β-glucan

The patented soluble beta-1,3/1,6-glucan (SBG®), developed by Biotec Pharmacon AS, was utilized as the second active ingredient in this project. SBG® is produced by extraction of beta-1,3/1,6-glucan (βG) from *Saccharomyces cerevisiae*, also known as bakers' yeast, in a novel process involving specific heating and cooling steps in relatively rapid succession. This procedure forces a new molecular conformation of the present βG due to rapidly established intermolecular interactions, generating a βG with altered structure and properties. This yields a pharmaceutical grade product with a final concentration of 2.5% soluble βG (w/v) in water, forming a gel at room temperature (Engstad and Nøkland, 2017). Analysis of the compound has revealed that a large array of structures is formed; single chains co-existing with triple-stranded structures and even larger particulate structures. This demonstrates that the βG present in SBG® is structurally related to, but still different from other plant or fungal branched (1→3)-β-D-glucans (Qin et al., 2013). It has been established that some degree of chain association is necessary to activate the cellular receptors associated with β-glucans effect (Palma et al., 2006). Soluble β-glucans ability to form ordered triple stranded structures is thus assumed to be essential for facilitating an immunomodulatory effect. However, the specific mechanism behind this effect is not fully established.

The wound healing effect of SBG® as a topical treatment of diabetic foot and leg ulcers has been examined in a clinical trial, where the results indicate that the product has promising potential for accelerating cutaneous healing (Zykova et al., 2014). In addition, the nanofibrous wound dressing with SBG® as active ingredient, developed by Grip et al., exhibited improved wound healing in an animal *in vivo* trial using diabetic mice as test subjects (Grip et al., 2018).

1.8.2 Solvents

To achieve successful electrospinning, the selection of solvent is fundamental. The selection of solvent contributes in determining the polymer concentration applicable for electrospinning, in addition to the conductivity and surface tension of the solution. This will in turn affect the spinnability of the polymer solution and the morphology of the generated fibers. Established

solvents used in preparation of electrospinning solutions are chloroform, acetic acid, acetone, dimethylformamide, tetrahydrofuran, ethanol and distilled water (Rošic et al., 2012b). Distilled water is generally preferred as solvent when the generated nanofibers are intended for biomedical applications. This is mainly due to the biocompatibility of distilled water and the fact that possible solvent residues will not raise toxicity concerns. However, the use of distilled water as solvent alone is limited to hydrophilic polymers. Polymers that are not fully soluble in water could require the addition of small amounts of co-solvents to increase solubility (Pelipenko et al., 2015). Moreover, the addition of volatile solvents could be necessary to increase the evaporation rate of the solvent, decreasing the required distance from outlet to collector (Rošic et al., 2012b).

In this project distilled water and acetic acid were utilized to prepare an acetic aqueous media to enable the dissolution of CS. Ethanol was also used as solvent, to increase the volatility of the polymer solution for successful electrospinning.

1.8.3 Other excipients

The polymer formulation used for electrospinning nanofibers is often supplemented with additional excipients to improve the production process or functionality of the nanofibers, with regard to therapeutic efficacy and biocompatibility (Pelipenko et al., 2015).

1.8.3.1 Polyethylene oxide

Polyethylene oxide (PEO) is a hydrophilic, synthetic polymer, often utilized to impart viscosity and modify the flow of aqueous solutions. This polymer has several favorable properties, such as biocompatibility and good mechanical integrity, including high elongation and ability to orient when strained (Grkovic et al., 2017). Due to its linear structure, good spinnability and ability to form hydrogen bonds with other polymers, PEO is often added to polymer formulations, which have proven to be challenging to electrospin alone (Klossner et al., 2008; Rošic et al., 2012a). Consequently, PEO was chosen as copolymer in this project mainly to improve the spinnability of the polymer solutions.

1.8.3.2 Hydroxypropyl methylcellulose

Hydroxypropyl methylcellulose (HPMC) is a cellulose ether obtained by chemical alteration of cellulose. The polymer is hydrophilic, biocompatible and biodegradable, with broad applications in food industry, cosmetics, textiles, agriculture and drug delivery (Deshmukh et al., 2017). Several cellulose derivates, including HPMC, has been applied in electrospinning and proven to form homogenous nanofibers of uniform quality (Frenot et al., 2007). This establishes the incentive for utilizing HPMC as copolymer in this project.

2 Aims of the study

This thesis represents a first step towards the development of active nanofibrous wound dressings containing CS and βG as active ingredients. To enable the production of nanofibers with favorable properties by electrospinning, numerous aspects of the production process has to be assessed. The aim of this thesis was thus to explore the influence of polymer- and solvent composition on polymer solution characteristics, spinnability of solutions and properties of produced nanofibers. Another focal point was to control specific parameters of the electrospinning process, to facilitate production of uniform fibers.

More specifically, we aimed to:

- Characterize the different polymer solutions by establishing their conductivity, surface tension and rheological properties through the utilization of suitable methods.
- Develop an optimized method for the electrospinning of the polymer solutions by controlling specific settings of the Nanospider™ and controlling ambient parameters, and evaluate its effect on morphology of produced nanofibers.
- Determine the spinnability of the different solutions and establish the highest obtainable concentration of active ingredients in successfully produced nanofibers.
- Characterize the produced nanofibers by establishing tensile properties, morphologies, diameters and absorption capacities through the use of appropriate methods.
- Assess the nanofibers suitability as wound dressings by evaluating potential limitations or favorable properties, based on their composition and determined characteristics.

3 Materials and methods

3.1 Materials

3.1.1 Chemicals

Acetic acid (≥99.8%), Sigma-Aldrich, St. Louis, MO, USA

Acetone (≥99.5%), Sigma-Aldrich, St. Louis, MO, USA

Benecel™ E4M hydroxypropyl methylcellulose (HPMC), Ashland Global Specialty Chemicals Inc, Ashland, KY, USA

Calcium chloride dihydrate (≥99.0%), Sigma-Aldrich, St. Louis, MO, USA

Chitopharm™ M, average MW of 426 kD, 87.4% degree of deacetylation, Chitinor AS, Tromsø, Norway

Distilled water

Ethanol (96% v/v), VWR International, Radnor, PA, USA

Polyethylene oxide (PEO), Dow Chemical Company, Midland, MI, USA

Sodium Chloride (≥99.5%), Sigma-Aldrich, St. Louis, MO, USA

Soluble beta-1,3/1,6-glucan, 2.5% (w/w) (SBG®), Biotec BetaGlucans AS, Tromsø, Norway

3.1.2 Instruments

Discovery HR-2 Hybrid Rheometer, TA Instruments, New Castle, DE, USA

Elmarco Nanospider™ Lab electrospinning machine, Liberec, Czech Republic

Force Tensiometer – K6, Krüss GmbH, Hamburg, Germany

IP54 Digital Micrometer 0-25/0.001 mm, Wilson Wolpert Instruments, Aachen, Germany

Polaron SC7640, Quorum Technologies LTD, Kent, UK

Sartorius LP620S, scale, Sartorius Lab Instruments GmbH & Co. KG, Göttingen, Germany

Sartorius Quintix 124-1S Analytical Balance, Sartorius Lab Instruments GmbH & Co. KG, Göttingen, Germany

SensION™+ EC7 Basic Conductivity Laboratory Meter, Hach Company, Loveland, CO, USA

SensION™+ PH3 Basic pH Benchtop Meter, Hach Company, Loveland, CO, USA

Shaking water bath 1083, Gesellschaft für Labortechnik mbH, Burgwedel, Germany

TA.XT plus Texture analyzer, Stable Micro Systems, Surrey, UK

TES-1364 Humidity-Temperature meter, TES Electrical Electronic Corp., Taipei, Taiwan

Qlima H509 Humidifier, PVG International B.V., Oss, Netherlands

Zeiss Sigma FE-SEM, Carl Zeiss, Oberkochen, Germany

3.1.3 Software and programs

Exponent Connect software v. 6.1.16.0, Stable Micro Systems, Surrey, UK

ImageJ software version 1.52u, National Institutes of Health, MD, USA

Trios software v. 5.0.0.44608, TA Instruments, New Castle, DE, USA

3.2 Methods

3.2.1 Preparation of polymer solutions

The preparation of the polymer solutions was grounded on the method of Grip et al. (Grip et al., 2018). A total of 37 polymer solutions were prepared in two separate rounds, utilizing CS and βG as active ingredients, and HPMC and PEO as co-polymers. Both solutions containing CS as the single active ingredient and solutions containing CS and βG were prepared, with gradually increasing concentrations. All solutions had a total polymer concentration of 2.1% (w/w). Therefore, as the concentration of the active ingredient(s) was increased, the amount of HPMC was decreased to the same extent. The concentration of PEO was kept constant at 0.315% (w/w). The relative concentrations (%) of the different polymers in the prepared solutions are presented in **Figure 10**, exact values are listed in the Appendix; **Table A2**, **Table A3**.

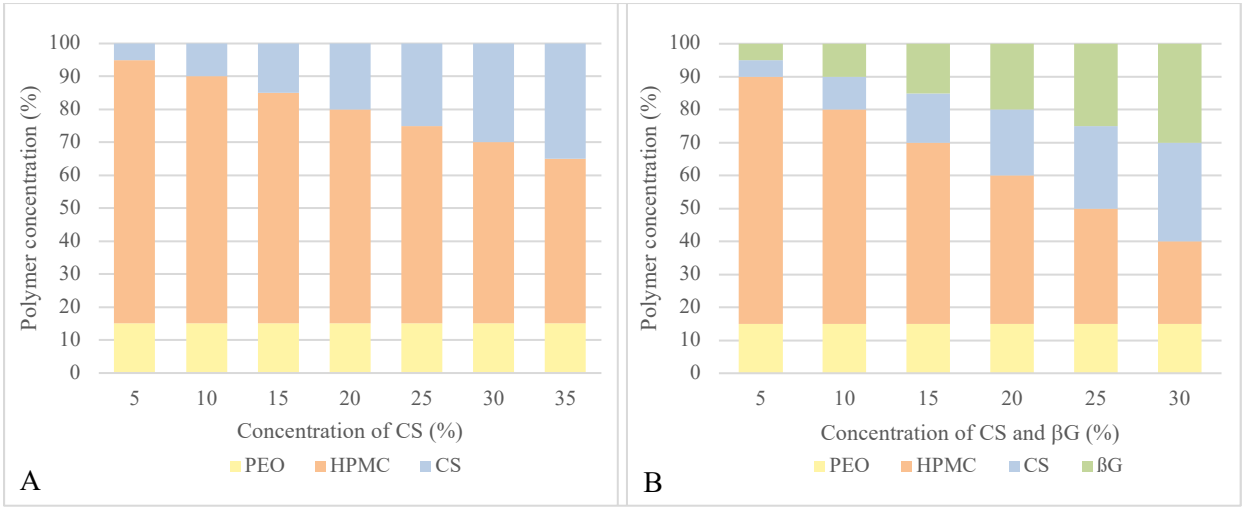

Figure 10: Distribution of polymers in solutions with increasing concentrations of (A) CS and (B) CS and βG, equaling a total polymer concentration of 2.1% (w/w).

Distilled water, ethanol (96%) and acetic acid (≥99.8%) were applied as solvents. Each polymer solution was prepared three times with pre-determined ethanol concentrations of 50%, 60% and

70% (w/w). The concentration of acetic acid was kept constant at 3% (w/w) in every solution, while the water content was adjusted to reach a total solvent concentration of 97.9% (w/w).

All polymers were provided as dry materials, except βG that was acquired from SBG® (2.5% w/w). To assure a homogeneous polymer distribution in the final spinning solutions, the polymers were first dissolved separately before mixing. The CS solutions were prepared by dissolving CS in distilled water and acetic acid. When βG was included in the formulation, SBG® was first heated in a water bath at 50°C for 10 minutes, to reduce the viscosity. Heated and liquefied SBG® was then diluted by adding the same solvents as applied for the CS solutions. The blend was then stirred on a magnetic stirrer for approximately 10 minutes, before CS was added and dissolved. Lastly, the solutions were left to stir overnight to ensure complete hydration of the polymers (step 1, **Figure 11**).

The PEO solution (5% w/w) was prepared in ethanol and heated at 70°C under constant stirring on a magnetic stirrer for 30 minutes, before being placed in a water bath at the same temperature for 1 hour. The formulation was then cooled to room temperature. The HPMC solution was prepared in ethanol at room temperature and stirred on a magnetic stirrer for 10 minutes. Finally, the three separate polymer solutions were mixed and stirred overnight creating the finished polymer solution (step 2 and 3, **Figure 11**).

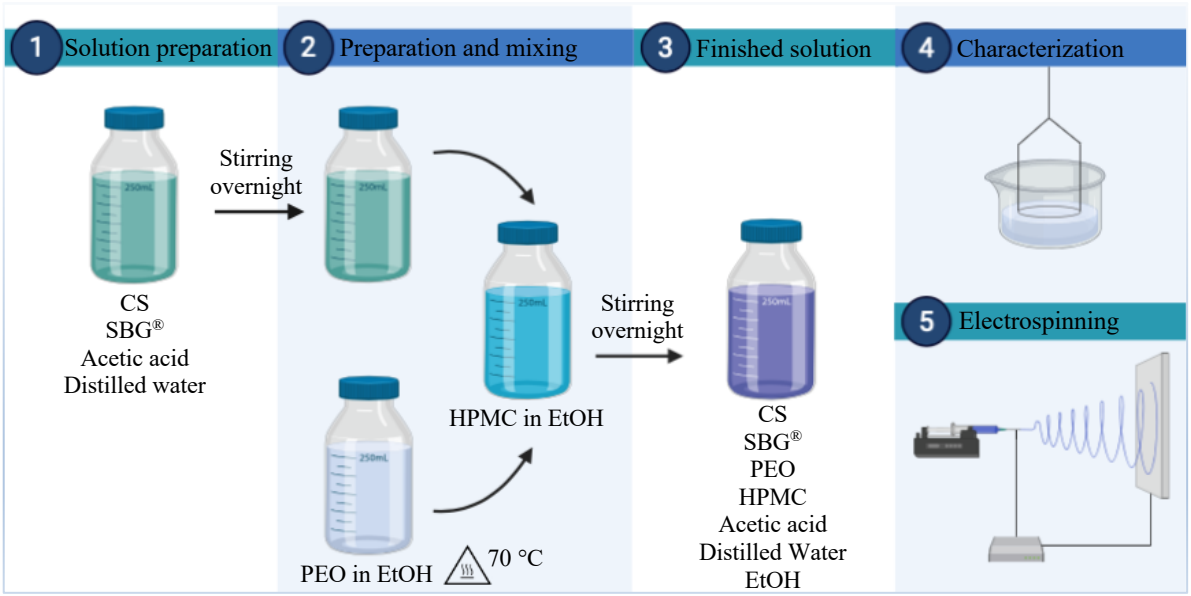

Figure 11: Presentation of the process of preparing a polymer solution. (1) Preparing solution with active ingredients, (2) preparing separate PEO- and HPMC solutions before mixing the polymer solutions in the HPMC solution, (3) finished solution. (4) Characterization and (5) electrospinning. Created with Biorender.com.

3.2.2 Characterization of polymer solutions

The surface tension, conductivity and rheological properties were determined for all of the solutions. The polymer solutions were prepared and characterized twice, and the average values reported.

3.2.2.1 Conductivity and surface tension

Conductivity of the solutions was measured at room temperature (25 ± 1°C) using a SensION^{TM}+ EC7 Basic Conductivity Laboratory Meter (Hach Company, Loveland, CO, USA). The conductivity was measured in triplicate for each solution.

The surface tension of the polymer solutions was measured at room temperature (25 ± 1°C) by applying the ring method, using a Force Tensiometer – K6 (Krüss GmbH, Hamburg, Germany). The tensiometer consists of a torsion wire which is connected to a thin wire ring. To conduct the measurement, approximately 20 ml of polymer solution was transferred to the sample vessel and placed on the sample platform of the instrument. The ring was then immersed in the sample and slowly withdrawn by lowering the sample platform. During this process, the surface tension of the liquid caused the wire to twist, and its deflection was presented on a scale calibrated for the surface tension (Krüss GmbH, 2007). The surface tension was determined by the value indicated by the scale, at the moment the connection between the liquid and the wire ring broke; when the applied force overcame the surface tension. The surface tension was measured in triplicate for each solution using this method.

3.2.2.2 Rheological measurements

The rheological characterization included determination of flow properties and viscoelastic properties. Therefore, both oscillatory and rotational rheological tests were performed using a Discovery HR-2 Hybrid Rheometer (TA Instruments, New Castle, DE, USA), with a parallel plate measuring system. The results were processed and evaluated with the Trios software v.5.0.0.44608 (TA Instruments, New Castle, DE, USA).

For the rotational tests a 40 mm cross-hatched plate geometry was used. The gap between the plate and the platform was set to 1050 μm for the trimming of the sample, and further lowered to an operational height of 1000 μm. The samples were soaked for 180 seconds to achieve a

stable temperature of 25°C for the measurements. The flow characteristics were determined by controlling the shear stress and plotting the viscosity as a function of the shear rate. The tests were conducted as logarithmic sweeps (0.5-500 Pa) registering 10 points per decade using a steady state sensing.

A 40 mm smooth steel plate geometry was applied for the oscillation tests. An amplitude sweep was initially performed to determine the linear viscoelastic range, using a frequency of 10 rad/s and a logarithmic sweep of strain from 0.01 to 1000%. The oscillation tests were all conducted within this established linear region. The test parameters, in terms of the gap- and operational height, temperature and soak time were the same for the oscillation tests as the rotary tests.

3.2.3 Electrospinning of polymer solutions

The Elmarco Nanospider™ Lab electrospinning machine (Liberec, Czech Republic), with a stationary wire electrode system, was utilized to perform the electrospinning of the polymer solutions. The instrument has an adjustable spinning distance of 120-240 mm, a substrate speed in the range of 0-5000 mm/min and a maximum spinning voltage of 80 kV. A spinning carriage with a volume of 50 ml was used in the spinning process to ensure that the metal wire would be coated with sufficient solution throughout the spinning time. The metal insert used had an orifice size of 0.8 mm. The electrospinning was performed at room temperature (24 ± 3°C), with a relative humidity of 23 ± 3%.

The highest voltage of 80 kV was applied for the spinning of all the solutions and the carriage speed was kept constant at 300 mm/s. The substrate speed and the spinning distance was, however, adjusted for each solution depending on the spinnability of the solution, to prevent droplets of solution from forming on the substrate. The spinning distance applied for the solutions was between 200 and 240 mm, while the chosen substrate speed was between 2 and 4 mm/min.

To determine the spinning distance, a preliminary round of spinning was executed for every solution. This process was initiated at a spinning distance of 240 mm. The spinnability of the solution and the formation of fibers on the substrate was then observed for approximately 3 minutes. If the polymer solution did not produce droplets on the surface of the substrate, the spinning distance was lowered by 10 mm. This procedure was continued either until droplets

were observed, or until the lowest distance of 200 mm was reached. The purpose of this exercise was to determine the optimal spinning distance for each solution, to promote the formation of an even fiber surface by avoiding the creation of droplets. The substrate speed of 2 mm/min was only adjusted if the electrospinning of a polymer solution resulted in the formation of droplets at the highest spinning distance of 240 mm. The substrate speed was then increased by 1 mm/min, followed by an observation period of 3 minutes to determine a suitable substrate speed. An upper limit of 4 mm/min substrate speed was established to prevent the formation of too thin fiber mats.

3.2.4 Characterization of nanofibers

The tensile properties, absorption capacity, nanofiber morphology and diameter were examined for all of the produced nanofibrous scaffolds. Each nanofibrous formulation was produced and characterized twice, and the average value was reported.

3.2.4.1 Tensile properties of nanofibers

The tensile properties of the spun nanofibers were measured using a Texture analyzer (TA.XT plus, Stable Micro Systems, Surrey, UK). The instrument was calibrated with a 5 kg load cell and fitted with tensile grips, before proceeding with height calibration. Grip separation was adjusted to 50 mm with a crosshead speed of 10 mm/min. A template was used to create test specimens of uniform width and length of 10 mm and 80 mm respectively, according to the ASTM D882-18 standard (ASTM International, 2018). The thickness of the nanofibers was determined by using an IP54 Digital Micrometer (Wilson Wolpert Instruments, Aachen, Germany), and the values were entered prior to each analysis to adjust for variations in thickness of the samples. The tensile strength (TS), elastic modulus (EM) and percent elongation at break (PEB) were evaluated in five samples from each fiber by use of the Exponent Connect software v.6.1.16.0 (Stable Micro Systems, Surrey, UK), through the establishment of tensile stress-strain curves (**Figure 12**).

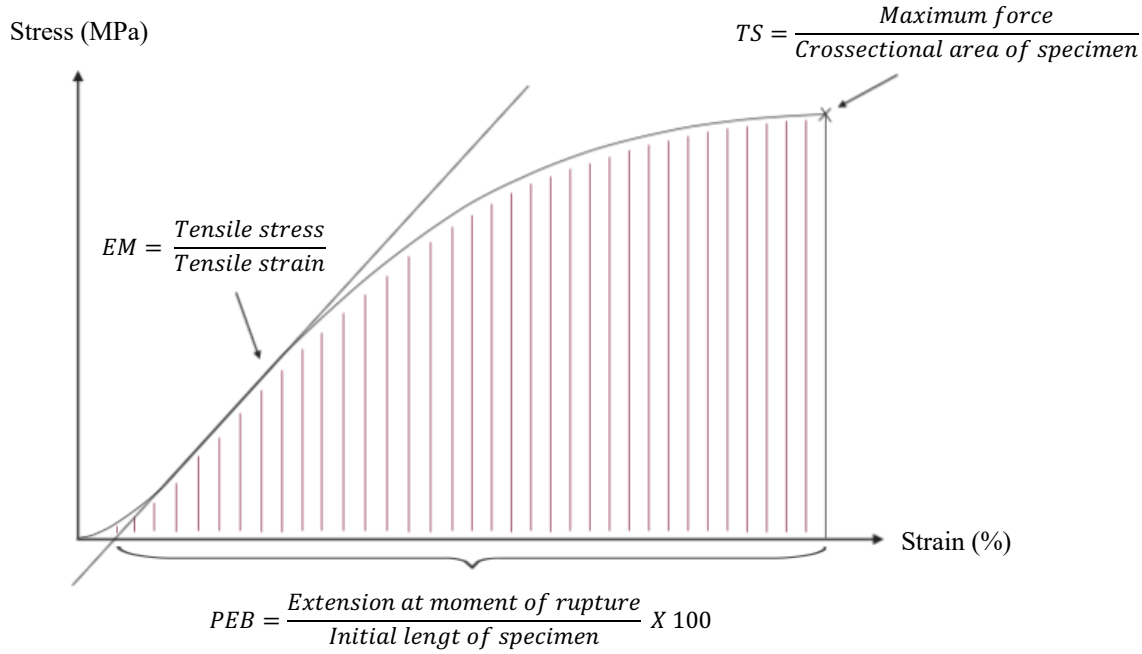

Figure 12: Tensile stress-strain curve, where load and displacement of the specimen was measured and plotted as stress over strain. (EM) elastic modulus, (TS) tensile strength, (PEB) percent elongation at break. Created with Biorender.com.

3.2.4.2 Diameter and morphology of nanofibers

The morphology and microstructure of the electrospun nanofibers was observed through Field Emission Scanning Electron Microscopy (FE-SEM), using the Zeiss Sigma FE-SEM (Carl Zeiss, Oberkochen, Germany), operated at an accelerating voltage of 2 kV. Small samples were cut from each of the spun fibers and fixed onto metallic studs with double-sided carbon tape. Further, the samples were splutter coated with a thin layer of gold-palladium using a Polaron SC7640 (Quorum Technologies LTD, Kent, UK), to secure a conductive layer of metal on the sample. After coating, the nanofibers were examined by FE-SEM under high vacuum, where five images were obtained from each fiber sample with varying magnifications of 1, 3 and 15 kX.

Nanofiber diameter was examined by analyzing the images obtained from FE-SEM utilizing the ImageJ software (NIH, MD, USA). The diameter distribution was determined by measuring 100 arbitrarily chosen fibers in three separate SEM-images per nanofiber sample. Consequently, 300 fibers were measured for each fiber specimen, ensuring a representative selection of fiber measurements for the establishment of the average fiber diameter.

3.2.4.3 Absorption capacity of nanofibers

The absorption capacity of the nanofibers was examined by immersing them into simulated wound fluid; "Solution A" from the ISO standard BS EN 13726-1 (British Standards Institution, 2002). To determine the absorption time, a preliminary round of tests was conducted, and the absorption capacity of samples compared after 1, 2, 5 and 10 minutes. A time interval of five minutes was chosen, due to the negligible difference in absorption capacity of the fibers after five and ten minutes.

The tests were conducted by pipetting 600 µl simulated wound fluid into 140 mm Petri dishes for each sample. Fiber samples (2×2 cm) were cut, weighed in their dry state and then immersed in the wound fluid at room temperature (25 ± 1°C) for five minutes. Excess fluid was removed from the fiber sample by deliberate transference of the sample from one weighing dish to another before weighing. The experiment was done in triplicate and the percentage absorption capacity (C_a) was calculated according to the following equation:

$$C_a(\%) = \frac{W_s - W_d}{W_d}\ x\ 100 \qquad \textbf{Eq. 1}$$

Where W_d was the weight of the dry nanofiber sample and W_s denotes the weight of the fiber sample after absorption.

3.2.5 Statistical evaluation

The presented results are expressed as mean ± SD from two independent experiments. The strength and direction of observed associations was examined statistically by calculation of the Pearson's correlation coefficient.

4 Results and discussion

4.1 Optimization of polymer solution composition

The composition of the electrospinning solutions; polymers and solvents, was selected based on the composition previously described by Grip et al. (Grip et al., 2018). However, for the solutions created in this project CS was added as a second active ingredient, in addition to βG, to introduce an antimicrobial effect to the nanofibrous scaffolds. When adding CS, the total polymer concentration had to be reassessed to ensure a composition that allowed a gradual increase in concentration of active ingredients, while still maintaining required features for successful nanofiber formation by electrospinning. Preliminary experiments involving the electrospinning of polymer solutions with differing total polymer concentration, were therefore executed by the research group before initiation of this project. Consequently, a total polymer concentration of 2.1% (w/w) was deemed most suitable (results not included).

When incorporating CS as active ingredient, the solvent composition also had to be adjusted. This was due to the insolubility of CS in aqueous solutions at neutral to high pH-levels. The polymer can, however, be partially protonated and thus solubilized in acidic aqueous solutions (Sogias et al., 2010). Hence, to enable the solubilization of CS, acetic acid was included as solvent in addition to water and ethanol.

To be better equipped to assess the effect of adding CS as a second active ingredient, two sets of solutions were prepared; one containing CS as the single active ingredient and one containing both CS and βG.

4.2 Characterization of polymer solutions

Successful formation of nanofibers by electrospinning is largely dependent on specific properties of the polymer solution. Solution conductivity, surface tension and rheology were properties examined in this project.

4.2.1 Conductivity and surface tension

Conductivity is an important parameter affecting the polymer solutions ability to produce nanofibers during electrospinning. This is due to the establishment of repulsive charges at the surface of the fluid, which enables the formation of a Taylor cone by application of an external

electric field. The surface tension of the solution is also significant for the initiation of electrospinning, because it determines the force required from the applied electric field for the repulsive charges to overcome it (Pelipenko et al., 2015). By establishing the exact surface tension and conductivity of each polymer solution, the influence of varying polymer- and solvent composition could be evaluated. The information could further be utilized to evaluate the conductivity and surface tensions potential influence on solution spinnability and properties of produced nanofibers.

The surface tension of the polymer solutions as a function of solution composition, is presented in **Figure 13**.

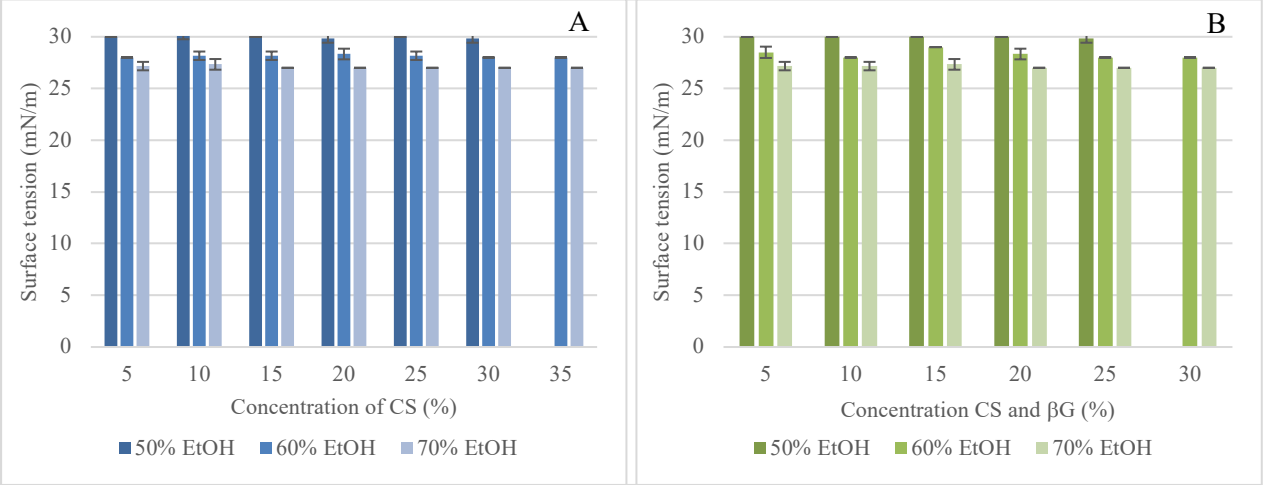

Figure 13: Surface tension of (A) CS and (B) CS and βG solutions as a function of solution composition (n=2).

The results show that the surface tension remained practically unchanged regardless of the adjustments made in polymer composition of the solutions. However, the surface tension appears to be affected by the solvent composition. A slight decrease in surface tension can be observed with an increase in ethanol concentration of the polymer solutions (**Figure 13**). This observation is supported by Khattab et al. who obtained similar results examining the surface tension of ethanol and water mixtures with varying ethanol concentrations (Khattab et al., 2012).

The association between ethanol concentration and surface tension of polymer solutions was examined statistically by calculating the Pearson correlation coefficient. The calculated

correlation coefficient was -0.97 for the CS solutions, and -0.95 for the CS and βG solutions. Correlation coefficients so close to -1 indicate a very strong negative association, which substantiates the observation of decreasing surface tension with increasing ethanol concentration (Schober et al., 2018).

The conductivity of the polymer solutions as a function of solution composition, is presented in **Figure 14**.

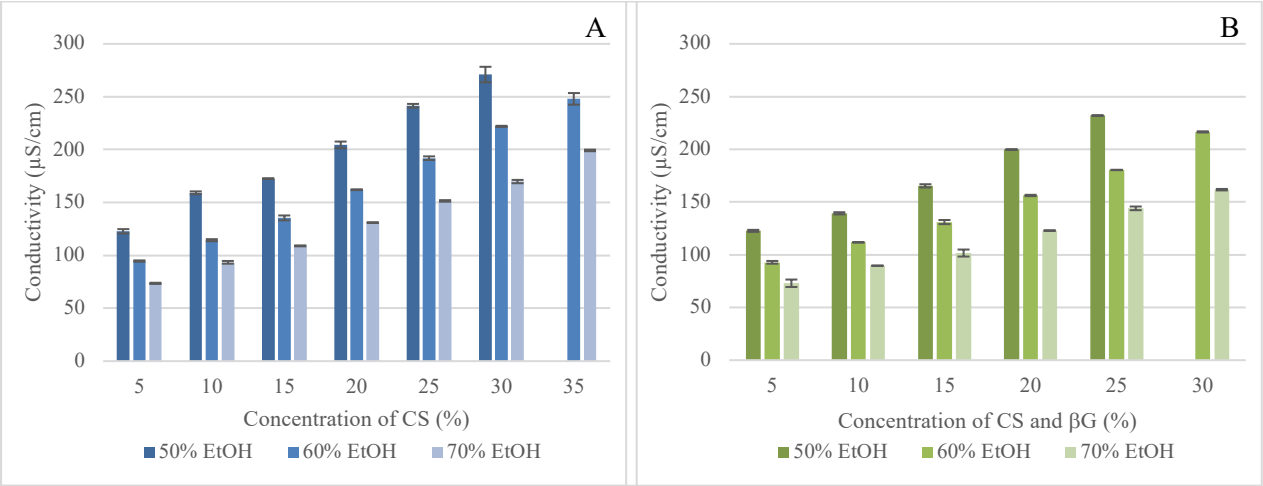

Figure 14: Conductivity of (A) CS and (B) CS and βG solutions as a function of solution composition (n=2).

The results show that the conductivity of the polymer solutions is affected by the concentration of CS. As the concentration of CS gradually increases, a corresponding increase in conductivity can be observed (**Figure 14**). This observed correlation can be explained by the polymers ability to exhibit polyelectrolyte properties in aqueous medium. The pKa value of CS is 6.5, which makes the polymer positively charged and soluble in acidic to neutral solutions (Sudhakar et al., 2018). Thus, the presence of acetic acid in the aqueous media of the polymer solutions establishes a suitable environment to promote the protonation and solubilization of CS, which enables the polymer to conduct electricity. Increasing conductivity of polymer solutions with increasing concentrations of CS has previously been reported in literature (Rošic et al., 2012a; Van der Schueren et al., 2012).

βG and HPMC does not function as polyelectrolytes. Hence, increasing concentrations of βG and decreasing concentrations of HPMC, does not affect the conductivity of the solutions. This

is confirmed by the observed similarity in conductivities of solutions containing CS and solutions containing both active ingredients, at corresponding concentrations (**Figure 14**).

The Pearson correlation coefficient was utilized to examine the association between CS concentration and conductivity of polymer solutions. The calculated correlation coefficient for the CS solutions was 0.82, while the correlation coefficient for CS and βG solutions was 0.76, which indicates a strong positive correlation. This strengthens the observed association between increasing CS concentration and subsequently increasing conductivity (Schober et al., 2018).

Also observed in **Figure 14**, was a continuous trend where solutions containing higher concentrations of ethanol were associated with lower conductivities. The solutions containing higher amounts of ethanol would consequently consist of lower amounts of water. Water can conduct electricity because of its ability to function as an electrolyte. However, ethanol does not have this ability and is therefore not conductive, which can explain the observed trend in conductivity.

4.2.2 Rheological properties

Viscosity is an important parameter in the electrospinning process due to its direct influence on the extent of polymer chain entanglement within the polymer solutions. Sufficient entanglement of polymer molecules is integral for the production of uniform nanofibers. Solutions consisting of polymers with low chain entanglement generally exhibit low viscoelastic force, which elicits fragmentation of the polymer chains under electrospinning. These fragments cause the formation of beads or droplets rather than continuous fibers. Viscosity of polymer solutions is dependent on polymer type, polymer concentration and type of solvent (Haider et al., 2018).

To evaluate rheological properties as a function of solution composition, rotational and oscillatory rheological measurements were performed on all solutions. The rotational measurements were utilized to determine the viscosity of the solutions as a function of shear rate. The results from these measurements depicted graphs with distinctly declining curves (**Appendix; Figure A3, Figure A4**) . The declining curves represent decreasing solution viscosity with increasing shear rate, which indicates that all of the solutions behaved as standard non-Newtonian, shear thinning fluids. This observed shear thinning effect is classical for polymer solutions and can be explained by the structure of the polymer chains. Without an external

influence, the macromolecules constituting the polymers exist in their lowest energy state, a three-dimensional coil. However, with applied shear the molecules will orientate parallel to the direction of shear and elongate. Consequently, this lowers their flow resistance and results in a decreased viscosity (Rošic et al., 2012a).

Due to the large amount of polymer solutions included in the rotational analysis, it was not possible to conduct a more detailed interpretation using the aforementioned graphs. Thus, to be able to evaluate potential differences in viscosity of polymer solutions of different composition, another set of graphs were constructed. Viscosity values were plotted as a function of solution composition and examined under varied controlled shear stresses. Small differences in viscosity were detected using this approach, and these differences were most pronounced at a controlled shear stress of 19.90 Pa. Viscosity presented as a function of solution composition at a controlled shear stress of 19.90 Pa is displayed in **Figure 15**.

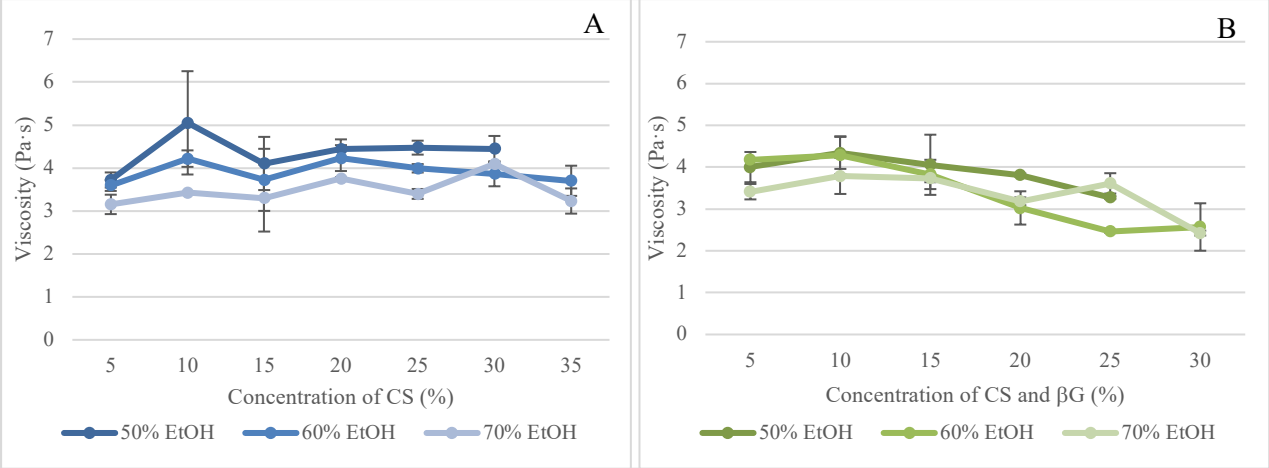

Figure 15: Viscosity of (A) CS and (B) CS and βG solutions as a function of solution composition at a controlled shear stress of 19.90 Pa (n=2).

As presented in **Figure 15**, the viscosity of solutions containing both active ingredients, was slightly decreasing with increasing concentrations of CS and βG. These observed differences in viscosity are likely to be caused by viscoelastic differences between the polymers constituting the solutions. With increasing concentrations of CS and βG, the concentration of the copolymer HPMC was consequently reduced. Celluloses such as HPMC are often utilized in pharmaceutical applications as viscosity increasing agents, which substantiates the polymers importance for the viscosity of the polymer solutions (Oh et al., 2015). Thus, with gradually

decreasing concentrations of HPMC, the viscosity of the solutions containing CS and βG were decreased. Decreased viscosity of polymer solutions with decreasing concentrations of HPMC have previously been reported by Aydogdu et al., who produced nanofibers from HPMC and PEO blends (Aydogdu et al., 2018).

The reduction in viscosity as a function of increasing concentrations of active ingredient(s) was only prominent for the solutions containing both active ingredients (**Figure 15**). This could be explained by the decrease in HPMC being double in these solutions compared to the CS solutions, for each increase in concentration of active ingredients, as previously presented in **Figure 10**. However, another likely explanation is that CS was able to replace HPMCs viscoelastic properties to a greater extent than βG, since no change in viscosity can be observed for CS solutions with increasing concentrations of CS.

The association between concentration of active ingredient(s) and viscosity of polymer solutions was examined statistically by calculating the Pearson correlation coefficient. For CS solutions the calculated correlation coefficient was 0.06, which indicates that no distinct association was found between the two variables. No observable change in viscosity with increasing concentrations of CS is thus confirmed statistically. Contrastingly, for solutions containing both active ingredients, the correlation coefficient was -0.73, which indicates a strong negative association (Schober et al., 2018). This means that as the concentration of CS and βG in the polymer solutions increased, the viscosity decreased, which is consistent with the observations made from **Figure 15**.

Also presented in **Figure 15**, is a slight difference in viscosity for solutions containing different concentrations of ethanol. The viscosity of the polymer solutions looks to be increasing with decreasing ethanol concentrations, which can be attributed to greater interactions between the hydrophilic polymer molecules and water. With larger amounts of available water the hydrophilic polymers are more readily susceptible to solubilizing or swelling which increases the viscosity of the solutions (Schmidt, 2019). The association of decreasing viscosity with increasing ethanol concentration, was more prominent for the CS solutions, which is confirmed by a moderately high negative correlation coefficient of -0.63, compared to the weak negative correlation coefficient for CS and βG solutions of -0.32 (Schober et al., 2018).

The oscillatory measurements were used to determine the dynamic modulus of the polymer solutions, expressed through storage and loss modulus. The storage modulus (G') is a measure of the elasticity of a material, depicting its ability to store energy, while the loss modulus (G") is a measure of the energy dissipated as heat when a material changes structure (Rošic et al., 2012a). Thus, the oscillatory measurements could help us evaluate if the polymer solutions remained solutions when altering the composition, or if they converted into gels. When the measured G" > G', the solution displays fluid-like behavior, but when the G' exceeds the G", it displays solid-like behavior which demonstrates the formation of a gel (Picout and Ross-Murphy, 2003).

Tan δ is defined as the ratio between loss- and storage modulus in a viscoelastic material, which can be calculated by dividing the G" by the G' (Picout and Ross-Murphy, 2003). Thus, tan δ indicates the relative degree of energy dissipation or damping of the material. The results from the oscillatory measurements were presented by plotting tan δ as a function of solution composition (**Figure 16**).

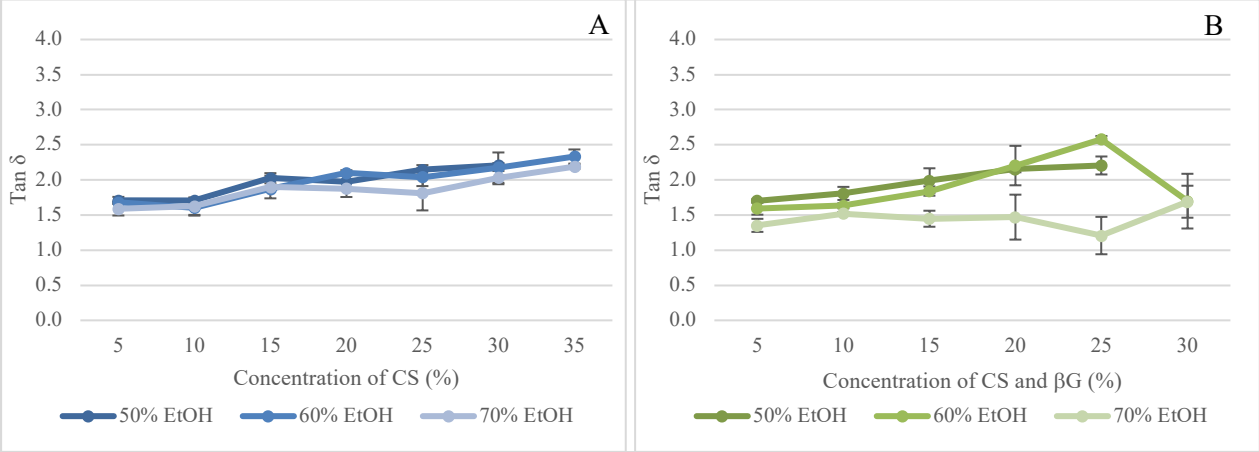

Figure 16: Tan δ as a function of solution composition of (A) CS solutions and (B) CS and βG solutions (n=2).

As depicted by **Figure 16**, all of the polymer solutions exhibited a tan δ > 1, which indicates that the loss modulus was continuously higher than the storage modulus in the viscoelastic area. This means that energy was dissipating and that the viscous component was the defining component of the material's viscoelastic characteristic (Tie et al., 2019). Conclusively, all of our polymer solutions exhibited fluid-like behavior independent of solution composition.

Hence, potential differences in fiber formation cannot be attributed the formation of gels with increasing concentrations of active ingredients.

4.3 Electrospinning

The Nanospider™ electrospinning technology was utilized for the spinning of the polymer solutions (Liberec, Czech Republic). This technology is based on the needleless electrospinning method for production of nanofibers directly from an open liquid surface (Yan et al., 2019). In the Nanospider™, this open surface is a conveyor wire where solution is deposited by a closed carriage. Advantages of this instrumentation is the establishment of a highly effective electrostatic field on the wire, in addition to the stabilization of solution viscosity. When electrospinning from an open surface, some hygroscopic solutions can readily absorb moisture from the environment, which could alter the viscosity of the solution (Yalcinkaya, 2019; Yan et al., 2019). Hence, the closed carriage system of the Nanospider™ prevents this effect. Moreover, fibers of small diameters and narrow standard deviations, have been reported to be easily formed on the thin wire (Yalcinkaya, 2019). Finally, the productivity rate is high, which makes the Nanospider™ technology promising for large scale production, as previously established by Grip et al. (Grip et al., 2018).

For the electrospinning of our solutions we wanted to optimize the electrospinning process by adjusting various parameters. We also wanted to examine the impact of gradually increasing the concentration of active ingredients on the spinnability of the solutions, to potentially determine a limit where solutions were not able to spin. This would give us an estimate of how large concentrations of active polymers it was possible to obtain in successfully produced fibers. Each polymer solution was prepared and electrospun two times.

4.3.1 Optimization of the electrospinning process

The distance to the collector is a process parameter capable of influencing morphology of electrospun nanofibers. However, as other electrospinning parameters, its influence varies depending on the polymer system (Haider et al., 2018). The optimal collector distance is dependent on the fluids evaporation rate, whipping interval and deposition time (Subbiah et al., 2005). Too short collector distance could prevent solidification of the jet before deposition on the collector, potentially resulting in fusion of nanofibers. Therefore, a minimal distance is

required to assure adequate time for the jet stream to dry before reaching the collector (Bhardwaj and Kundu, 2010; Robb and Lennox, 2011). Increasing the collector distance will increase the time for thinning of the jet to occur. However, with increasing collector distance, the electric field weakens, which can affect its ability to accelerate the polymer jet over the complete distance (Robb and Lennox, 2011).

To secure production of smooth and uniform fibers we attempted to optimize the electrospinning process by varying specific electrospinning settings of the Nanospider™. The electrospinning of the polymer solutions was performed according to the method previously described in section **3.2.3**, which included adjustment of the substrate (collector) distance and substrate speed. The electrospinning settings utilized for spinning each polymer solution in two separate rounds of spinning are presented in **Table 2**.

Table 2: Applied settings for the electrospinning of polymer solutions in the first and second round of spinning.

Name of solution	Round I		Round II	
	Substrate speed (mm/min)	Substrate distance (cm)	Substrate speed (mm/min)	Substrate distance (cm)
5%CS-50%EtOH	4	24	2	22
5%CS-60%EtOH	2	20	4	24
5%CS-70%EtOH	2	23	4	24
5%CS-5%βG-50%EtOH	2	20	2	22
5%CS-5%βG-60%EtOH	2	20	4	24
5%CS-5%βG-70%EtOH	2	21	2	23
10%CS-50%EtOH	2	23	2	23
10%CS-60%EtOH	3	24	4	24
10%CS-70%EtOH	2	20	2	24
10%CS-10%βG-50%EtOH	2	20	2	23
10%CS-10%βG-60%EtOH	4	24	4	24
10%CS-10%βG-70%EtOH	2	22	4	24
15%CS-50%EtOH	2	20	4	24
15%CS-60%EtOH	4	24	4	24
15%CS-70%EtOH	4	24	4	24
15%CS-15%βG-50%EtOH	2	22	2	23
15%CS-15%βG-60%EtOH	2	20	2	23
15%CS-15%βG-70%EtOH	4	24	4	24
20%CS-50%EtOH	2	20	4	24
20%CS-60%EtOH	2	23	2	24
20%CS-70%EtOH	2	24	4	24
20%CS-20%βG-50%EtOH	2	22	2	22
20%CS-20%βG-60%EtOH	2	22	4	24
20%CS-20%βG-70%EtOH	4	24	4	24
25%CS-60%EtOH	4	24	4	24
25%CS-70%EtOH	4	24	4	24
25%CS-25%βG-60%EtOH	4	24	4	24
25%CS-25%βG-70%EtOH	4	24	4	24
30%CS-60%EtOH	4	24	4	24
30%CS-70%EtOH	4	24	2	24
30%CS-30%βG-60%EtOH	4	24	4	24
30%CS-30%βG-70%EtOH	4	24	4	24
35%CS-60%EtOH	4	24	4	24
35%CS-70%EtOH	4	24	4	24

As presented in **Table 2**, the electrospinning settings varied between solutions of different compositions, but also between solutions of identical composition in the two rounds of spinning. Out of the 37 electrospun solutions, just 16 had the same settings in both rounds of spinning. These inconsistencies can be attributed to the difficulty in determining the optimal instrumentation for each polymer solution. The substrate distance and speed were selected through visual inspection and subjective evaluation of the spinnability of the solutions and their tendency to produce droplets on the substrate. Due to limited visibility of the spinning process this method of determination was perceived as challenging and might have resulted in discrepant evaluations. Hence, it was not possible to detect a trend in spinnability of the solutions by comparing process settings and solution composition.

Based on the experienced difficulties in achieving a consistent evaluation and determination of electrospinning settings, it can be considered favorable to utilize standard settings for solutions of similar composition to ensure a comparable result. Several reports from literature have concluded that the nanofiber diameter is reduced with increasing distance to the collector (Matabola and Moutloali, 2013; Wang and Kumar, 2006). However, there are also reports presenting results that indicates that an altered collector distance has no significant effect on fiber morphology (Zhang et al., 2005a). Hence, the potential impact of varying the electrospinning settings on the resultant fiber morphology will be discussed when evaluating the results from the nanofiber diameter analysis (section **4.4.2**).

4.3.1.1 Controlling ambient parameters

Temperature and humidity are ambient parameters that can influence the morphology of fibers produced by electrospinning (Robb and Lennox, 2011). An important part of the optimization of the electrospinning process, was therefore to control these parameters to secure production of nanofibers with consistent morphologies. The temperature and relative humidity were attempted controlled within the theoretical ranges of 24 ± 3°C and 23 ± 3%, respectively. The ambient parameters measured during the first and second round of electrospinning are presented in **Figure 17** and **Figure 18**.

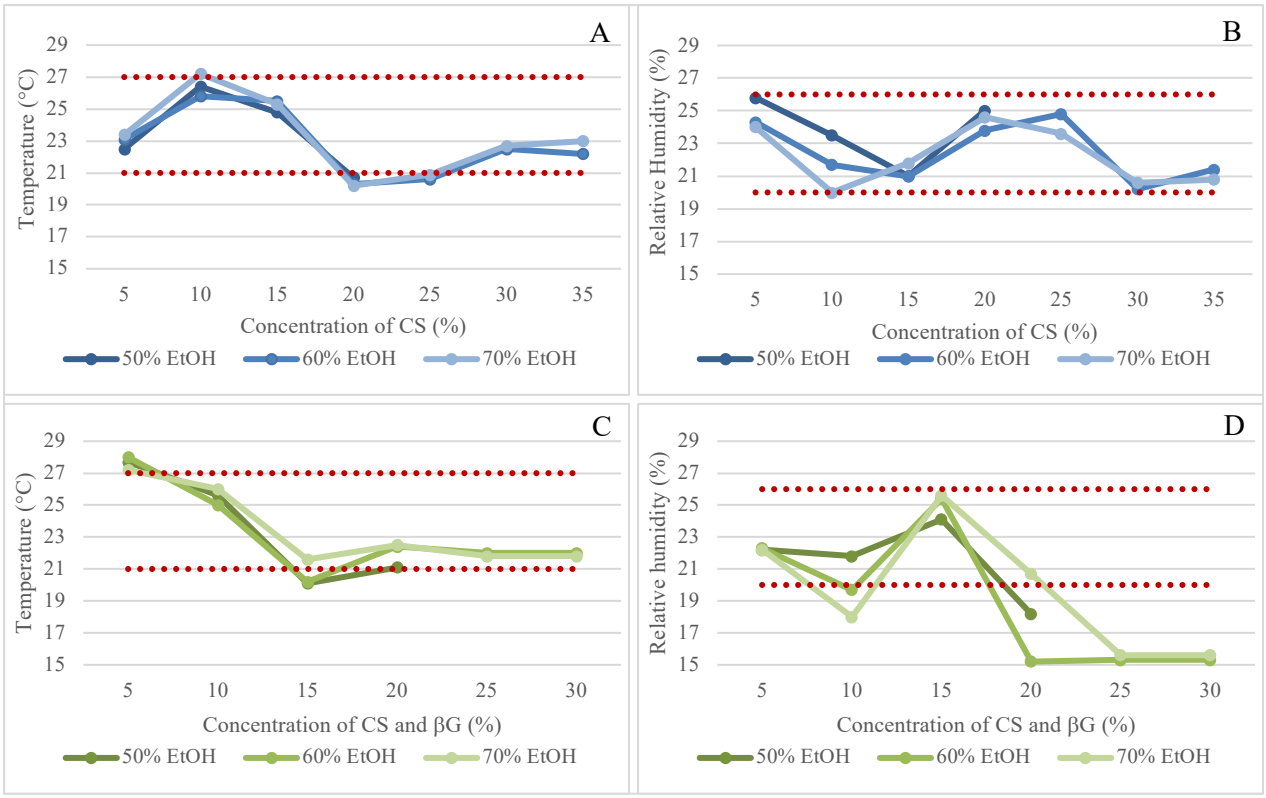

Figure 17: The ambient parameters measured during electrospinning of solutions in round I. Temperature of (A) CS and (C) CS and βG solutions, and relative humidity of (B) CS and (D) CS and βG solutions.

As illustrated in **Figure 17**, large fluctuations were observed in the measurements of ambient parameters during the first round of electrospinning. In addition, the measured temperature and humidity during spinning of some of the solutions were outside of the predetermined range. These fluctuations and deviating measurements have the ability to affect the morphology of the produced nanofibers, due to their influence on nanofiber diameter. According to literature, increasing temperature will result in production of fibers with reduced diameters due to the combined effect of an increase in evaporation rate of solvent and a decrease in solution viscosity (De Vrieze et al., 2009; Oğulata and İçoğlu, 2015; Shahabadi et al., 2015). Contrarily, the effect of the relative humidity on nanofiber diameter has proven to be largely dependent on polymer composition, which is substantiated by conflicting reports from literature. Pelipenko et al. examined changes in nanofiber diameter by varying the relative humidity under electrospinning of different polymer solutions. They found that fiber diameter was increased with decreasing relative humidity, which they attributed to a rapid solidification of the liquid jet and consequent reduced voltage-induced stretching. However, with increasing relative humidity, they observed the opposite effect with production of smaller diameter fibers (Pelipenko et al., 2013).

Contrarily, Oğulata and İçoğlu found that nanofiber diameter increased with increasing relative humidity when electrospinning polyetherimide, which they explained by the polymers rapid precipitation caused by more available water in the surrounding air (Oğulata and İçoğlu, 2015).

The observed fluctuations in the ambient parameter measurements were determined to be a result of an insufficient ability to control the parameters before and during spinning. This challenge was attempted solved for the second round of spinning by altering the location of the electrospinning instrument, to where the environmental aspects affecting spinning could be more readily controlled.

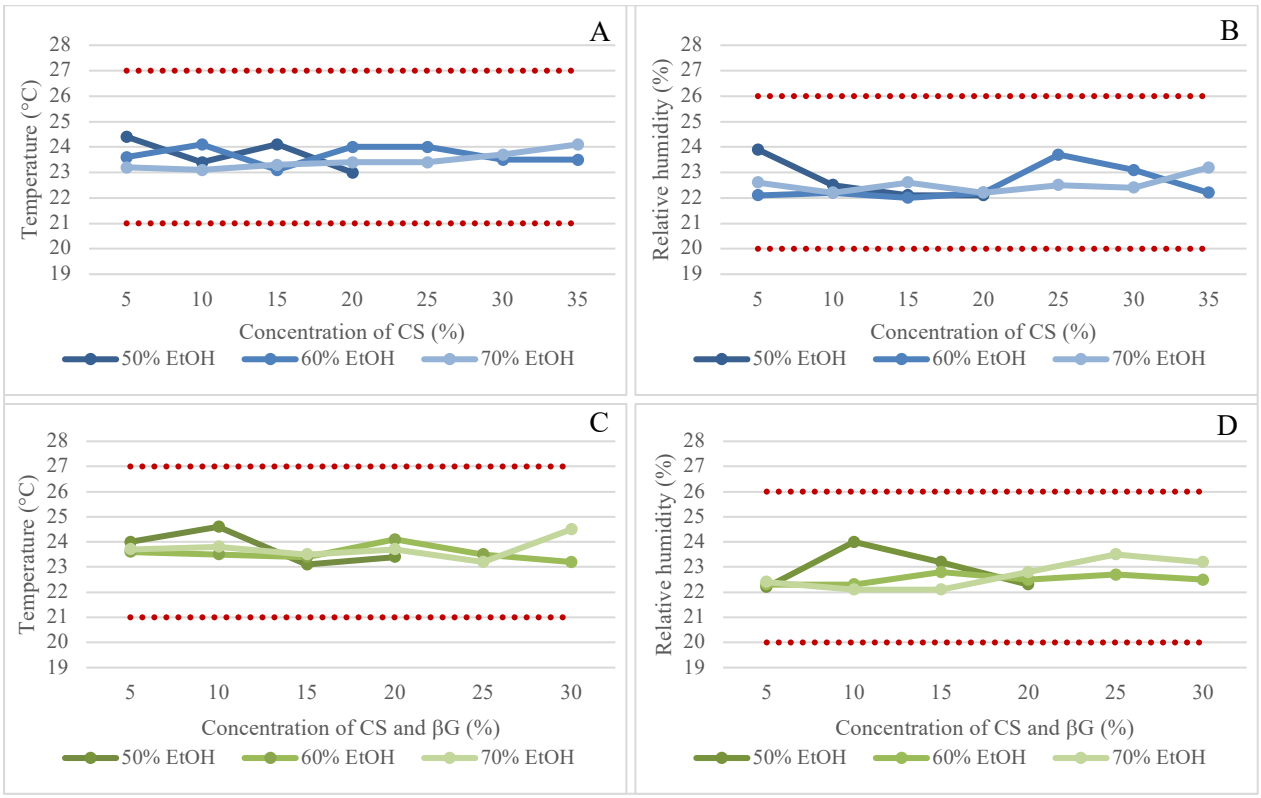

Figure 18: The ambient parameters measured during electrospinning of solutions in round II. Temperature of (A) CS and (C) CS and βG solutions, and relative humidity of (B) CS and (D) CS and βG solutions.

As presented in **Figure 18**, the ambient parameters were successfully controlled for the second round of spinning, which indicates that the relocation of the Nanospider™ was effective.

Due to poor control over the ambient parameters during the first round of spinning, their potential effect on morphology of the produced nanofibers will be further assessed when

evaluating the results from the nanofiber diameter analysis (section **4.4.2**). Preferably, a third replicate of the preparation and spinning of the solutions, with adequately controlled ambient parameters, would have been beneficial.

4.3.2 Spinnability of solutions

The design of the polymer solutions and the flexibility of the electrospinning process enabled the successful spinning of a majority of the solutions. Out of the 37 prepared solutions a total of 34 solutions were spinnable, as presented in **Table 3**. By gradually increasing the concentration of active ingredient(s), an upper limit of spinnability was identified for the solutions prepared with 50% (w/w) ethanol. When reaching a CS and βG concentration of 25% (w/w), both the solution containing just CS and the solution containing both active polymers could not produce continuous fibers and was deemed non-spinnable (**Table 3**). These observations were confirmed in the second round of spinning. Interestingly, the solutions prepared with equal concentrations of active ingredients but higher concentrations of ethanol, were spinnable and producing fibers. This indicated that the solvent composition was a determining factor.

Table 3: Overview of spinnable and non-spinnable solutions. Spinnable solutions are marked green, while non-spinnable solutions are marked red. Solutions that were not prepared or spun are marked grey.

Concentration of CS (%)	**5**	**10**	**15**	**20**	**25**	**30**	**35**	**Concentration of CS and βG (%)**	**5**	**10**	**15**	**20**	**25**	**30**
50% EtOH								***50% EtOH***						
60% EtOH								***60% EtOH***						
70% EtOH								***70% EtOH***						

This observation can be explained by the polymer solutions conductivity. As previously presented in **Figure 14**, the conductivity of the polymer solutions was gradually increasing with increasing CS concentration and decreasing ethanol concentration. The inability to spin some of the solutions prepared with higher CS concentrations and lower ethanol concentrations, can therefore be attributed to their high conductivities preventing them from forming Taylor cones. This reasoning is based on the findings of Angammana and Jayaram, who examined the effect of solution conductivity on the electrospinning process by varying the conductivity of solutions containing PEO and water. They found that polymer solutions that exhibited very high

conductivities would not promote the formation of a Taylor cone, due to a depleted tangential electric field along the surface of the fluid (Angammana and Jayaram, 2011).

This observed correlation can be substantiated by the proven spinnability of solutions containing equally high or higher CS concentrations prepared with increased concentrations of ethanol. The increased ethanol content and subsequently decreased water content in these solutions, caused a decrease in the conductivity, which enabled the formation of Taylor cones and production of fibers by electrospinning. It is also important to note, that solutions produced with higher ethanol concentrations also exhibited a slightly reduced surface tension (**Figure 13**), which could have contributed to improved spinnability by lowering the force resisting the formation of Taylor cones and the formation of fluid jets.

For polymer solutions containing both active polymers, the upper limit of preparation was reached at CS and βG concentrations of 30% (w/w). The design of the solutions would not allow for polymer concentrations exceeding this, due to the water content of SBG®. The SBG® utilized in this project is prepared as a 2.5% (w/v) hydrogel in water (Biotec BetaGlucans AS, Tromsø, Norway). Thus, some of the water used as solvent in the polymer solutions originated from SBG®, and this amount increased with increasing concentrations of βG in the solutions. When attempting to prepare a solution containing 35% (w/w) CS and βG, the water content introduced by the SBG® was higher than intended for solutions of higher ethanol content. Hence, the preparation of solutions containing higher concentrations of βG was not obtainable with the current design of the solutions.

For the polymer solutions just containing CS, the highest achieved concentration was 35% (w/w). Theoretically, solutions of higher CS content could have been prepared and potentially successfully spun.

4.4 Characterization of nanofibers

Tensile properties, morphologies, diameters and absorption capacities were examined for all of the produced nanofibrous scaffolds, to assess the success of the formulations.

4.4.1 Tensile properties

An adequate mechanical strength of nanofibrous scaffolds is important to facilitate easy application and handling. Moreover, sufficient durability of nanofibrous scaffolds is integral to provide lasting support for wound healing, by withstanding mechanical forces while maintaining flexibility (MacEwan et al., 2017). As previously established, nanofibers can stimulate wound healing by mimicking the ECM and facilitating cellular responses (Beachley and Wen, 2010). The mechanical properties of the fibrous scaffolds are important in this regard, because the fibers should degrade as the new ECM starts regenerating. Very high tensile strength could result in the fibers remaining in the wound bed after regeneration, possibly obstructing tissue development, while fibers of weak tensile strength might not support regenerative processes for the required time (Chandrasekaran et al., 2011).

The tensile properties of the nanofibers were analyzed through the establishment of stress–strain curves, enabling calculation of the nanofibrous scaffolds tensile strength, elastic modulus and percentage elongation at break. The results from the mechanical characterization are presented in **Figure 19**, **Figure 20** and **Figure 21**.

The tensile strength describes the amount of tensile stress a material can sustain before experiencing permanent deformation, and can be utilized to quantify the intermolecular fiber connectivity of the nanofibrous scaffold (Yuan et al., 2016). The average tensile strength of fibers produced in two rounds of electrospinning, was plotted as a function of solution composition and presented in **Figure 19**.

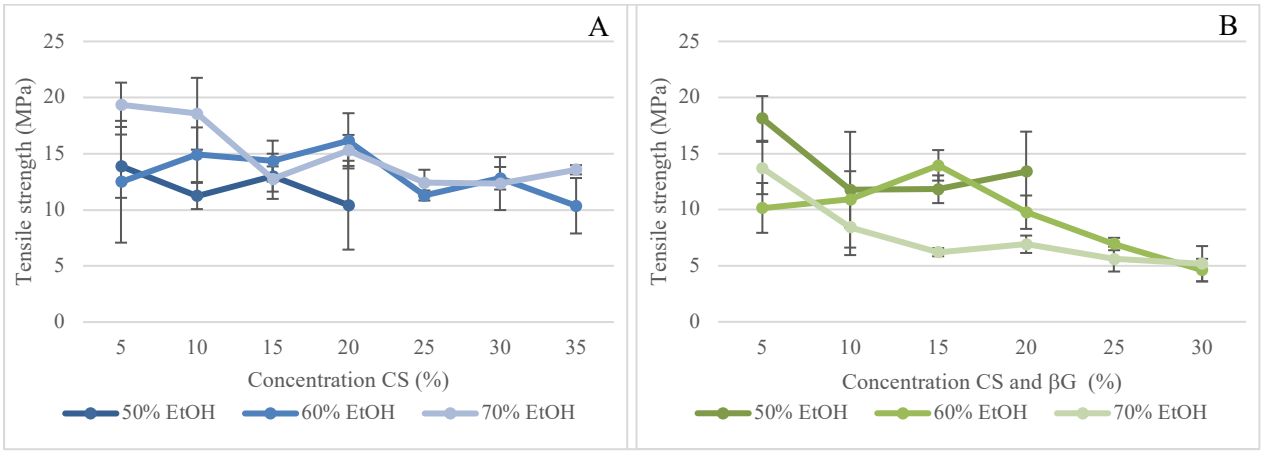

Figure 19: Tensile strength of (A) CS and (B) CS and βG nanofibers as a function of solution composition (n=2). Exact values are listed in the Appendix; **Table A4**.

Fluctuations can be observed in measured tensile strength of fibers containing CS as active ingredient, which makes it challenging to evaluate the effect of increasing CS concentration. Naturally, CS is relatively rigid and brittle, which causes it to have limited mechanical strength (Wahba, 2020). This is confirmed by reports from literature with Gu et al. presenting a tensile strength of 2.4 MPa for CS fibers, and Yuan et al. a tensile strength of 2.8 MPa for CS and PEO nanofibers (Gu et al., 2013; Yuan et al., 2016). In comparison, the values obtained for the tensile strength of CS fibers in this study are higher. This increased mechanical strength can potentially be attributed to the presence of HPMC in the nanofibers. Only a limited number of publications can be found on electrospinning of HPMC and none of these publications have evaluated the tensile properties of the produced nanofibers (Aydogdu et al., 2018; Frenot et al., 2007; Grip et al., 2018; Verreck et al., 2003). However, HPMC is a cellulose derivate widely applied in the production of films, and several reports from literature present high tensile strengths for such formulations (Ghadermazi et al., 2019; Pooponpun et al., 2015; Saringat et al., 2005). This indicates that HPMC has the ability to confer structural support to the nanofibers, which is consistent with general attributes of cellulose. Due to the reinforcing presence of cellulose microfibrils in natural fibers, they display increased tensile strength with elevated cellulose content (Djafari Petroudy, 2017; Komuraiah et al., 2014).

Theoretically, a decrease in tensile strength should be observed with increasing concentrations of CS, and such observations are also supported in literature (Chen et al., 2008; Chen et al., 2010). However, no clear decrease can be detected. Contrastingly, a decrease in tensile strength can be observed for fibers containing both CS and βG with gradually increasing concentrations. This observation can complement the assumed structural importance of HPMC, due to the reduction in HPMC concentration for CS and βG fibers being twice as high as the reduction in the CS fibers, for each increase in concentration of active ingredients (**Figure 10**). Due to the more prominent decrease of HPMC concentrations for fibers consisting of both active ingredients, the graph is thus more clearly decreasing. This also indicates that the addition of βG does not improve the mechanical strength of the fibers.

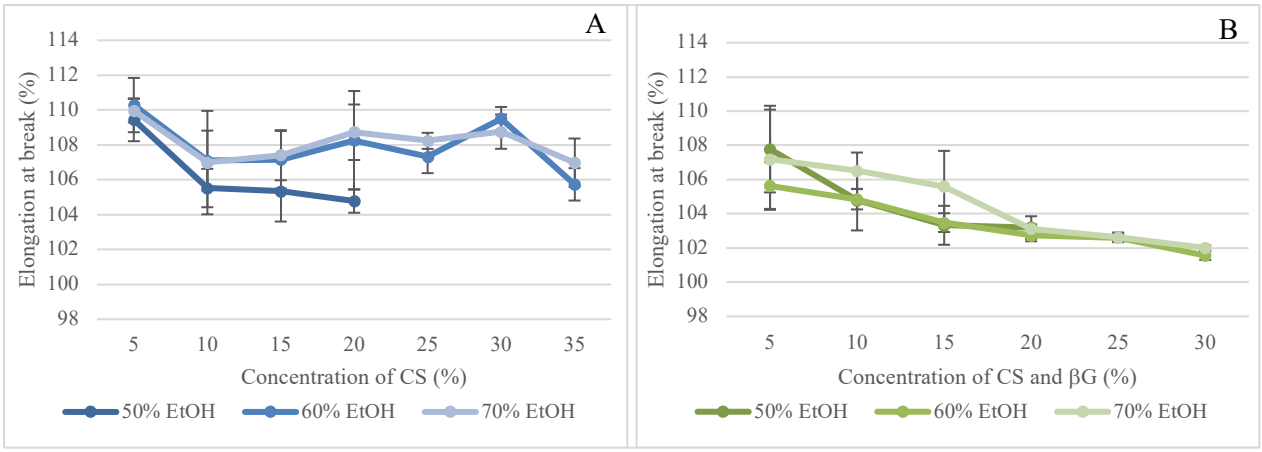

Figure 20: Elongation at break of (A) CS and (B) CS and βG nanofibers as a function of solution composition (n=2). Exact values are listed in the Appendix; **Table A4**.

A similar trend can be observed in **Figure 20**, presenting the average elongation at break as a function of solution composition. Elongation at break is the ratio between changed length and initial length after breakage of the test specimen. It expresses the capability of the fibers to resist changes in shape without breaking (Djafari Petroudy, 2017). The observed decrease in elongation at break for fibers containing both active ingredients, can substantiate the importance of HPMC in the nanofibrous structure.

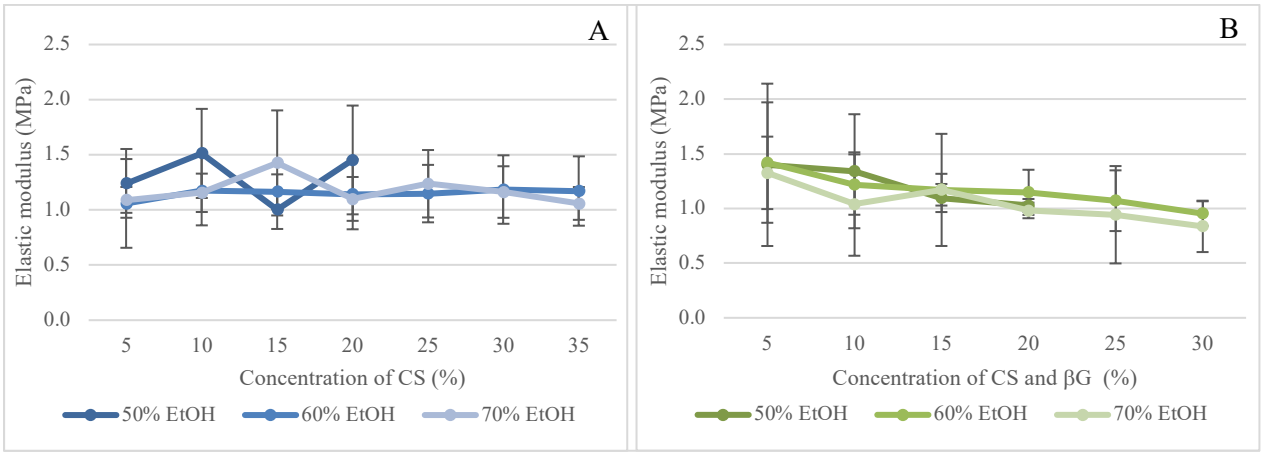

Figure 21: Elastic modulus of (A) CS and (B) CS and βG nanofibers as a function of solution composition (n=2). Exact values are listed in the Appendix; **Table A4**.

Elastic modulus measures the flexibility of a material and can be used to evaluate its resistance to elastic deformation (Yuan et al., 2016). As presented in **Figure 21**, a slight decrease in elastic

modulus can be observed with increasing concentrations of active ingredients for CS and βG fibers, while the elastic modulus of the CS fibers was relatively stable. However, the reduction in elastic modulus for CS and βG fibers was not very pronounced, which could suggest that the decrease in HPMC did not affect the flexibility of the fibers to such a large extent. Due to the consistently high standard deviations of these measurements, several parallels would be favorable to enable a more conclusive interpretation.

The association between concentration of active ingredient(s) and tensile properties of nanofibrous scaffolds was examined statistically by calculating the Pearson correlation coefficient. The calculated correlation coefficient for CS fibers was relatively low for all of the tensile properties, indicating a weak to negligible negative association (**Table 4**). Contrastingly, a moderate to strong negative association was detected for nanofibers containing both active ingredients for both the tensile strength, elongation at break and elastic modulus (Schober et al., 2018) (**Table 4**). This indicates that the observed association between decreasing tensile properties of nanofibers with increasing concentrations of CS and βG, can be confirmed statistically.

Table 4: Calculated Pearson correlation coefficients depicting the strength of the association between tensile properties and concentration of active ingredient(s) in CS and CS and βG nanofibers.

CS nanofibers	Correlation coefficient	CS and βG nanofibers	Correlation coefficient
Tensile strength	-0.33	***Tensile strength***	-0.64
Elongation at break	-0.17	***Elongation at break***	-0.77
Elastic modulus	-0.06	***Elastic modulus***	-0.51

Generally, the mechanical properties of the nanofibrous scaffolds were experienced as sufficient to facilitate uncomplicated handling. However, an increased brittleness could be observed for CS and βG fibers with increasing concentrations, which is disfavored with regards to easy application and handling and could therefore limit their utilization as wound dressings.

Based on reports from literature, the measured mechanical strength of the produced fibers is sufficient to support tissue regenerative processes *in vitro* and/or *in vivo* (Li et al., 2019; Waghmare et al., 2018). However, it is not assessed to what degree the nanofibrous scaffolds are able to sustain their mechanical integrity in the wound fluid, which will be further discussed when evaluating the fibers absorption capacity (section **4.4.3**).

4.4.2 Diameter and morphology

The morphology and dimensions of nanofibers are essential in eliciting tissue growth through interactions with cellular components in the wound bed (Beachley and Wen, 2010). However, more research is required to establish how to optimally exploit these interactions to enable more effective tissue regeneration.

The morphology and microstructure of the generated nanofibers were analyzed with FE-SEM (Carl Zeiss, Oberkochen, Germany). The obtained micrographs confirmed nanofiber formation for all of the spinnable polymer solutions and revealed randomly aligned fibers displaying smooth and uniform fiber surfaces. The diameters of the produced nanofibers were analyzed using ImageJ (NIH, MD, USA) and the results showed a relatively narrow diameter distribution, as depicted by **Figure 22**.

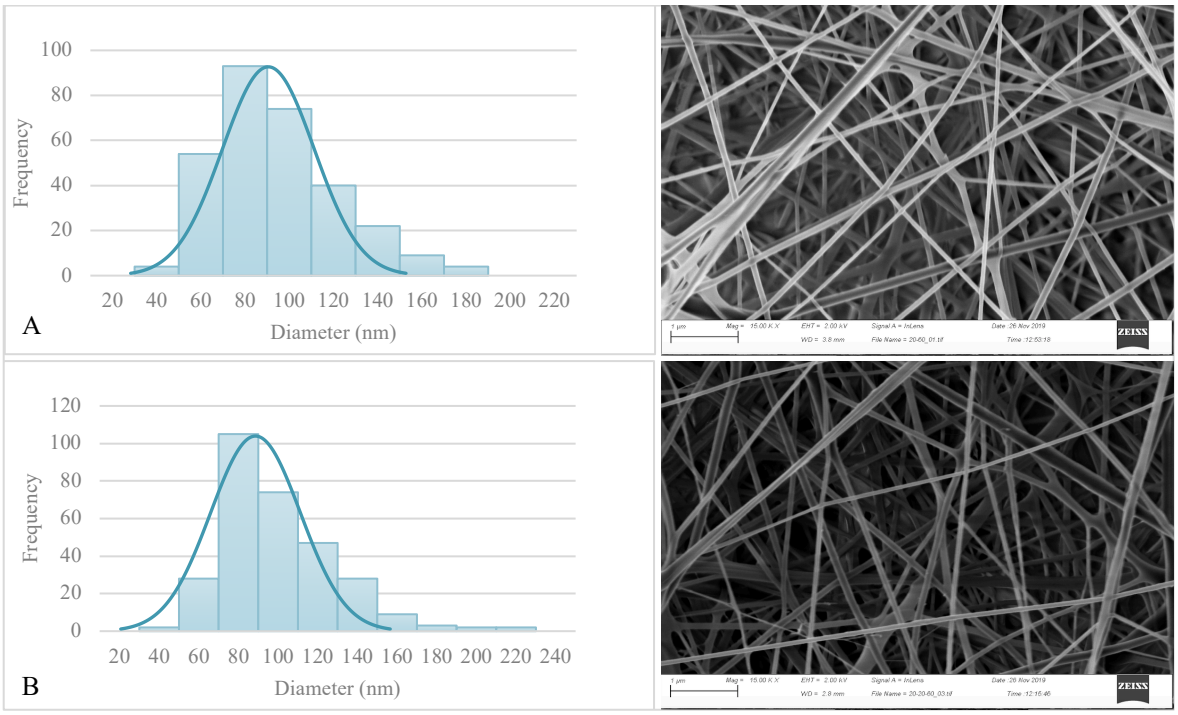

Figure 22: Representative diameter distribution histograms and FE-SEM micrographs of electrospun scaffolds. (A) 20% CS – 60% EtOH, (B) 20% CS – 20% βG – 60 % EtOH.

The average diameter of fibers produced in two rounds of electrospinning was calculated and plotted as a function of solution composition, as presented in **Figure 23**. The average fiber diameter ranges from 73.1 ± 0.9 to 103.4 ± 7.1 nm for the fiber scaffolds produced with CS, and from 67.7 ± 3.3 to 112.3 ± 38.4 nm for scaffolds produced with CS and βG. Considering

the narrow diameter distributions and small standard deviations, it suffices to state that uniform nanofibers were obtained by electrospinning. The results also indicate that addition of βG to the fiber composition does not affect the fiber diameter notably, which correlates with the rheological results presenting relatively similar viscosities of solutions containing CS and solutions containing both active ingredients.

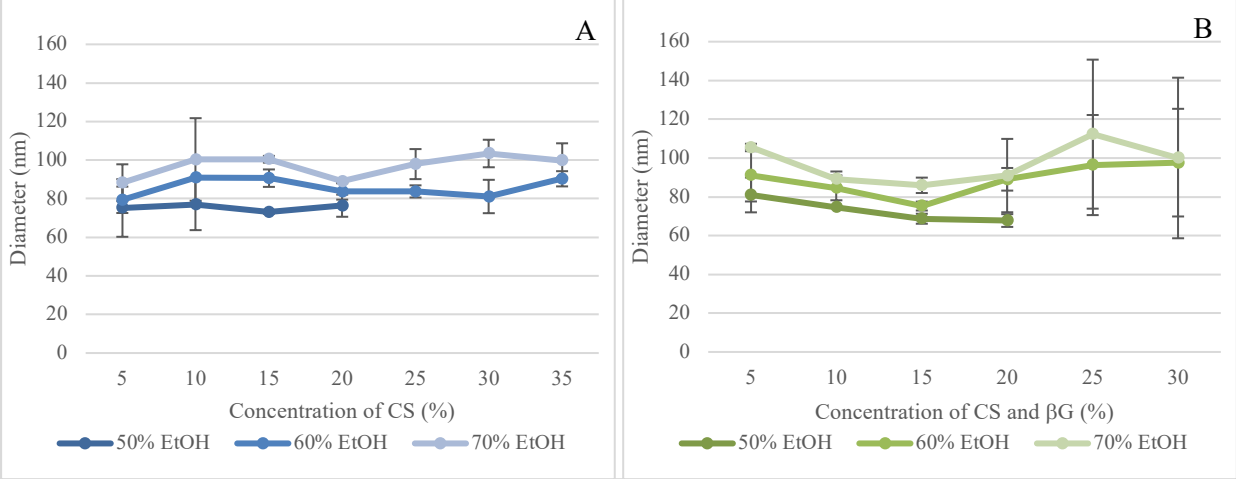

Figure 23: Average diameter of (A) CS and (B) CS and βG nanofibers, plotted as a function of solution composition (n=2). Exact values are listed in the Appendix; **Table A7**.

As previously established (section **4.3.1.1**), ambient parameters are important determinants of nanofiber diameter. An increase in average fiber diameter can be observed for CS and βG fibers of higher concentrations, specifically for the fibers containing 25% and 30% (w/w) active ingredients. This increase could potentially be attributed the very low relative humilities measured during production of these fibers in the first round of electrospinning (**Figure 17**). This reasoning can be substantiated by the high standard deviations depicted for the fibers under consideration, indicating that the diameters measured for the same fibers in the two rounds of spinning were different.

Table 5: Nanofiber diameter of CS and βG fibers containing 25% and 30% (w/w) active ingredients, produced in round I and round II of electrospinning.

CS and βG fibers	Diameter round I (nm)	Diameter round II (nm)
25%CS-25%βG-60% EtOH	114.6	78.1
25%CS-25%βG-70% EtOH	139.5	85.2
30%CS-30%βG-60% EtOH	117.3	78.0
30%CS-30%βG-70% EtOH	129.3	70.8

As presented in **Table 5**, fibers of larger diameters were produced in the first round of spinning, compared to the second round. The average diameter for these fibers would thus most likely be reduced with better controlled ambient parameters in the first round of spinning. The observation of increased fiber diameter with decreased relative humidity is in accordance with previously published results (Pelipenko et al., 2013).

As previously introduced in section **4.3.1**, the distance to the collector could also potentially have an effect on the nanofiber diameter. Because this selected distance varied under electrospinning of solutions of different composition and solutions of identical composition, it is important to evaluate its potential influence on the diameter of the produced fibers. As presented in **Figure 23**, the most prominent difference in fiber diameter was found for the nanofibers produced with a concentration of 25% and 30% (w/w) CS and βG, as previously established. When examining the distance to the collector utilized under the spinning of these fibers, it was found that the same distance had been used under both rounds of spinning. The observed increase in average fiber diameter for these fibers is thus more likely to be attributed to the influence of the relative humidity. As the measured diameters for the rest of the fibers were relatively stable, the differences in distance from the wire to the collector under electrospinning, does not seem to have affected the fiber diameter notably.

It is not possible to observe a distinct correlation between average nanofiber diameter and concentration of active ingredient(s), which could be due to the total polymer concentration being constant in all of the solutions, generating a relatively consistent viscosity. However, a correlation between solvent composition and fiber diameter is observed. As illustrated in **Figure 23**, polymer solutions containing higher concentrations of ethanol are inclined to produce fibers of larger diameters. This association can be explained by the high volatility of ethanol compared to water. Increased volatility of solvent results in a fast evaporation and consequently rapid solidification of fibers during electrospinning. Due to rapid solidification, the polymer solution is subjected to voltage-induced stretching for a restricted time, resulting in formation of fibers of larger diameters (Golecki et al., 2014; Wannatong et al., 2004; Yang et al., 2004).

However, conductivity of polymer solutions is also an essential determinant of fiber diameter. As previously established, electrospinning is initiated by the formation of Taylor cones caused by generation of electrostatic interactions between repulsive surface charges of the liquid and an external electric field. When the applied electric field is sufficiently high for the electrostatic

force to overcome the surface tension, a charged jet of fluid emanates from the tip of the cone. Repulsive charges at the surface of this jet causes the solution to stretch, which draws the fluid jet into nanoscale (Haider et al., 2018). A more conductive solution will generate a higher charge density on the surface of the jet, which allows for infliction of stronger elongation forces under the electric field, favoring a reduction in fiber diameter. Zong et al. examined this effect by utilizing three different salts to modify the conductivity of the spinning solution. Their results indicated that fiber diameter decreased with addition of salts and that different salts exhibited different effects based on their ability to generate conductivity (Zong et al., 2002). Decreased fiber diameter facilitated by increased electrical conductivity is in conformity with other reports from literature (Angammana and Jayaram, 2011; Zhang et al., 2005a). The previously presented trend in conductivity (**Figure 14**), displaying higher conductivities of solutions containing lower concentrations of ethanol, is thus consistent with the observed trend in diameter (**Figure 23**).

The association between concentration of ethanol and nanofiber diameter was examined statistically by calculation of the Pearson correlation coefficient. The correlation coefficient was 0.72 for the CS fibers, indicating a strong positive association, and 0.52 for the fibers containing both active ingredients, indicating a moderate positive association (Schober et al., 2018). The statistical analysis is thus consistent with the observations of increasing fiber diameter with increasing concentrations of ethanol. To evaluate if ethanol's influence on solution conductivity could be the source of this effect, the association between conductivity and fiber diameter was examined. The calculated correlation coefficient was 0.12 for both solutions containing CS and solutions containing CS and βG, which indicates a weak positive correlation. The observed effect of ethanol on nanofiber diameter in this project, is thus less likely to be facilitated by the influence of conductivity and more likely to be attributed the volatility of the solvent.

4.4.4 Absorption capacity

The importance of maintaining a moist wound environment to improve wound healing is well established (Lionelli and Lawrence, 2003). However, the presence of excessive amounts of exudate in the wound bed can cause maceration and increase the risk of infection, potentially resulting in impaired wound healing. Effective wound dressings must thus be able to absorb sufficient amounts of wound exudate, while still maintaining a level of tissue hydration that is consistent with a moist wound environment (Ousey et al., 2016).

The nanofibers efficacy in absorbing wound fluid was evaluated by measuring their absorption capacity. The nanofibers absorption capacity as a function of fiber composition, is presented in **Figure 24**.

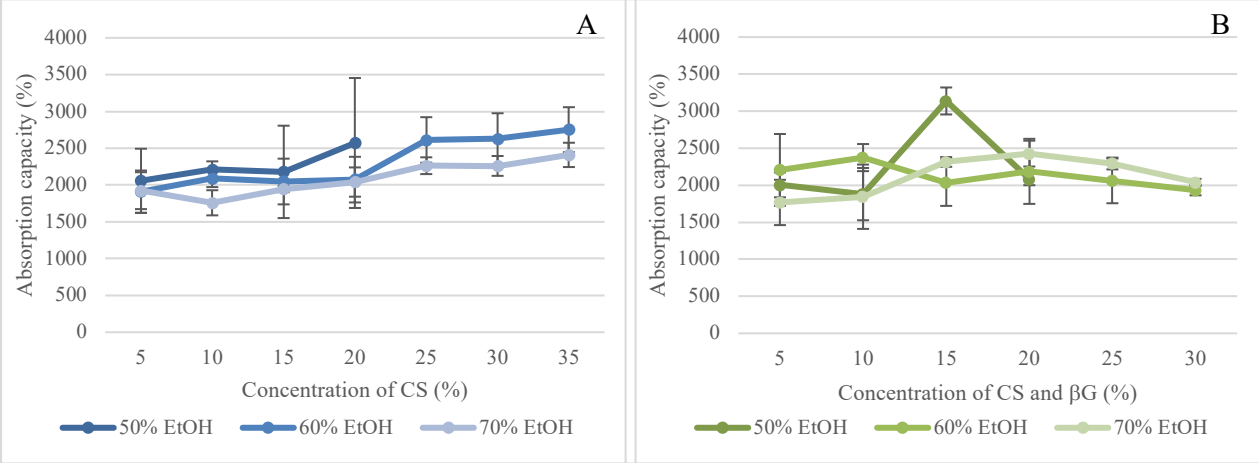

Figure 24: Absorption capacity of (A) CS and (B) CS and βG fibers as a function of fiber composition (n=2). Exact values are listed in the Appendix; **Table A8**.

The average absorption capacity was 2207.5 ± 283.3% for the CS fibers and 2161.5 ± 323.5% (w/w) for the fibers composed of both active ingredients. Compared to reports from literature, the obtained absorption capacity was quite high. The highest located absorption capacity for CS based nanofibers was presented by Archana et al. who produced fibers containing CS and pectin that exhibited a maximum absorption of 1215% (Archana et al., 2013). Other studies have shown lower absorption capacities for CS fibers ranging from 350% to 1000% depending on the fiber composition (Çay et al., 2014; Li et al., 2011; Sencadas et al., 2012). Grip et al. presented an average absorption of 1287% for βG nanofibers consisting of the same copolymers as the fibers produced in this study. Important to note, is that differences

in fiber composition as well as differences in execution of the absorption experiments hinders results from other studies from being directly comparable to the results obtained in this project. For example, choice of absorption time, simulated wound fluid, and method of removal of excess fluid from the fiber sample, are discrepancies observed in different studies that could have an impact on measured absorption capacity. Specifically observed, is that several of the mentioned studies have utilized filter paper to absorb excess fluid from the sample before weighing. However, in this study, excess fluid was removed by deliberate transference of the fiber sample from one weighing dish to another. The higher absorption capacities in this study could thus potentially be partially attributed to reduced removal of fluid from the sample before weighing.

Apart from the potential influence of the execution method, the large absorption capacity of the produced nanofibers is likely caused by the hydrophilic nature of the polymers composing the fibers, as the degree of swelling is dependent on the affinity between the polymers and the external solution (Sencadas et al., 2012). Both HPMC and PEO are hydrophilic polymers that exhibit good swelling abilities and fast hydration characteristics, which enables them to bind large amounts of water (Asghar et al., 2012; Joshi, 2011; Wang et al., 2017). In addition, CS appears to be able to increase the fluid absorption, as the absorption capacity of the CS fibers gradually increases with increasing concentrations of CS (**Figure 24**). CS can contribute to the high absorption capacity due to the hydrophilic property of CS in acidic to neutral medium. In this environment the CS molecules acquire positive charges along their backbone caused by protonation of their amino groups, which causes a relaxation of the polymer chains. This relaxation enables greater interactions with surrounding water molecules, resulting in an increased absorption (Kumirska et al., 2011). Similar results have been reported by Zarghami et al. who evaluated the liquid adsorption of nanofibers of different compositions and found that the swelling was enhanced with increased hydrophilic properties (Zarghami et al., 2015).

Compared to the CS fibers, the fiber samples containing both CS and βG had an equally high average absorption capacity. This could suggest that βG was able to replace the absorptive properties of HPMC to a certain extent. However, no increase in absorption capacity can be detected as a result of increasing concentrations of active ingredients for these fibers, as observed for the CS fibers (**Figure 24**). Another important observation in **Figure 24**, is an increased absorption capacity for the CS and βG fibers with a concentration of 15% (w/w)

active ingredients and a concentration of 50% (w/w) ethanol. This raised absorption capacity cannot be explained by previously measured properties of the fibers. In addition, the measured absorption capacity seems to be relatively similar for the fibers produced in both rounds of electrospinning, due to the low standard deviation. It could therefore be interesting to repeat the production and characterization of these fibers with regards to the absorption capacity, to assess if the same effect can be observed in a third replicate.

By calculation of the Pearson correlation coefficient, the association between concentration of active ingredient(s) and absorption capacity of nanofibrous scaffolds was examined statistically. The calculated correlation coefficient for CS fibers was 0.51, which indicated a moderate positive association between the variables. The observed association between increasing CS concentration and subsequently increasing absorption capacity, can thus be substantiated. Contrastingly, the calculated correlation coefficient for fibers containing both active ingredients was 0.07. A correlation coefficient so close to zero indicates that no distinct association was detected, which is consistent with the observations made from **Figure 24** (Schober et al., 2018).

Upon exposure to the simulated wound fluid the nanofibrous specimens quickly hydrated and swelled but remained intact. It was anticipated that the fibers would partially dissolve and create a structured gel when exposed to the fluid for a longer duration, which was confirmed. This presumption was grounded on the fiber composition being highly similar to the composition of the βG nanofibers produced by Grip et al., who observed this effect (Grip et al., 2018). It is not certain to what degree the nanofibers are able to sustain their nanofibrous structure and mechanical integrity in the gel for longer time intervals. Some studies have examined this phenomenon by drying the fiber specimens after swelling in the wound liquid and analyzing them using FE-SEM (Çay et al., 2014; Mengistu Lemma et al., 2016). This approach could be useful in evaluating the produced nanofibers ability to exert an additional wound healing effect, by facilitating cellular responses through their fibrous structure, provided that they are able to maintain their structure to a certain extent. Regardless, the formation of a gel contributes to efficient absorption of wound liquid and establishes an occluded and moist wound environment which is beneficial for wound healing.

5 Conclusions

In the present study, composite nanofibers with increasing concentrations of chitosan (CS) and β-glucan (βG) were successfully produced by electrospinning. The highest achieved concentration of active ingredients in successfully spun fibers was 35% (w/w) for the CS fibers and 30% (w/w) for each of the active polymers in the CS and βG fibers. The results revealed that optimization of electrospinning conditions was crucial to obtain uniform nanofibers, as relative humidity was found to affect the nanofiber morphology notably. Specifically, an increase in nanofiber diameter was observed with a decrease in relative humidity during electrospinning. Contrastingly, the applied settings of the Nanospider^{TM}, which included variation of substrate speed and distance from the wire to the substrate, was not found to influence nanofiber morphology.

Adjustment of polymer- and solvent composition was determined to influence both the conductivity, surface tension and viscosity of the solutions. However, the conductivity was determined to be the primary factor influencing the spinnability of the polymer solutions, as solutions of too high conductivity could not be successfully spun. Based on this, an upper limit of spinnability was detected for solutions of 25% (w/w) active ingredient(s) and 50% (w/w) ethanol. Moreover, polymer solutions containing higher amounts of ethanol were found to produce nanofibers with increased diameters, which was attributed to an increased solvent volatility. The tensile tests indicated that the mechanical strength of the nanofibrous scaffolds containing CS and βG was limited, due to a gradual reduction in tensile strength, elongation at break and elastic modulus with increasing concentrations of active ingredients. The limited durability of the nanofibers is disfavored in wound healing, as it can present challenges with regards to application and handling. Lastly, the absorption capacity of the nanofibers was found to be high, which was attributed to the hydrophilic nature of the polymers constituting the nanofibrous scaffold. The high absorption capacity suggests that the nanofibrous scaffolds would be suitable for treatment of wounds with moderate to high exudate production.

Conclusively, the results from the present study were promising and can serve as a strong base for further development of the nanofibers.

6 Perspectives

Firstly, continuance of the optimization of the electrospinning process should be emphasized in further research to secure production of beadles, continuous nanofibers.

A further research objective should also include the structure elucidation of nanofibers *in situ*. By evaluating the fibers ability to sustain their fibrous structure in contact with wound fluid, more information on their potential structural wound healing effect could be obtained. If the fibers were proven to fully disintegrate relatively rapidly, techniques to increase the mechanical strength of the fibers could be considered.

Furthermore, both the antimicrobial and wound healing effects of the fibers should be examined *in vitro*, using suitable bacterial- and cell cultures. Conducting these experiments would contribute to quantifying the effect of gradually increasing the concentrations of active ingredients in the nanofibers. Moreover, the structural importance of the nanofibers could be further assessed through the *in vitro* tests, by for example comparing the wound healing effect of fibers with elevated mechanical strength to the original fibers.

If exhibiting promising effects in the *in vitro* studies, the next appropriate step would be examining the nanofibers effect *in vivo*, by for example utilizing a suitable animal model capable of simulating the chronic wound environment.

7 References

Abrigo, M., McArthur, S.L., Kingshott, P., 2014. Electrospun nanofibers as dressings for chronic wound care: Advances, challenges, and future prospects. Macromol. Biosci. 14, 772-792.

Agarwal, S., Wendorff, J.H., Greiner, A., 2008. Use of electrospinning technique for biomedical applications. Polym. J. 49, 5603-5621.

Agnihotri, S.A., Mallikarjuna, N.N., Aminabhavi, T.M., 2004. Recent advances on chitosan-based micro- and nanoparticles in drug delivery. J. Control. Release. 100, 5-28.

Ahmed, S., Ikram, S., 2016. Chitosan based scaffolds and their applications in wound healing. Achiev. Life Sci. 10, 27-37.

Alberti, T., Coelho, D.S., Voytena, A., Pitz, H., de Pra, M., Mazzarino, L., Kuhnen, S., Ribeiro-do-Valle, R.M., Maraschin, M., Veleirinho, B., 2017. Nanotechnology: A promising tool towards wound healing. Curr. Pharm. Des. 23, 3515-3528.

Alghoraibi, I., Alomari, S., 2018. Different methods for nanofiber design and fabrication, in: Barhoum, A., Bechelany, M., Makhlouf, A. (Eds.), Handbook of Nanofibers, 1st ed. Springer International Publishing, Cham, pp. 1-46.

Andreu, V., Mendoza, G., Arruebo, M., Irusta, S., 2015. Smart dressings based on nanostructured fibers containing natural origin antimicrobial, anti-inflammatory, and regenerative compounds. Materials. 8, 5154-5193.

Angammana, C., Jayaram, S., 2011. Analysis of the effects of solution conductivity on electrospinning process and fiber morphology. IEEE Trans. Ind. Appl. 47, 1109-1117.

Archana, D., Dutta, J., Dutta, P.K., 2013. Evaluation of chitosan nano dressing for wound healing: Characterization, in vitro and in vivo studies. Int. J. Biol. Macromol. 57, 193-203.

Asghar, A., Samad, Y.A., Hashaikeh, R., 2012. Cellulose/PEO blends with enhanced water absorption and retention functionality. J. Appl. Polym. Sci. 125, 2121-2127.

ASTM International, 2018. ASTM D882-18, Standard test method for tensile properties of thin plastic sheeting. ASTM International, West Conshohocken.

Aydogdu, A., Sumnu, G., Sahin, S., 2018. A novel electrospun hydroxypropyl methylcellulose/polyethylene oxide blend nanofibers: Morphology and physicochemical properties. Carbohydr. Polym. 181, 234-246.

Bano, I., Arshad, M., Yasin, T., Ghauri, M.A., Younus, M., 2017. Chitosan: A potential biopolymer for wound management. Int. J. Biol. Macromol. 102, 380-383.

Baroni, A., Buommino, E., De Gregorio, V., Ruocco, E., Ruocco, V., Wolf, R., 2012. Structure and function of the epidermis related to barrier properties. Clin. Dermatol. 30, 257-262.

Baum, C.L., Arpey, C.J., 2005. Normal cutaneous wound healing: Clinical correlation with cellular and molecular events. Dermatol. Surg. 31, 674-686.

Beachley, V., Wen, X., 2010. Polymer nanofibrous structures: Fabrication, biofunctionalization, and cell interactions. Prog. Polym. Sci. 35, 868-892.

Bhardwaj, N., Kundu, S.C., 2010. Electrospinning: A fascinating fiber fabrication technique. Biotechnol. Adv. 28, 325-347.

Bielefeld, K.A., Amini-Nik, S., Alman, B.A., 2013. Cutaneous wound healing: Recruiting developmental pathways for regeneration. Cell. Mol. Life. Sci. 70, 2059-2081.

Boateng, J., Catanzano, O., 2015. Advanced therapeutic dressings for effective wound healing - A review. J. Pharm. Sci. 104, 3653-3680.

Boateng, J.S., Matthews, K.H., Stevens, H.N., Eccleston, G.M., 2008. Wound healing dressings and drug delivery systems: A review. J. Pharm. Sci. 97, 2892-2923.

British Standards Institution, 2002. BS EN 13726-1 Test methods for primary wound dressings, Part 1: Aspects of absorbency. BSI, Milton Keynes., p. 20.

Çay, A., Miraftab, M., Perrin, E., 2014. Characterization and swelling performance of physically stabilized electrospun poly(vinyl alcohol)/chitosan nanofibres. Eur. Polym. J. 61, 253-262.

Chandrasekaran, A.R., Venugopal, J., Sundarrajan, S., Ramakrishna, S., 2011. Fabrication of a nanofibrous scaffold with improved bioactivity for culture of human dermal fibroblasts for skin regeneration. Biomed. Mater. 6, 015001.

Chen, F., Li, X., Mo, X., He, C., Wang, H., Ikada, Y., 2008. Electrospun chitosan-P(LLA-CL) nanofibers for biomimetic extracellular matrix. J. Biomater. Sci. Polym. Ed. 19, 677-691.

Chen, Z.G., Wang, P.W., Wei, B., Mo, X.M., Cui, F.Z., 2010. Electrospun collagen-chitosan nanofiber: A biomimetic extracellular matrix for endothelial cell and smooth muscle cell. Acta Biomater. 6, 372-382.

Clark, R., 2014. Chapter 76 - Wound repair: Basic biology to tissue engineering, in: Lanza, R., Langer, R., Vacanti, J. (Eds.), Principles of Tissue Engineering, 4 ed. Academic Press, Waltham, pp. 1595-1617.

De Vrieze, S., Van Camp, T., Nelvig, A., Hagström, B., Westbroek, P., De Clerck, K., 2009. The effect of temperature and humidity on electrospinning. J. Mater. Sci. 44, 1357-1362.

Demidova-Rice, T.N., Hamblin, M.R., Herman, I.M., 2012. Acute and impaired wound healing: Pathophysiology and current methods for drug delivery, part 1: Normal and chronic wounds: Biology, causes, and approaches to care. Adv. Skin Wound Care. 25, 304-314.

Deshmukh, K., Basheer Ahamed, M., Deshmukh, R.R., Khadheer Pasha, S.K., Bhagat, P.R., Chidambaram, K., 2017. 3 - Biopolymer composites with high dielectric performance: Interface engineering, in: Sadasivuni, K.K., Ponnamma, D., Kim, J., Cabibihan, J.J., AlMaadeed, M.A. (Eds.), Biopolymer Composites in Electronics, 1st ed. Elsevier, Cambridge, MA., pp. 27-128.

Dhivya, S., Padma, V.V., Santhini, E., 2015. Wound dressings - A review. BioMedicine (Taipei). 5, 24-28.

Djafari Petroudy, S.R., 2017. 3 - Physical and mechanical properties of natural fibers, in: Fan, M., Fu, F. (Eds.), Advanced High Strength Natural Fibre Composites in Construction. Woodhead Publishing, Cambridge, MA., pp. 59-83.

Doostmohammadi, M., Forootanfar, H., Ramakrishna, S., 2020. Regenerative medicine and drug delivery: Progress via electrospun biomaterials. Mater. Sci. Eng. C. 109, 110521.

Du, B., Bian, Z., Xu, B., 2014. Skin health promotion effects of natural beta-glucan derived from cereals and microorganisms: A review. Phytother. Res. 28, 159-166.

Elsabee, M.Z., Naguib, H.F., Morsi, R.E., 2012. Chitosan based nanofibers, review. Mater. Sci. Eng. C. 32, 1711-1726.

Engstad, R., Nøkland, T., 2017. Glucans, US9623043B2.

Enoch, S., Leaper, D.J., 2008. Basic science of wound healing. Surgery (Oxford). 26, 31-37.

Fong, H., Chun, I., Reneker, D.H., 1999. Beaded nanofibers formed during electrospinning. Polym. J. 40, 4585-4592.

Frenot, A., Henriksson, M.W., Walkenström, P., 2007. Electrospinning of cellulose-based nanofibers. J. Appl. Polym. Sci. 103, 1473-1482.

Fujihara, K., Teo, W.E., Lim, T.-C., Ma, Z., 2005. An Introduction to Electrospinning and Nanofibers, 1st ed. World Scientific Publishing Co. Pte. Ltd., London, pp. 15.

Ghadermazi, R., Hamdipour, S., Sadeghi, K., Ghadermazi, R., Khosrowshahi Asl, A., 2019. Effect of various additives on the properties of the films and coatings derived from hydroxypropyl methylcellulose - A review. Food. Sci. Nutr. 7, 3363-3377.

Goldberg, S.R., Diegelmann, R.F., 2017. Basic science of wound healing, in: Dieter, R.S., Dieter, J.R.A., Dieter, I.I.I.R.A., Nanjundappa, A. (Eds.), Critical Limb Ischemia: Acute and Chronic, 1st ed. Springer International Publishing, Cham, pp. 131-136.

Golecki, H.M., Yuan, H., Glavin, C., Potter, B., Badrossamay, M.R., Goss, J.A., Phillips, M.D., Parker, K.K., 2014. Effect of solvent evaporation on fiber morphology in rotary jet spinning. Langmuir. 30, 13369-13374.

Grip, J., Engstad, R.E., Skjæveland, I., Škalko-Basnet, N., Isaksson, J., Basnet, P., Holsæter, A.M., 2018. Beta-glucan-loaded nanofiber dressing improves wound healing in diabetic mice. Eur. J. Pharm. Sci. 121, 269-280.

Grkovic, M., Stojanovic, D.B., Pavlovic, V.B., Rajilic-Stojanovic, M., Bjelovic, M., Uskokovic, P.S., 2017. Improvement of mechanical properties and antibacterial activity of crosslinked electrospun chitosan/poly (ethylene oxide) nanofibers. Compos. B. Eng. 121, 58-67.

Gu, B., Park, S., Kim, M.S., Kang, C., Kim, J.-I., Kim, C.-H., 2013. Fabrication of sonicated chitosan nanofiber mat with enlarged porosity for use as hemostatic materials. Carbohydr. Polym. 97, 65-73.

Gunn, J., Zhang, M., 2010. Polyblend nanofibers for biomedical applications: Perspectives and challenges. Trends Biotechnol. 28, 189-197.

Guo, S., Dipietro, L.A., 2010. Factors affecting wound healing. J. Dent. Res. 89, 219-229.

Haider, A., Haider, S., Kang, I.-K., 2018. A comprehensive review summarizing the effect of electrospinning parameters and potential applications of nanofibers in biomedical and biotechnology. Arab. J. Chem. 11, 1165-1188.

Han, G., Ceilley, R., 2017. Chronic wound healing: A review of current management and treatments. Adv. Ther. 34, 599-610.

Hayes, T.R., Su, B., 2011. 15 - Wound dressings, in: Bosworth, L.A., Downes, S. (Eds.), Electrospinning for Tissue Regeneration, 1st ed. Woodhead Publishing, Cambridge, UK., pp. 317-339.

Howling, G.I., Dettmar, P.W., Goddard, P.A., Hampson, F.C., Dornish, M., Wood, E.J., 2001. The effect of chitin and chitosan on the proliferation of human skin fibroblasts and keratinocytes in vitro. Biomaterials. 22, 2959-2966.

Hurler, J., Škalko-Basnet, N., 2012. Potentials of chitosan-based delivery systems in wound therapy: Bioadhesion study. J. Funct. Biomater. 3, 37-48.

Jones, V., Grey, J.E., Harding, K.G., 2006. Wound dressings. BMJ. 332, 777-780.

Joshi, S.C., 2011. Sol-Gel behavior of hydroxypropyl methylcellulose (HPMC) in ionic media including drug release. Materials (Basel). 4, 1861-1905.

Järbrink, K., Ni, G., Sönnergren, H., Schmidtchen, A., Pang, C., Bajpai, R., Car, J., 2017. The humanistic and economic burden of chronic wounds: A protocol for a systematic review. Syst. Rev. 6, 15.

Kenry, Lim, C.T., 2017. Nanofiber technology: Current status and emerging developments. Prog. Polym. Sci. 70, 1-17.

Khattab, I.S., Bandarkar, F., Fakhree, M.A.A., Jouyban, A., 2012. Density, viscosity, and surface tension of water+ethanol mixtures from 293 to 323K. Korean J. Chem. Eng. 29, 812-817.

Kim, H.-L., Lee, J.-H., Lee, M.H., Kwon, B.J., Park, J.-C., 2012. Evaluation of electrospun (1,3)-(1,6)-β-D-glucans/biodegradable polymer as artificial skin for full-thickness wound healing. Tissue Eng. Part A. 18, 2315-2322.

Klossner, R.R., Queen, H.A., Coughlin, A.J., Krause, W.E., 2008. Correlation of chitosan's rheological properties and its ability to electrospin. Biomacromolecules. 9, 2947-2953.

Komuraiah, A., Kumar, N.S., Prasad, B.D., 2014. Chemical composition of natural fibers and its influence on their mechanical properties. Mech. Compos. Mater. 50, 359-376.

Krüss GmbH, 2007. Force Tensiometer – K6 manual, The measurement. Krüss GmbH, Hamburg.

Kumirska, J., Weinhold, M., Thöming, J., Stepnowski, P., 2011. Biomedical activity of chitin/chitosan based materials - Influence of physicochemical properties apart from molecular weight and degree of N-acetylation. Polymers (Basel). 3, 1875-1901.

Lazarus, G.S., Cooper, D.M., Knighton, D.R., Margolis, D.J., Pecoraro, R.E., Rodeheaver, G., Robson, M.C., 1994. Definitions and guidelines for assessment of wounds and evaluation of healing. Arch. Dermatol. 130, 489-493.

Leaper, D., Assadian, O., Edmiston, C.E., 2015. Approach to chronic wound infections. Br. J. Dermatol. 173, 351-358.

Li, J., Chen, J., Kirsner, R., 2007. Pathophysiology of acute wound healing. Clin. Dermatol. 25, 9-18.

Li, M., Han, B., Liu, W., 2011. Preparation and properties of a drug release membrane of mitomycin C with N-succinyl-hydroxyethyl chitosan. J. Mater. Sci. Mater. Med. 22, 2745-2755.

Li, Z., Mei, S., Dong, Y., She, F., Kong, L., 2019. High efficiency fabrication of chitosan composite nanofibers with uniform morphology via centrifugal spinning. Polymers (Basel). 11, 1550.

Lionelli, G.T., Lawrence, W.T., 2003. Wound dressings. Surg. Clin. North Am. 83, 617-638.

Liu, Y., Zhou, S., Gao, Y., Zhai, Y., 2019. Electrospun nanofibers as a wound dressing for treating diabetic foot ulcer. Asian J. Pharm. Sci. 14, 130-143.

MacEwan, M.R., MacEwan, S., Kovacs, T.R., Batts, J., 2017. What makes the optimal wound healing material? A review of current science and introduction of a synthetic nanofabricated wound care scaffold. Cureus 9, 1736-1736.

Majtan, J., Jesenak, M., 2018. β-Glucans: Multi-functional modulator of wound healing. Molecules. 23, 806.

Marks, J.G., Miller, J.J., 2019. 2 - Structure and function of the skin, in: Marks, J.G., Miller, J.J. (Eds.), Lookingbill and Marks' Principles of Dermatology, 6th ed. Elsevier Saunders, London, pp. 2-10.

Matabola, K.P., Moutloali, R.M., 2013. The influence of electrospinning parameters on the morphology and diameter of poly(vinyledene fluoride) nanofibers- effect of sodium chloride. J. Mater. Sci. 48, 5475-5482.

Matica, M.A., Aachmann, F.L., Tøndervik, A., Sletta, H., Ostafe, V., 2019. Chitosan as a wound dressing starting material: Antimicrobial properties and mode of action. Int. J. Mol. Sci. 20, 5889.

Megelski, S., Stephens, J.S., Chase, D.B., Rabolt, J.F., 2002. Micro- and nanostructured surface morphology on electrospun polymer fibers. Macromolecules. 35, 8456-8466.

Mele, E., 2016. Electrospinning of natural polymers for advanced wound care: Towards responsive and adaptive dressings. J. Mater. Chem. B. 4, 4801-4812.

Memic, A., Abudula, T., Mohammed, H.S., Joshi Navare, K., Colombani, T., Bencherif, S.A., 2019. Latest progress in electrospun nanofibers for wound healing applications. ACS Appl. Bio Mater. 2, 952-969.

Mengistu Lemma, S., Bossard, F., Rinaudo, M., 2016. Preparation of pure and stable chitosan nanofibers by electrospinning in the presence of poly(ethylene oxide). Int. J. Mol. Sci. 17, 1790.

Menke, N.B., Ward, K.R., Witten, T.M., Bonchev, D.G., Diegelmann, R.F., 2007. Impaired wound healing. Clin. Dermatol. 25, 19-25.

Mescher, A., 2009. Junqueira's Basic Histology: Text and Atlas, 12th ed. McGraw Hill Medical, New York, pp. 806.

Mohiti-Asli, M., Loboa, E.G., 2016. 23 - Nanofibrous smart bandages for wound care, in: Ågren, M.S. (Ed.), Wound Healing Biomaterials, 1st ed. Woodhead Publishing, Cambridge, MA., pp. 483-499.

Mustoe, T.A., O'Shaughnessy, K., Kloeters, O., 2006. Chronic wound pathogenesis and current treatment strategies: A unifying hypothesis. Plast. Reconstr. Surg. 117, 35-41.

Nafisi, S., Maibach, H.I., 2018. Chapter 3 - Skin penetration of nanoparticles, in: Shegokar, R., Souto, E.B. (Eds.), Emerging Nanotechnologies in Immunology, 1st ed. Elsevier, Boston, pp. 47-88.

Nemati, S., Kim, S.-J., Shin, Y.M., Shin, H., 2019. Current progress in application of polymeric nanofibers to tissue engineering. Nano Converg. 6, 36.

Oğulata, R.T., İçoğlu, H.İ., 2015. Interaction between effects of ambient parameters and those of other important parameters on electrospinning of PEI/NMP solution. J. Text. Inst. 106, 57-66.

Oh, C.M., Heng, P.W.S., Chan, L.W., 2015. A study on the impact of hydroxypropyl methylcellulose on the viscosity of PEG melt suspensions using surface plots and principal component analysis. AAPS PharmSciTech. 16, 466-477.

Ousey, K., Cutting, K.F., Rogers, A.A., Rippon, M.G., 2016. The importance of hydration in wound healing: Reinvigorating the clinical perspective. J. Wound Care. 25, 122, 124-130.

Palma, A.S., Feizi, T., Zhang, Y., Stoll, M.S., Lawson, A.M., Diaz-Rodriguez, E., Campanero-Rhodes, M.A., Costa, J., Gordon, S., Brown, G.D., Chai, W., 2006. Ligands for the beta-glucan receptor, Dectin-1, assigned using "designer" microarrays of oligosaccharide probes (neoglycolipids) generated from glucan polysaccharides. J. Biol. Chem. 281, 5771-5779.

Park, C.J., Gabrielson, N.P., Pack, D.W., Jamison, R.D., Wagoner Johnson, A.J., 2009. The effect of chitosan on the migration of neutrophil-like HL60 cells, mediated by IL-8. Biomaterials. 30, 436-444.

Pelipenko, J., Kocbek, P., Kristl, J., 2015. Critical attributes of nanofibers: Preparation, drug loading, and tissue regeneration. Int. J. Pharm. 484, 57-74.

Pelipenko, J., Kristl, J., Janković, B., Baumgartner, S., Kocbek, P., 2013. The impact of relative humidity during electrospinning on the morphology and mechanical properties of nanofibers. Int. J. Pharm. 456, 125-134.

Periayah, M.H., Halim, A.S., Saad, A.Z.M., 2016. Chitosan: A promising marine polysaccharide for biomedical research. Pharmacogn Rev. 10, 39-42.

Pham, Q.P., Sharma, U., Mikos, A.G., 2006. Electrospinning of polymeric nanofibers for tissue engineering applications: A review. Tissue Eng. 12, 1197-1211.

Picout, D.R., Ross-Murphy, S.B., 2003. Rheology of biopolymer solutions and gels. ScientificWorldJournal. 3, 105-121.

Pooponpun, S., Polnok, A., Paeratakul, O., Kraisit, P., Sarisuta, N., 2015. Mechanical and adhesive properties of cellulosic film coats containing polymeric additives. Pharmazie. 70, 300-305.

Qin, F., Sletmoen, M., Stokke, B.T., Christensen, B.E., 2013. Higher order structures of a bioactive, water-soluble (1→3)- β -d-glucan derived from Saccharomyces cerevisiae. Carbohydr. Polym. 92, 1026-1032.

Reinke, J.M., Sorg, H., 2012. Wound repair and regeneration. Eur. Surg. Res. 49, 35-43.

Rivera, A.E., Spencer, J.M., 2007. Clinical aspects of full-thickness wound healing. Clin. Dermatol. 25, 39-48.

Robb, B., Lennox, B., 2011. 3 - The electrospinning process, conditions and control, in: Bosworth, L.A., Downes, S. (Eds.), Electrospinning for Tissue Regeneration, 1st ed. Woodhead Publishing, Cambridge, UK., pp. 51-66.

Robson, M.C., Steed, D.L., Franz, M.G., 2001. Wound healing: Biologic features and approaches to maximize healing trajectories. Curr. Probl. Surg. 38, 72-140.

Rošic, R., Kocbek, P., Pelipenko, J., Kristl, J., Baumgartner, S., 2013. Nanofibers and their biomedical use. Acta. Pharm. 63, 295-304.

Rošic, R., Pelipenko, J., Kocbek, P., Baumgartner, S., Bešter-Rogač, M., Kristl, J., 2012a. The role of rheology of polymer solutions in predicting nanofiber formation by electrospinning. Eur. Polym. J. 48, 1374-1384.

Rošic, R., Pelipenko, J., Kristl, J., Kocbek, P., Baumgartner, S., 2012b. Properties, engineering and applications of polymeric nanofibers: Current research and future advances. Chem. Biochem. Eng. Q. 26, 417-425.

Sahariah, P., Másson, M., 2017. Antimicrobial chitosan and chitosan derivatives: A review of the structure - activity relationship. Biomacromolecules. 18, 3846-3868.

Santos, M.R.E., Fonseca, A.C., Mendonça, P.V., Branco, R., Serra, A.C., Morais, P.V., Coelho, J.F.J., 2016. Recent developments in antimicrobial polymers: A review. Materials. 9, 599.

Saringat, H., Alfadol, K., Khan, G.M., 2005. The influence of different plasticizers on some physical and mechanical properties of hydroxypropyl methylcellulose free films. Pak. J. Pharm. Sci. 18, 25-38.

Schmidt, B.V.K.J., 2019. Hydrophilic polymers. Polymers (Basel). 11, 693.

Schober, P., Boer, C., Schwarte, L., 2018. Correlation coefficients: Appropriate use and interpretation. Anesth. Analg. 126, 1763-1768.

Sencadas, V., Correia, D.M., Ribeiro, C., Moreira, S., Botelho, G., Gómez Ribelles, J.L., Lanceros-Mendez, S., 2012. Physical-chemical properties of cross-linked chitosan electrospun fiber mats. Polym. Test. 31, 1062-1069.

Seo, G., Hyun, C., Choi, S., Kim, Y.M., Cho, M., 2019. The wound healing effect of four types of beta-glucan. Appl. Biol. Chem. 62, 20.

Shahabadi, S.M.S., Kheradmand, A., Montazeri, V., Ziaee, H., 2015. Effects of process and ambient parameters on diameter and morphology of electrospun polyacrylonitrile nanofibers. Polym. Sci. Ser. A. 57, 155-167.

Sherwood, L., 2013. Introduction to Human Physiology, 8th ed. Cengage Learning, Independence, pp. 437-476.

Siddiqui, A.R., Bernstein, J.M., 2010. Chronic wound infection: Facts and controversies. Clin. Dermatol. 28, 519-526.

Singer, A.J., Clark, R.A.F., 1999. Cutaneous wound healing. N. Engl. J. Med. 341, 738-746.

Sogias, I.A., Khutoryanskiy, V.V., Williams, A.C., 2010. Exploring the factors affecting the solubility of chitosan in water. Macromol. Chem. Phys. 211, 426-433.

Subbiah, T., Bhat, G.S., Tock, R.W., Parameswaran, S., Ramkumar, S.S., 2005. Electrospinning of nanofibers. J. Appl. Polym. Sci. 96, 557-569.

Sudhakar, Y.N., Selvakumar, M., Bhat, D.K., 2018. Chapter 2 - Methods of preparation of biopolymer electrolytes, in: Sudhakar, Y.N., Selvakumar, M., Bhat, D.K. (Eds.), Biopolymer Electrolytes, 1st ed. Elsevier, Cambridge, MA., pp. 35-52.

Sun, B., Long, Y.Z., Zhang, H.D., Li, M.M., Duvail, J.L., Jiang, X.Y., Yin, H.L., 2014. Advances in three-dimensional nanofibrous macrostructures via electrospinning. Prog. Polym. Sci. 39, 862-890.

Tie, L., Yu, M., Li, X., Liu, W., Zhang, B., Chang, Z., Zheng, Y., 2019. Research on polymer solution rheology in polymer flooding for Qikou reservoirs in a Bohai Bay oilfield. J. Petrol. Expl. Produc. Tech. 9, 703-715.

Tortora, G.J., Derrickson, B., 2014. Principles of Anatomy & Physiology, 14th ed. Wiley, Hoboken, pp. 142-155.

Ueno, H., Mori, T., Fujinaga, T., 2001. Topical formulations and wound healing applications of chitosan. Adv. Drug Del. Rev. 52, 105-115.

Van den Berg, L.M., Zijlstra-Willems, E.M., Richters, C.D., Ulrich, M.M., Geijtenbeek, T.B., 2014. Dectin-1 activation induces proliferation and migration of human keratinocytes enhancing wound re-epithelialization. Cell. Immunol. 289, 49-54.

Van der Schueren, L., Steyaert, I., De Schoenmaker, B., De Clerck, K., 2012. Polycaprolactone/chitosan blend nanofibres electrospun from an acetic acid/formic acid solvent system. Carbohydr. Polym. 88, 1221-1226.

Velnar, T., Bailey, T., Smrkolj, V., 2009. The wound healing process: An overview of the cellular and molecular mechanisms. J. Int. Med. Res. 37, 1528-1542.

Verreck, G., Chun, I., Peeters, J., Rosenblatt, J., Brewster, M.E., 2003. Preparation and characterization of nanofibers containing amorphous drug dispersions generated by electrostatic spinning. Pharm. Res. 20, 810-817.

Waghmare, V.S., Wadke, P.R., Dyawanapelly, S., Deshpande, A., Jain, R., Dandekar, P., 2018. Starch based nanofibrous scaffolds for wound healing applications. Bioact. Mater. 3, 255-266.

Wahba, M.I., 2020. Enhancement of the mechanical properties of chitosan. J. Biomater. Sci. Polym. Ed. 31, 350-375.

Wang, H.S., Fu, G.D., Li, X.S., 2009. Functional polymeric nanofibers from electrospinning. Recent Pat. Nanotechnol. 3, 21-31.

Wang, L., Chen, K., Wen, H., Ouyang, D., Li, X., Gao, Y., Pan, W., Yang, X., 2017. Design and evaluation of hydrophilic matrix system containing polyethylene oxides for the zero-order controlled delivery of water-insoluble drugs. AAPS PharmSciTech 18, 82-92.

Wang, T., Kumar, S., 2006. Electrospinning of polyacrylonitrile nanofibers. J. Appl. Polym. Sci. 102, 1023-1029.

Wannatong, L., Sirivat, A., Supaphol, P., 2004. Effects of solvents on electrospun polymeric fibers: preliminary study on polystyrene. Polym. Int. 53, 1851-1859.

Wickett, R.R., Visscher, M.O., 2006. Structure and function of the epidermal barrier. Am. J. Infect. Control. 34, 98-110.

Wong, T.W., 2009. Chitosan and its use in design of insulin delivery system. Recent Pat. Drug Deliv. Formul. 3, 8-25.

Yalcinkaya, F., 2019. Preparation of various nanofiber layers using wire electrospinning system. Arab. J. Chem. 12, 5162-5172.

Yan, G., Niu, H., Lin, T., 2019. Chapter 7 - Needle-less electrospinning, in: Ding, B., Wang, X., Yu, J. (Eds.), Electrospinning: Nanofabrication and Applications, 1st ed. William Andrew Publishing, Cambridge, MA., pp. 219-247.

Yang, J., Tian, F., Wang, Z., Wang, Q., Zeng, Y.J., Chen, S.Q., 2008. Effect of chitosan molecular weight and deacetylation degree on hemostasis. J. Biomed. Mater. Res., Part B: Appl. Biomater. 84, 131-137.

Yang, Q., Li, Z., Hong, Y., Zhao, Y., Qiu, S., Wang, C., Wei, Y., 2004. Influence of solvents on the formation of ultrathin uniform poly(vinyl pyrrolidone) nanofibers with electrospinning. J. Polym. Sci., Part B: Polym. Phys. 42, 3721-3726.

Yu, M., Dong, R.-H., Yan, X., Yu, G.-F., You, M.-H., Ning, X., Long, Y.-Z., 2017. Recent advances in needleless electrospinning of ultrathin fibers: From academia to industrial production. Macromol. Mater. Eng. 302, 1700002.

Yuan, T., Jenkins, P., Foushee, A., Jockheck-Clark, A., Stahl, J., 2016. Electrospun chitosan/polyethylene oxide nanofibrous scaffolds with potential antibacterial wound dressing applications. J. Nanomater. 2016, 1-10.

Zahedi, P., Rezaeian, I., Ranaei-Siadat, S.-O., Jafari, S.-H., Supaphol, P., 2010. A review on wound dressings with an emphasis on electrospun nanofibrous polymeric bandages. Polym. Adv. Technol. 21, 77-95.

Zargham, S., Bazgir, S., Tavakoli, A., Rashidi, A., Damerchely, R., 2012. The effect of flow rate on morphology and deposition area of electrospun nylon 6 nanofiber. J. Eng. Fibers Fabr. 7, 42-49.

Zarghami, A., Irani, M., Mostafazadeh, A., Golpour, M., Heidarinasab, A., Haririan, I., 2015. Fabrication of PEO/chitosan/PCL/olive oil nanofibrous scaffolds for wound dressing applications. Fibers Polym. 16, 1201-1212.

Zhang, C., Yuan, X., Wu, L., Han, Y., Sheng, J., 2005a. Study on morphology of electrospun poly(vinyl alcohol) mats. Eur. Polym. J. 41, 423-432.

Zhang, Y., Lim, C.T., Ramakrishna, S., Huang, Z.M., 2005b. Recent development of polymer nanofibers for biomedical and biotechnological applications. J. Mater. Sci. Mater. Med. 16, 933-946.

Zhao, R., Liang, H., Clarke, E., Jackson, C., Xue, M., 2016. Inflammation in chronic wounds. Int. J. Mol. Sci. 17, 2085.

Zhu, F., Du, B., Xu, B., 2016. A critical review on production and industrial applications of beta-glucans. Food Hydrocoll. 52, 275-288.

Zong, X., Kim, K., Fang, D., Ran, S., Hsiao, B.S., Chu, B., 2002. Structure and process relationship of electrospun bioabsorbable nanofiber membranes. Polym. J. 43, 4403-4412.

Zykova, S.N., Balandina, K.A., Vorokhobina, N.V., Kuznetsova, A.V., Engstad, R., Zykova, T.A., 2014. Macrophage stimulating agent soluble yeast β-1,3/1,6-glucan as a topical treatment of diabetic foot and leg ulcers: A randomized, double blind, placebo-controlled phase II study. J. Diabetes Investig. 5, 392-399.

Appendix

Polymer solutions

Table A1: Theoretical distribution of polymers in the total selection of prepared solutions.

Name of solution	Final polymer concentration (%)	HPMC (%)	PEO (%)	CS (%)	*βG* (%)
5%CS-50%EtOH	2.1	80	15	5	0
5%CS-60%EtOH	2.1	80	15	5	0
5%CS-70%EtOH	2.1	80	15	5	0
5%CS-5%βG-50%EtOH	2.1	75	15	5	5
5%CS-5%βG-60%EtOH	2.1	75	15	5	5
5%CS-5%βG-70%EtOH	2.1	75	15	5	5
10%CS-50%EtOH	2.1	75	15	10	0
10%CS-60%EtOH	2.1	75	15	10	0
10%CS-70%EtOH	2.1	75	15	10	0
10%CS-10%βG-50%EtOH	2.1	65	15	10	10
10%CS-10%βG-60%EtOH	2.1	65	15	10	10
10%CS-10%βG-70%EtOH	2.1	65	15	10	10
15%CS-50%EtOH	2.1	70	15	15	0
15%CS-60%EtOH	2.1	70	15	15	0
15%CS-70%EtOH	2.1	70	15	15	0
15%CS-15%βG-50%EtOH	2.1	55	15	15	15
15%CS-15%βG-60%EtOH	2.1	55	15	15	15
15%CS-15%βG-70%EtOH	2.1	55	15	15	15
20%CS-50%EtOH	2.1	65	15	20	0
20%CS-60%EtOH	2.1	65	15	20	0
20%CS-70%EtOH	2.1	65	15	20	0
20%CS-20%βG-50%EtOH	2.1	45	15	20	20
20%CS-20%βG-60%EtOH	2.1	45	15	20	20
20%CS-20%βG-70%EtOH	2.1	45	15	20	20
25%CS-50%EtOH	2.1	60	15	25	0
25%CS-60%EtOH	2.1	60	15	25	0
25%CS-70%EtOH	2.1	60	15	25	0
25%CS-25%βG-50%EtOH	2.1	35	15	25	25
25%CS-25%βG-60%EtOH	2.1	35	15	25	25
25%CS-25%βG-70%EtOH	2.1	35	15	25	25
30%CS-50%EtOH	2.1	55	15	30	0
30%CS-60%EtOH	2.1	55	15	30	0
30%CS-70%EtOH	2.1	55	15	30	0
30%CS-30%βG-50%EtOH	2.1	25	15	30	30
30%CS-30%βG-60%EtOH	2.1	25	15	30	30
30%CS-30%βG-70%EtOH	2.1	25	15	30	30
35%CS-50%EtOH	2.1	50	15	35	0
35%CS-60%EtOH	2.1	50	15	35	0
35%CS-70%EtOH	2.1	50	15	35	0

Table A2: Exact distribution of polymers in the total selection of prepared solutions for the first round of spinning.

Name of solution	Final polymer concentration (%)	HPMC (%)	PEO (%)	CS (%)	*βG* (%)
5%CS-50%EtOH	2.10	80.18	14.90	4.91	0.00
5%CS-60%EtOH	2.10	80.03	15.09	4.88	0.00
5%CS-70%EtOH	2.10	80.10	14.94	4.95	0.00
5%CS-5%βG-50%EtOH	2.10	74.96	15.05	4.98	5.01
5%CS-5%βG-60%EtOH	2.10	74.95	15.06	4.99	5.00
5%CS-5%βG-70%EtOH	2.10	74.93	15.07	5.00	5.00
10%CS-50%EtOH	2.10	74.99	15.05	9.96	0.00
10%CS-60%EtOH	2.10	74.99	15.05	9.96	0.00
10%CS-70%EtOH	2.10	74.93	15.04	10.03	0.00
10%CS-10%βG-50%EtOH	2.20	66.66	14.29	9.53	9.52
10%CS-10%βG-60%EtOH	2.20	66.64	14.30	9.54	9.52
10%CS-10%SBG-70%EtOH	2.20	66.65	14.29	9.53	9.53
15%CS-50%EtOH	2.10	69.99	15.01	15.00	0.00
15%CS-60%EtOH	2.10	70.00	15.00	15.00	0.00
15%CS-70%EtOH	2.10	69.99	15.01	15.00	0.00
15%CS-15%βG-50%EtOH	2.10	55.01	15.00	14.99	15.00
15%CS-15%βG-60%EtOH	2.10	55.00	15.00	15.01	15.00
15%CS-15%βG-70%EtOH	2.10	54.99	15.00	15.01	15.00
20%CS-50%EtOH	2.10	65.00	15.01	20.00	0.00
20%CS-60%EtOH	2.10	64.99	15.01	20.00	0.00
20%CS-70%EtOH	2.10	64.98	14.99	20.02	0.00
20%CS-20%βG-50%EtOH	2.10	45.00	15.02	19.99	19.99
20%CS-20%βG-60%EtOH	2.10	45.00	15.00	20.01	19.99
20%CS-20%βG-70%EtOH	2.10	45.00	15.00	20.01	19.99
25%CS-50%EtOH	2.10	59.99	15.01	25.00	0.00
25%CS-60%EtOH	2.10	60.00	15.00	25.00	0.00
25%CS-70%EtOH	2.10	60.00	15.00	25.00	0.00
25%CS-25%βG-50%EtOH	2.10	35.01	15.00	25.00	24.99
25%CS-25%βG-60%EtOH	2.10	35.00	14.99	25.02	24.99
25%CS-25%βG-70%EtOH	2.10	35.00	14.99	25.02	24.99
30%CS-50%EtOH	2.10	54.99	15.00	30.01	0.00
30%CS-60%EtOH	2.10	55.00	15.00	30.00	0.00
30%CS-70%EtOH	2.10	55.00	15.00	30.00	0.00
30%CS-30%βG-60%EtOH	2.10	25.01	15.00	30.01	29.99
30%CS-30%βG-70%EtOH	2.10	25.01	15.00	29.99	30.00
35%CS-60%EtOH	2.10	49.99	15.00	35.01	0.00
35%CS-70%EtOH	2.10	50.00	15.00	35.00	0.00

Table A3: Exact distribution of polymers in the total selection of prepared solutions for the second round of spinning.

Name of solution	Final polymer concentration (%)	HPMC (%)	PEO (%)	CS (%)	*βG* (%)
5%CS-50%EtOH	2.10	80.00	15.00	5.00	0.00
5%CS-60%EtOH	2.10	80.00	15.00	5.00	0.00
5%CS-70%EtOH	2.10	80.01	15.00	4.99	0.00
5%CS-5%βG-50%EtOH	2.10	74.99	14.99	5.02	5.00
5%CS-5%βG-60%EtOH	2.10	74.99	15.00	5.01	5.00
5%CS-5%βG-70%EtOH	2.10	74.99	15.00	5.01	5.00
10%CS-50%EtOH	2.10	75.00	15.00	10.00	0.00
10%CS-60%EtOH	2.10	74.99	15.00	10.01	0.00
10%CS-70%EtOH	2.10	74.99	14.99	10.02	0.00
10%CS-10%βG-50%EtOH	2.10	65.00	15.00	10.01	10.00
10%CS-10%βG-60%EtOH	2.10	64.99	14.99	10.02	10.00
10%CS-10%βG-70%EtOH	2.10	65.00	15.00	10.00	10.00
15%CS-50%EtOH	2.10	69.99	15.00	15.02	0.00
15%CS-60%EtOH	2.10	69.99	15.00	15.01	0.00
15%CS-70%EtOH	2.10	70.00	15.00	15.00	0.00
15%CS-15%βG-50%EtOH	2.10	55.00	15.00	15.00	15.00
15%CS-15%βG-60%EtOH	2.10	55.01	15.00	15.00	15.00
15%CS-15%βG-70%EtOH	2.10	55.00	15.00	15.01	15.00
20%CS-50%EtOH	2.10	65.01	15.00	19.99	0.00
20%CS-60%EtOH	2.10	65.01	15.00	19.99	0.00
20%CS-70%EtOH	2.10	64.99	14.99	20.01	0.00
20%CS-20%βG-50%EtOH	2.10	45.01	15.00	19.99	20.00
20%CS-20%βG-60%EtOH	2.10	45.00	15.00	20.01	19.99
20%CS-20%βG-70%EtOH	2.10	45.00	15.00	20.01	19.99
25%CS-50%EtOH	2.10	60.00	15.00	25.00	0.00
25%CS-60%EtOH	2.10	60.00	15.00	24.99	0.00
25%CS-70%EtOH	2.10	60.00	15.00	25.00	0.00
25%CS-25%βG-50%EtOH	2.10	35.01	15.00	25.00	24.99
25%CS-25%βG-60%EtOH	2.10	35.00	15.00	25.01	24.99
25%CS-25%βG-70%EtOH	2.10	35.01	15.00	25.01	24.99
30%CS-50%EtOH	2.10	54.99	14.99	30.01	0.00
30%CS-60%EtOH	2.10	55.00	14.99	30.01	0.00
30%CS-70%EtOH	2.10	55.00	15.00	30.00	0.00
30%CS-30%βG-60%EtOH	2.10	25.01	15.00	30.00	29.99
30%CS-30%βG-70%EtOH	2.10	25.01	15.00	29.99	30.00
35%CS-60%EtOH	2.10	49.99	15.00	35.01	0.00
35%CS-70%EtOH	2.10	50.00	15.00	35.00	0.00

PH of polymer solutions

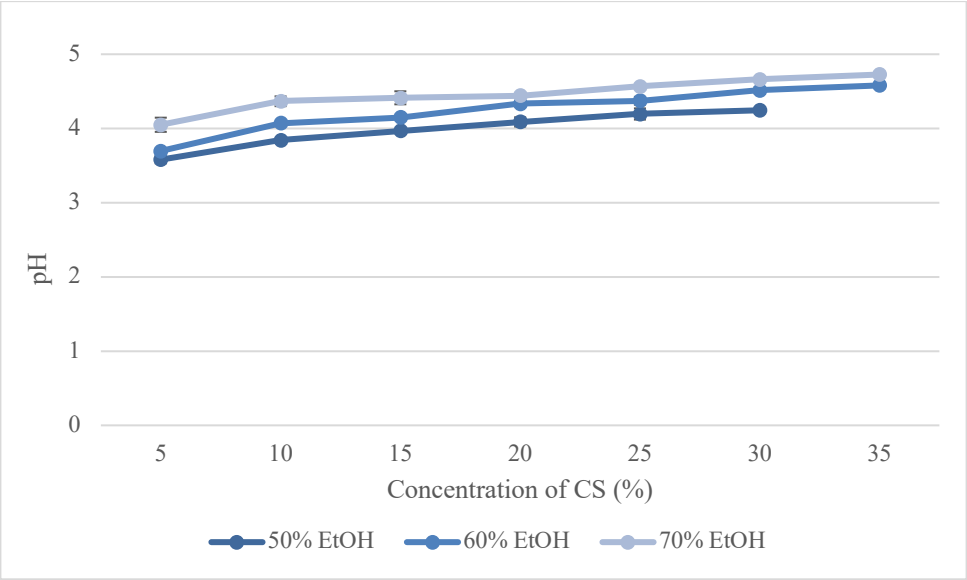

Figure A1: pH of CS solutions as a function of solution composition.

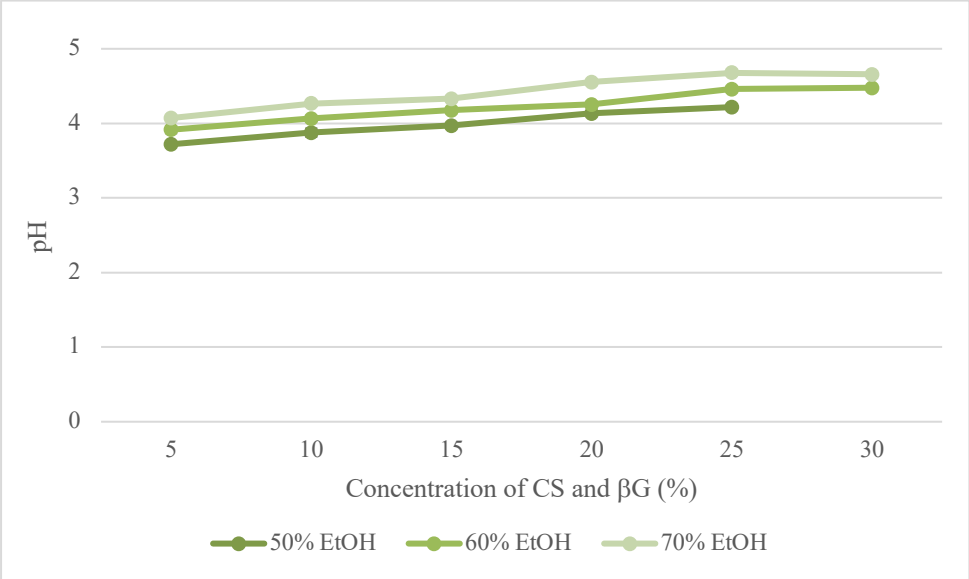

Figure A2: pH of CS and βG solutions as a function of solution composition.

Rheological properties

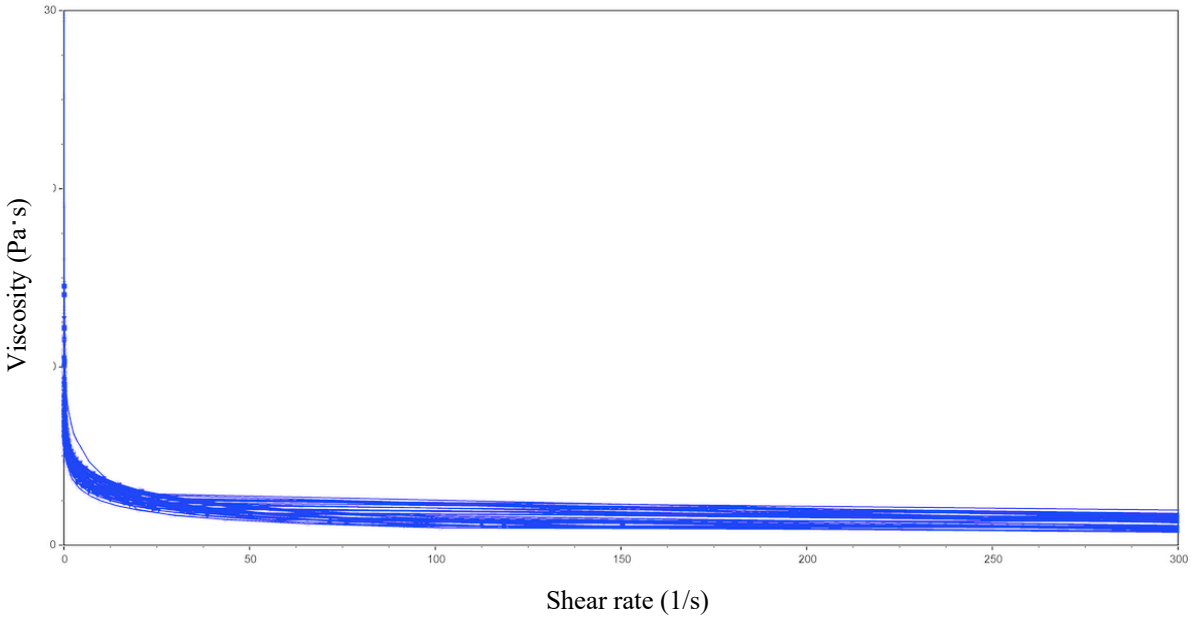

Figure A3: Viscosity of CS solutions as a function of shear rate.

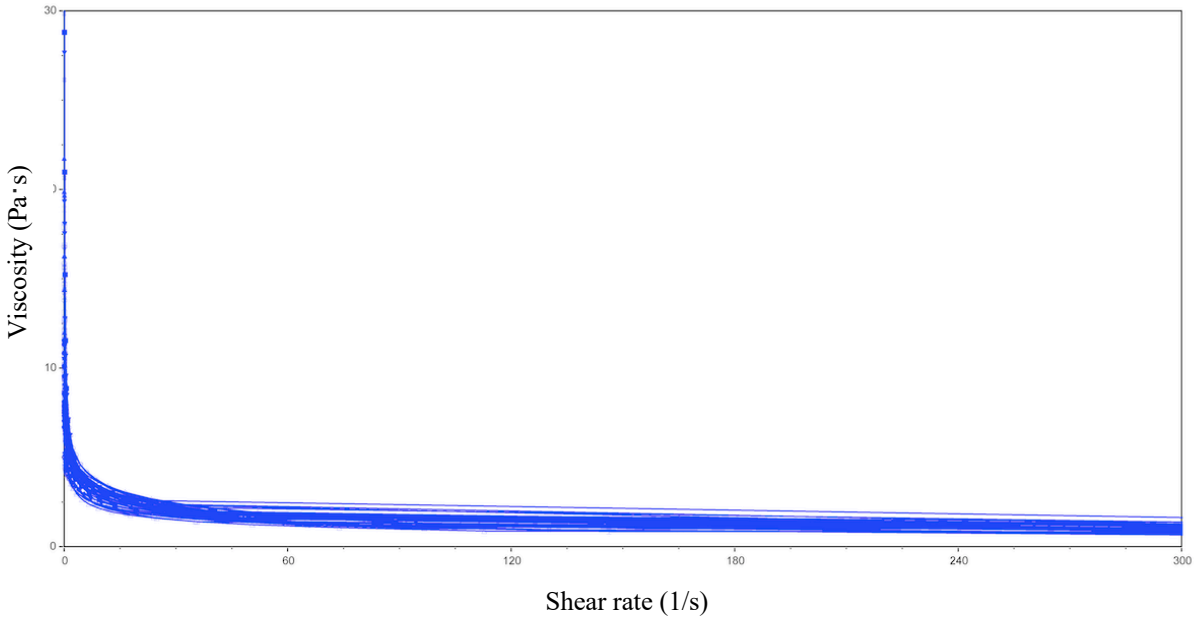

Figure A4: Viscosity for CS and βG solutions as a function of shear rate.

Tensile properties

Table A4: Tensile properties of the total selection of nanofiber scaffolds. The values are presented as mean ± SD (n = 2).

Name of fiber scaffold	Tensile strength (MPa)	Yong modulus (MPa)	Elongation at break (%)
5%CS-50%EtOH	13.89 ± 2.82	1.24 ± 0.31	109.44 ± 1.23
5%CS-60%EtOH	12.50 ± 5.43	1.06 ± 0.40	110.28 ± 1.56
5%CS-70%EtOH	19.36 ± 1.97	1.09 ± 0.12	109.96 ± 0.67
5%CS-5%βG-50%EtOH	18.13 ± 1.99	1.40 ± 0.74	107.78 ± 2.53
5%CS-5%βG-60%EtOH	10.16 ± 2.22	1.42 ± 0.55	105.63 ± 1.40
5%CS-5%βG-70%EtOH	13.71 ± 2.33	1.33 ± 0.33	107.19 ± 2.90
10%CS-50%EtOH	11.23 ± 1.17	1.51 ± 0.40	105.53 ± 1.10
10%CS-60%EtOH	14.91 ± 2.43	1.17 ± 0.31	107.10 ± 1.72
10%CS-70%EtOH	18.56 ± 3.20	1.16 ± 0.17	106.98 ± 2.97
10%CS-10%βG-50%EtOH	11.78 ± 5.16	1.34 ± 0.52	104.79 ± 1.76
10%CS-10%βG -60%EtOH	10.93 ± 2.50	1.22 ± 0.28	104.85 ± 0.59
10%CS-10%βG -70%EtOH	8.44 ± 2.49	1.04 ± 0.47	106.52 ± 1.06
15%CS-50%EtOH	12.99 ± 2.01	1.00 ± 0.17	105.33 ± 1.73
15%CS-60%EtOH	14.34 ± 1.82	1.16 ± 0.16	107.15 ± 1.65
15%CS-70%EtOH	12.74 ± 1.12	1.43 ± 0.48	107.41 ± 1.44
15%CS-15%βG -50%EtOH	11.82 ± 1.24	1.10 ± 0.13	103.33 ± 1.14
15%CS-15%βG -60%EtOH	13.95 ± 1.36	1.17 ± 0.15	103.48 ± 0.55
15%CS-15%βG -70%EtOH	6.21 ± 0.37	1.17 ± 0.51	105.60 ± 2.07
20%CS-50%EtOH	10.41 ± 3.96	1.45 ± 0.49	104.78 ± 0.68
20%CS-60%EtOH	16.15 ± 2.46	1.14 ± 0.32	108.26 ± 2.83
20%CS-70%EtOH	15.29 ± 1.38	1.10 ± 0.20	108.73 ± 1.59
20%CS-20%βG-50%EtOH	13.39 ± 3.57	1.03 ± 0.06	103.19 ± 0.67
20%CS-20%βG-60%EtOH	9.78 ± 1.49	1.15 ± 0.21	102.73 ± 0.34
20%CS-20%βG-70%EtOH	6.92 ± 0.77	0.98 ± 0.07	103.12 ± 0.26
25%CS-60%EtOH	11.28 ± 0.45	1.15 ± 0.26	107.31 ± 0.93
25%CS-70%EtOH	12.42 ± 1.15	1.24 ± 0.31	108.23 ± 0.46
25%CS-25%βG-60%EtOH	6.94 ± 0.55	1.07 ± 0.28	102.61 ± 0.21
25%CS-25%βG-70%EtOH	5.60 ± 1.11	0.94 ± 0.45	102.62 ± 0.28
30%CS-60%EtOH	12.81 ± 1.00	1.18 ± 0.31	109.50 ± 0.67
30%CS-70%EtOH	12.34 ± 2.36	1.16 ± 0.23	108.76 ± 0.98
30%CS-30%βG-60%EtOH	4.61 ± 1.00	0.95 ± 0.11	101.56 ± 0.25
30%CS-30%βG-70%EtOH	5.18 ± 1.57	0.84 ± 0.23	102.01 ± 0.15
35%CS-60%EtOH	10.36 ± 2.47	1.17 ± 0.31	105.74 ± 0.93
35%CS-70%EtOH	13.57 ± 0.41	1.06 ± 0.15	106.98 ± 1.39

Tensile energy to break

Table A5: Tensile energy required to break the total selection of nanofiber scaffolds. The values are presented as mean ± SD (n = 2).

Polymer concentration	Tensile energy to break (M/m^3)		
	50% EtOH	**60% EtOH**	**70% EtOH**
5%CS	0.85 ± 0.29	0.76 ± 0.44	1.24 ± 0.17
5%CS-5%βG	0.97 ± 0.38	0.36 ± 0.15	0.63 ± 0.37
10%CS	0.38 ± 0.12	0.63 ± 0.18	0.88 ± 0.39
10%CS-10%βG	0.41 ± 0.32	0.32 ± 0.12	0.34 ± 0.14
15%CS	0.43 ± 0.16	0.67 ± 0.22	0.60 ± 0.11
15%CS-15%βG	0.21 ± 0.11	0.30 ± 0.07	0.20 ± 0.09
20%CS	0.29 ± 0.13	0.89 ± 0.31	0.86 ± 0.10
20%CS-20%βG	0.26 ± 0.13	0.14 ± 0.04	0.11 ± 0.02
25%CS		0.53 ± 0.06	0.67 ± 0.08
25%CS-25%βG		0.09 ± 0.02	0.07 ± 0.01
30%CS		0.78 ± 0.11	0.70 ± 0.20
30%CS-30%βG		0.03 ± 0.01	0.05 ± 0.02
35%CS		0.36 ± 0.07	0.61 ± 0.12

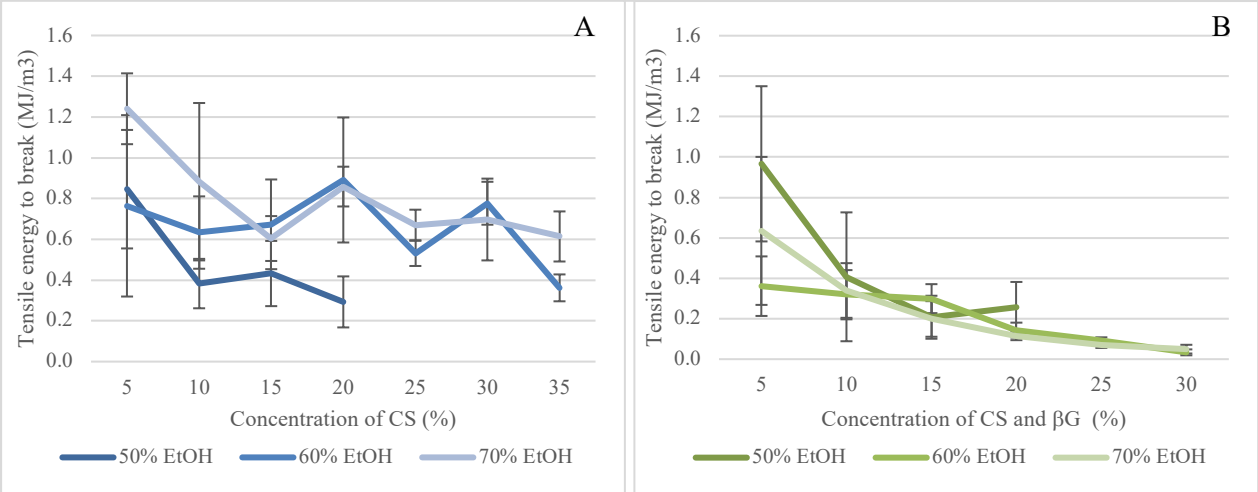

Figure A5: Tensile energy required to break (A) CS and (B) CS and βG fibers plotted as a function of polymer concentration.

Thickness of nanofiber scaffolds

Table A6: Average thickness of nanofiber scaffolds. The values are presented as mean ± SD (n = 2).

Polymer concentration	Thickness (mm)		
	50% EtOH	**60% EtOH**	**70% EtOH**
5%CS	0.03 ± 0.01	0.04 ± 0.01	0.04 ± 0.00
5%CS-5%βG	0.03 ± 0.00	0.04 ± 0.00	0.04 ± 0.01
10%CS	0.03 ± 0.00	0.03 ± 0.01	0.03 ± 0.00
10%CS-10%βG	0.03 ± 0.01	0.02 ± 0.00	0.05 ± 0.00
15%CS	0.03 ± 0.00	0.03 ± 0.00	0.04 ± 0.00
15%CS-15%βG	0.02 ± 0.00	0.03 ± 0.00	0.03 ± 0.01
20%CS	0.02 ± 0.01	0.03 ± 0.00	0.03 ± 0.00
20%CS-20%βG	0.02 ± 0.00	0.02 ± 0.00	0.02 ± 0.00
25%CS		0.03 ± 0.00	0.03 ± 0.00
25%CS-25%βG		0.02 ± 0.01	0.02 ± 0.01
30%CS		0.02 ± 0.00	0.03 ± 0.00
30%CS-30%βG		0.02 ± 0.00	0.02 ± 0.00
35%CS		0.02 ± 0.00	0.02 ± 0.00

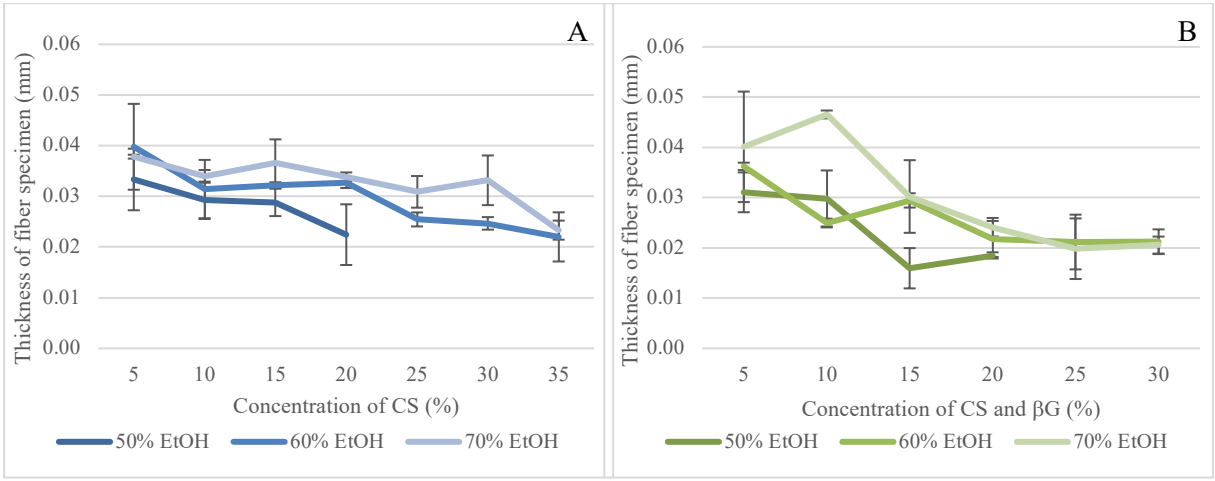

Figure A6: Thickness of (A) CS and (B) CS and βG nanofiber scaffolds.

Nanofiber diameter

Table A7: Average fiber diameter of the total selection of nanofiber scaffolds. The values are presented as mean ± SD (n = 2).

Polymer concentration	Diameter (nm)		
	50% EtOH	**60% EtOH**	**70% EtOH**
5%CS	75.19 ± 14.94	79.42 ± 6.84	88.27 ± 9.55
5%CS-5%βG	80.97 ± 8.98	91.08 ± 13.48	105.43 ± 1.91
10%CS	76.96 ± 13.26	90.91 ± 0.39	100.33 ± 21.40
10%CS-10%βG	74.61 ± 0.06	84.62 ± 6.40	89.17 ± 3.90
15%CS	73.12 ± 0.93	90.64 ± 4.52	100.44 ± 1.74
15%CS-15%βG	68.70 ± 2.57	75.24 ± 2.30	85.93 ± 3.97
20%CS	76.36 ± 5.73	83.75 ± 4.24	86.03 ± 2.41
20%CS-20%βG	67.78 ± 3.29	89.04 ± 5.84	90.96 ± 18.91
25%CS		83.76 ± 3.16	97.93 ± 7.79
25%CS-25%βG		96.38 ± 25.81	112.32 ± 38.42
30%CS		81.13 ± 8.65	103.42 ± 7.13
30%CS-30%βG		97.62 ± 27.76	100.03 ± 41.40
35%CS		90.31 ± 3.94	99.87 ± 8.84

Diameter distribution

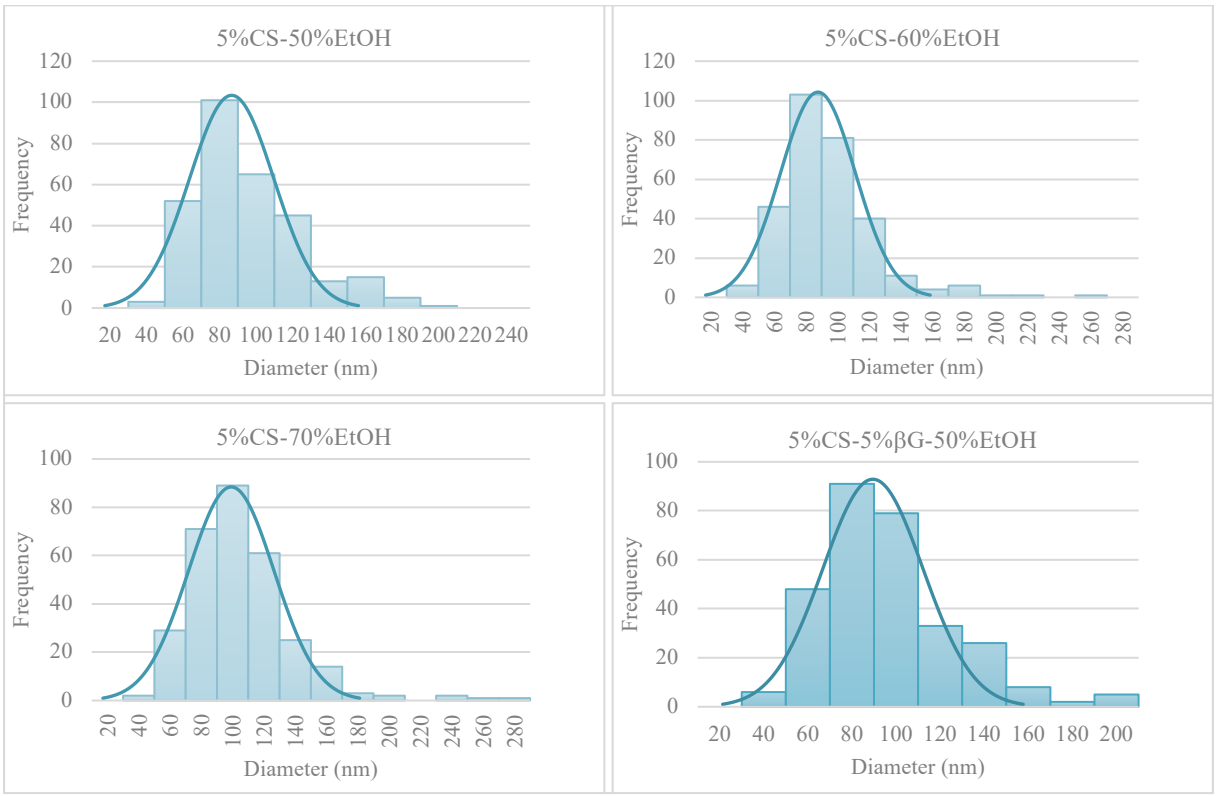

Figure A7: Diameter distribution histograms for fibers produced in the first round of electrospinning.

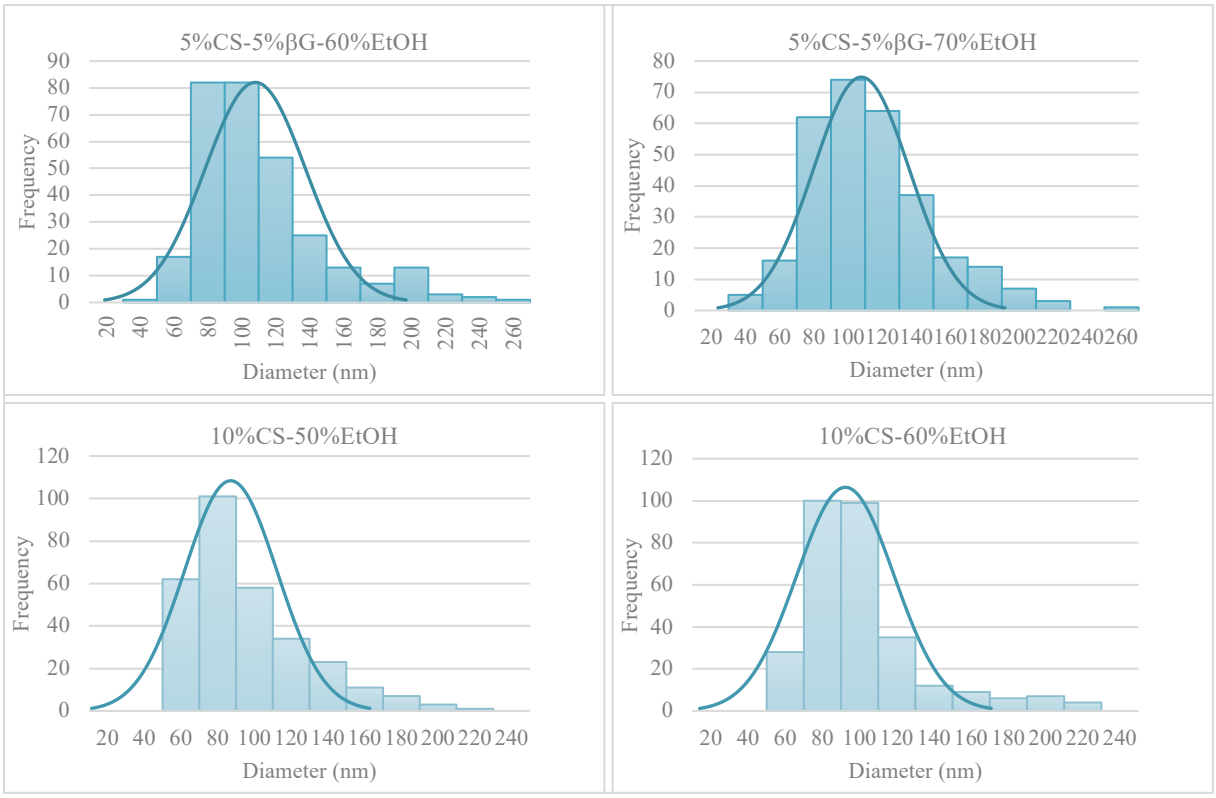

Figure A8: Diameter distribution histograms for fibers produced in the first round of electrospinning.

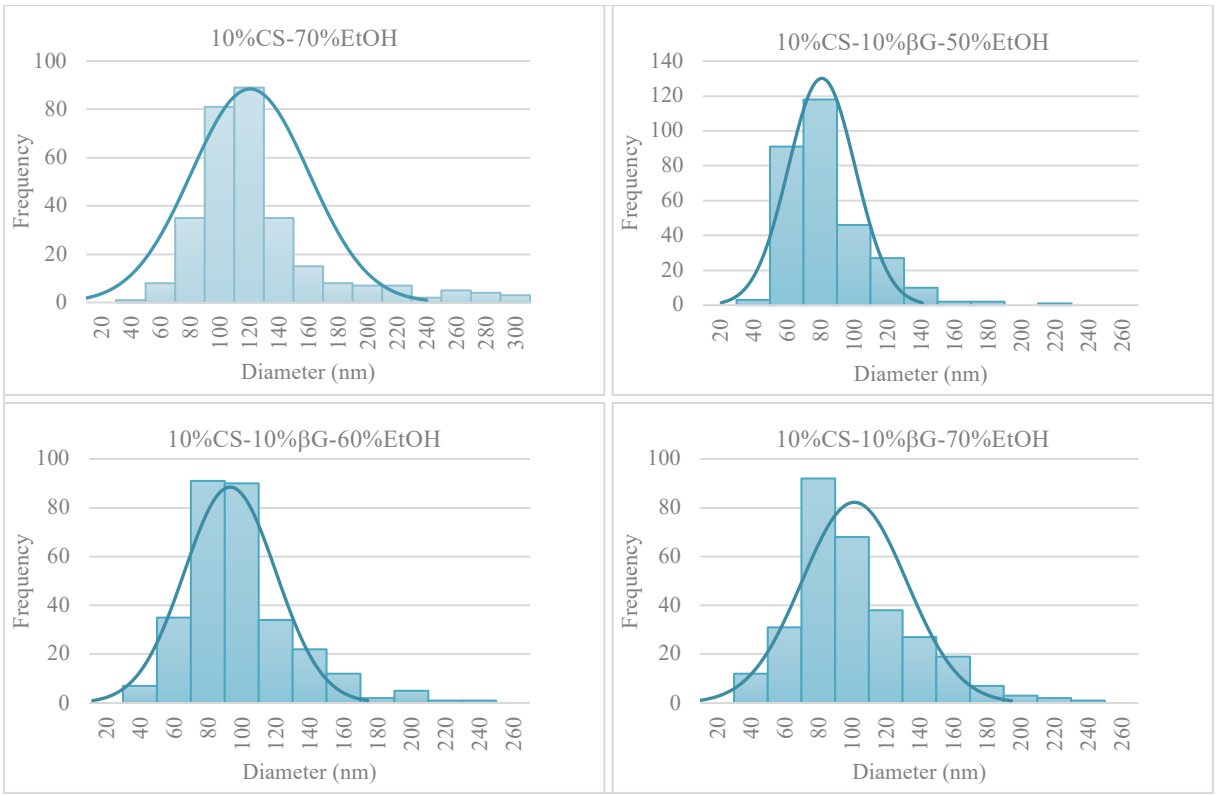

Figure A9: Diameter distribution histograms for fibers produced in the first round of electrospinning.

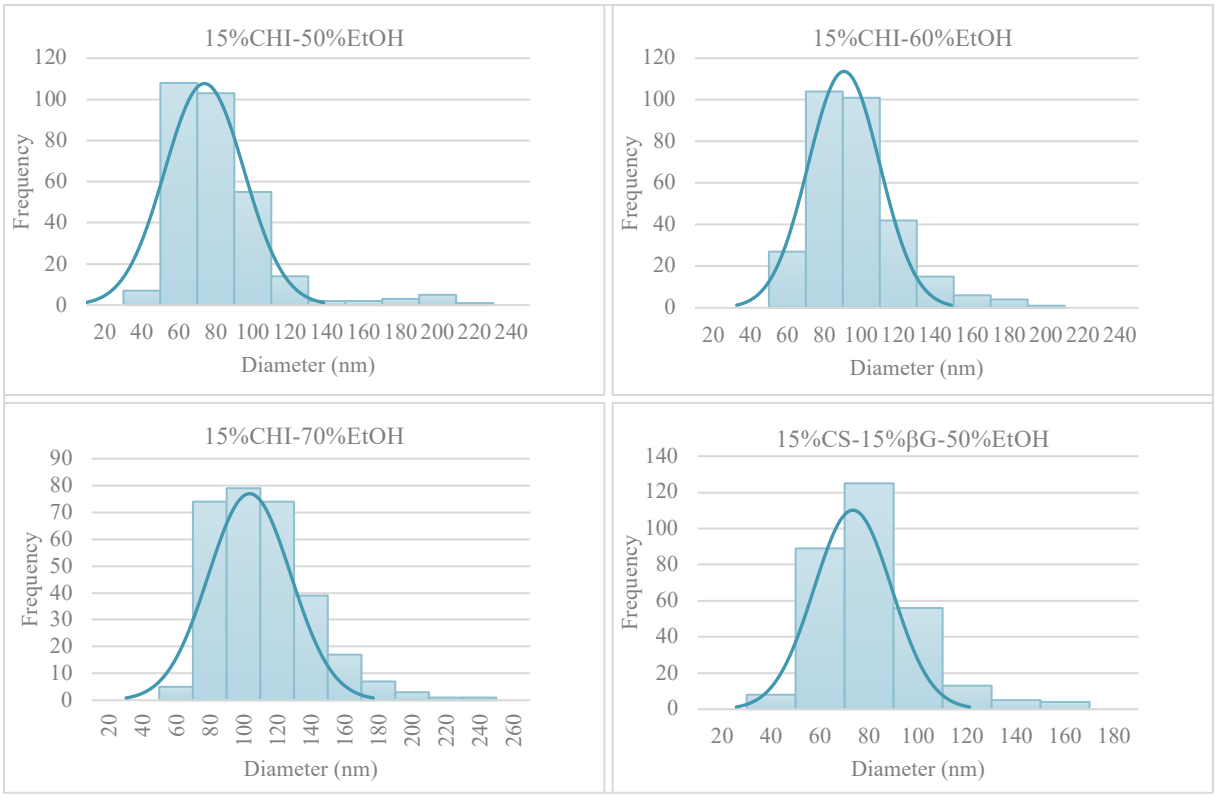

Figure A10: Diameter distribution histograms for fibers produced in the first round of electrospinning.

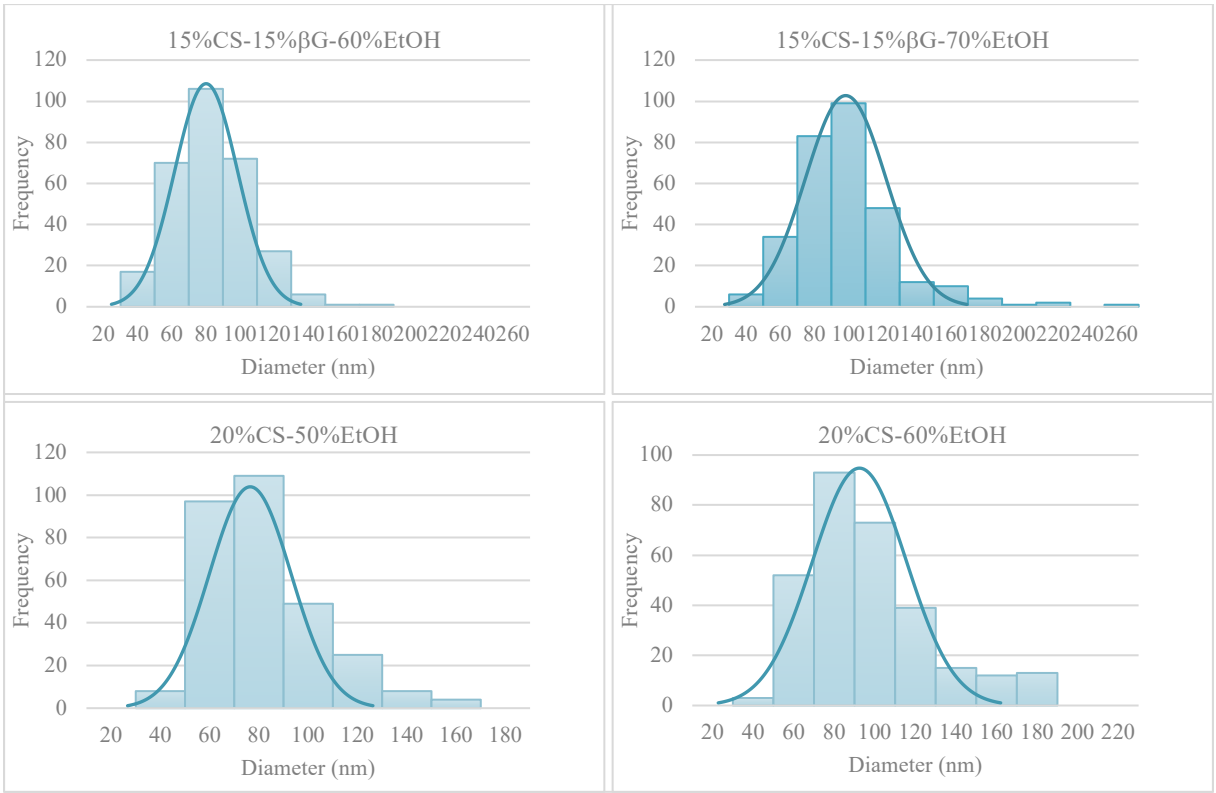

Figure A11: Diameter distribution histograms for fibers produced in the first round of electrospinning.

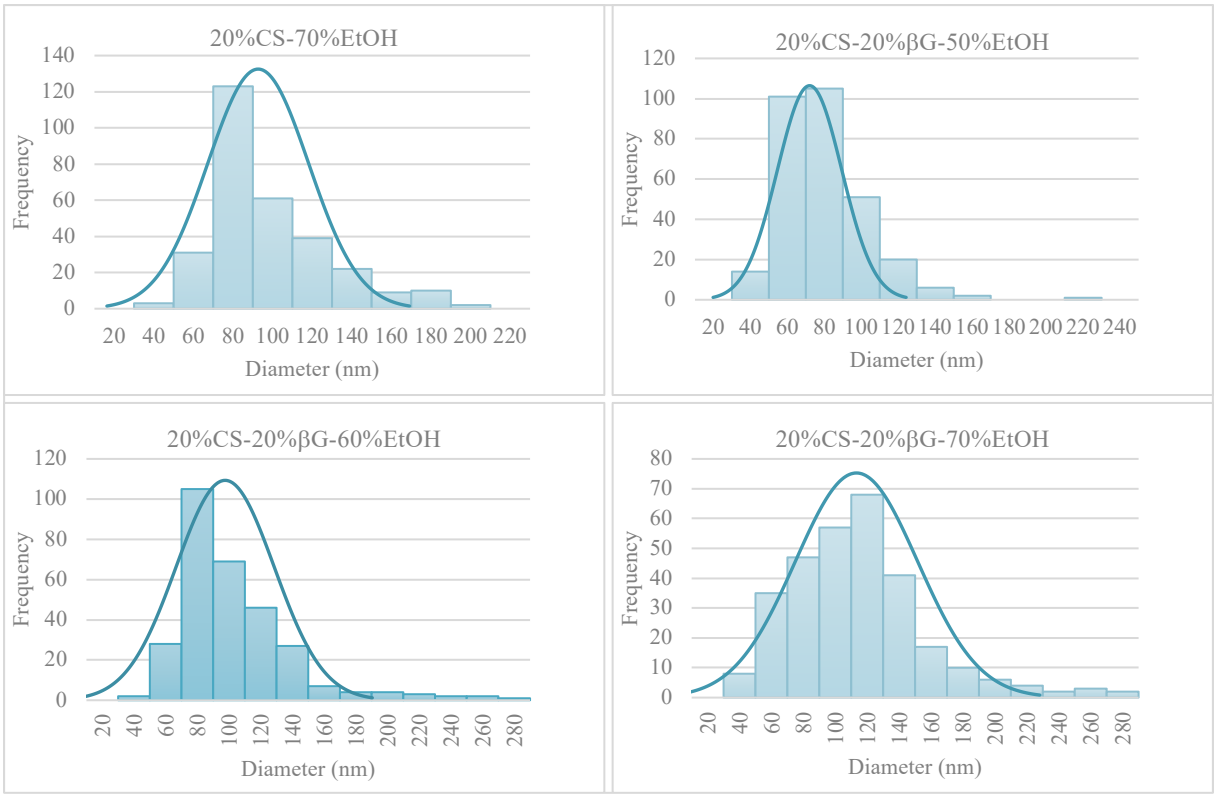

Figure A12: Diameter distribution histograms for fibers produced in the first round of electrospinning.

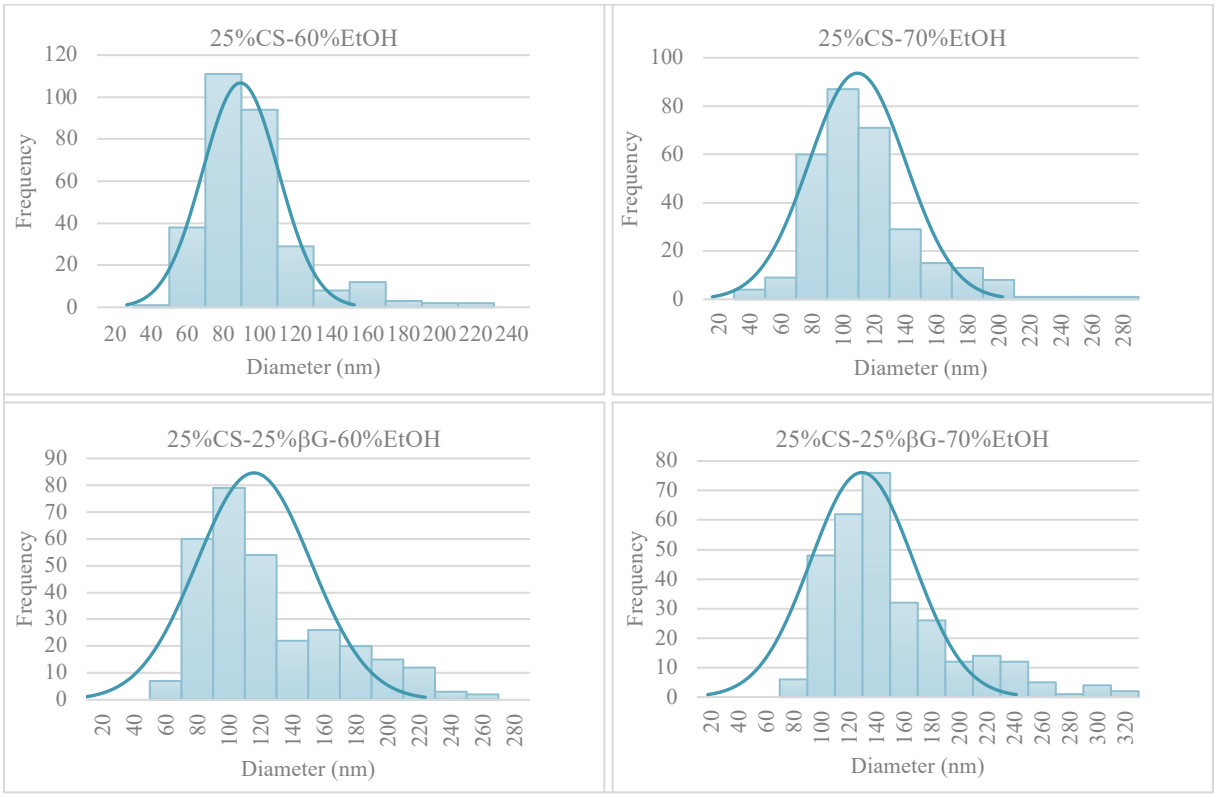

Figure A13: Diameter distribution histograms for fibers produced in the first round of electrospinning.

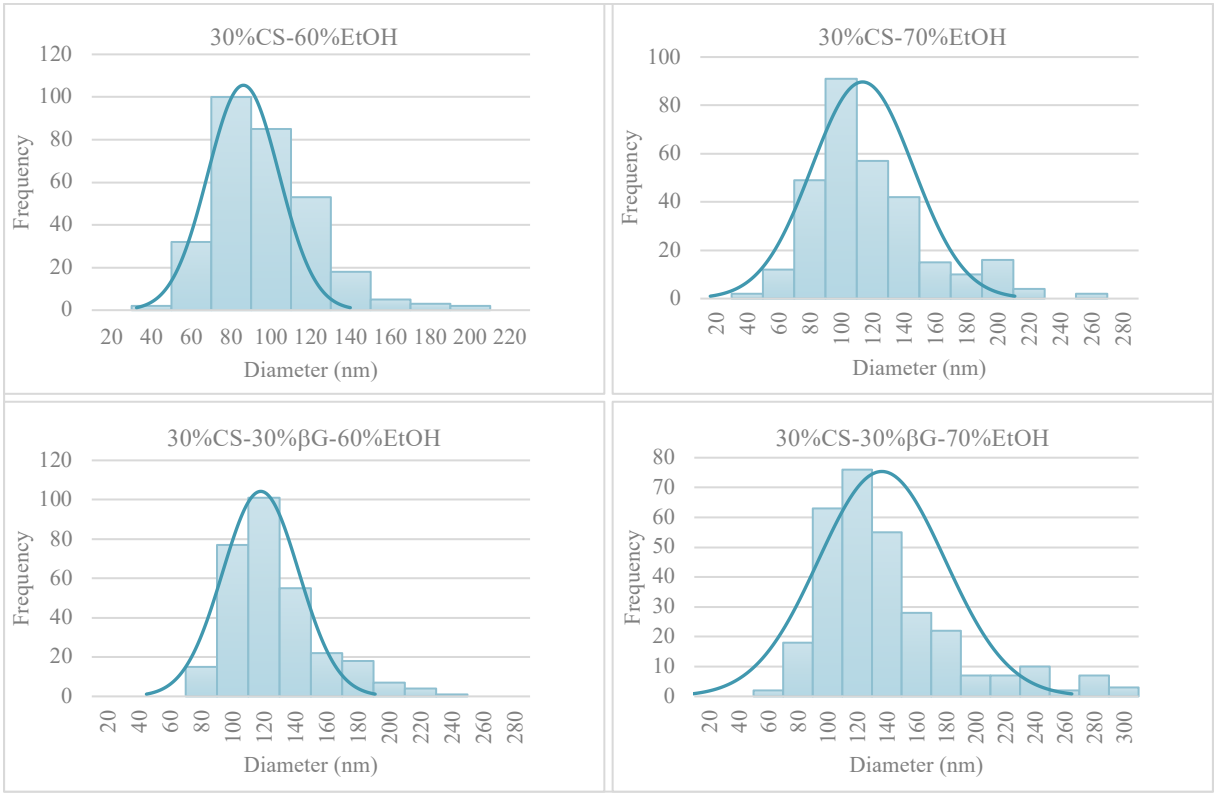

Figure A14: Diameter distribution histograms for fibers produced in the first round of electrospinning.

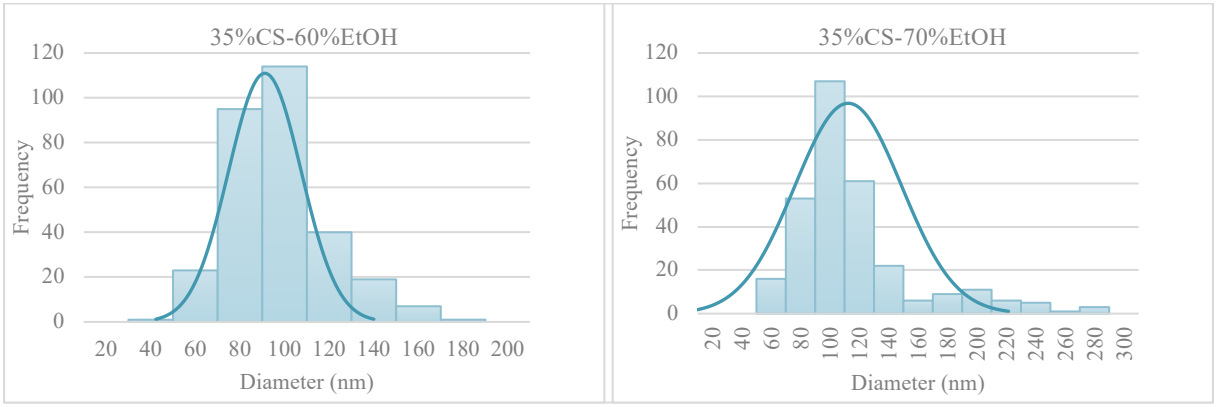

Figure A15: Diameter distribution histograms for fibers produced in the first round of electrospinning.

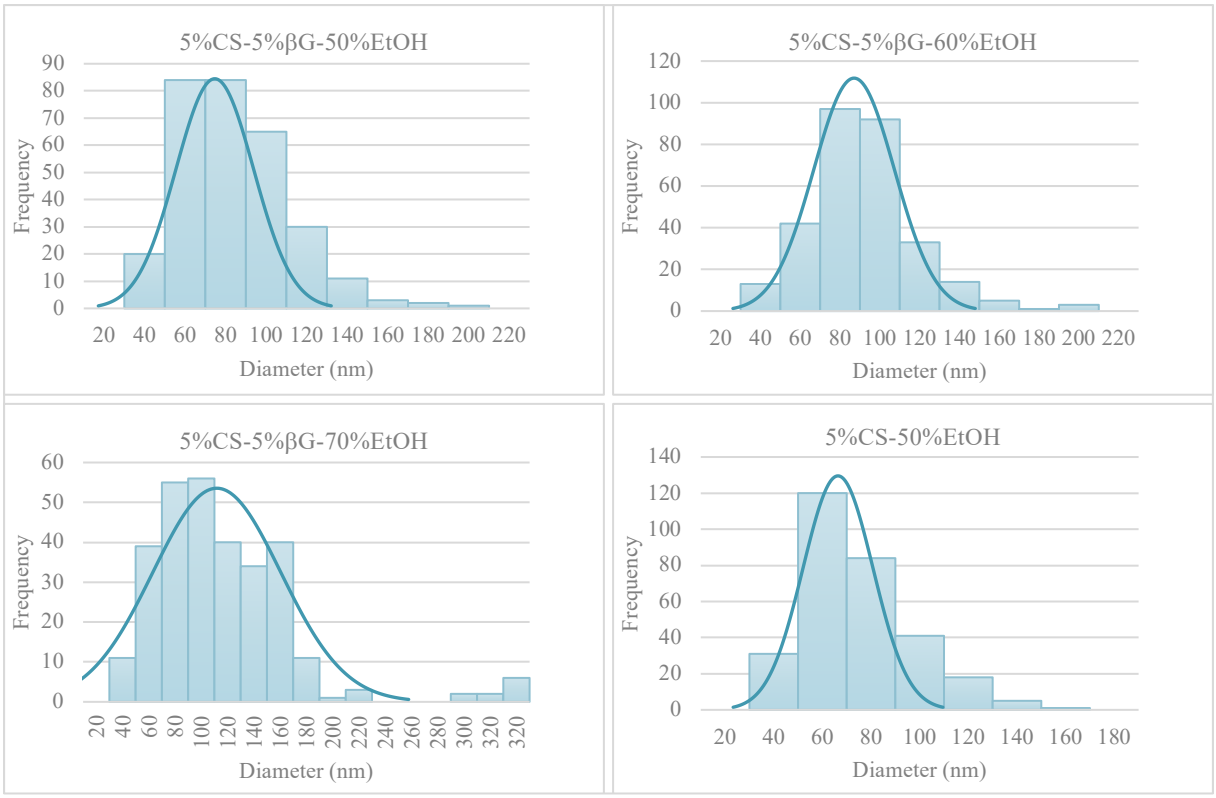

Figure A16: Diameter distribution histograms for fibers produced in the second round of electrospinning.

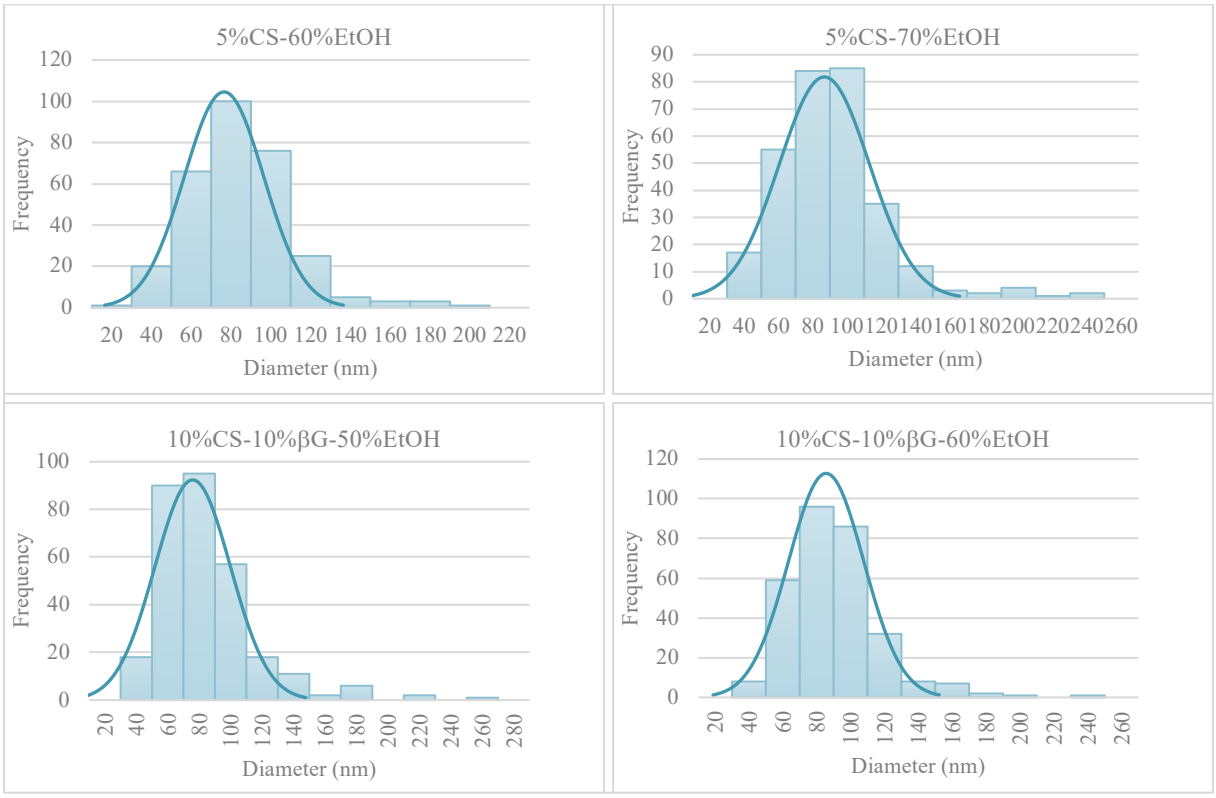

Figure A17: Diameter distribution histograms for fibers produced in the second round of electrospinning.

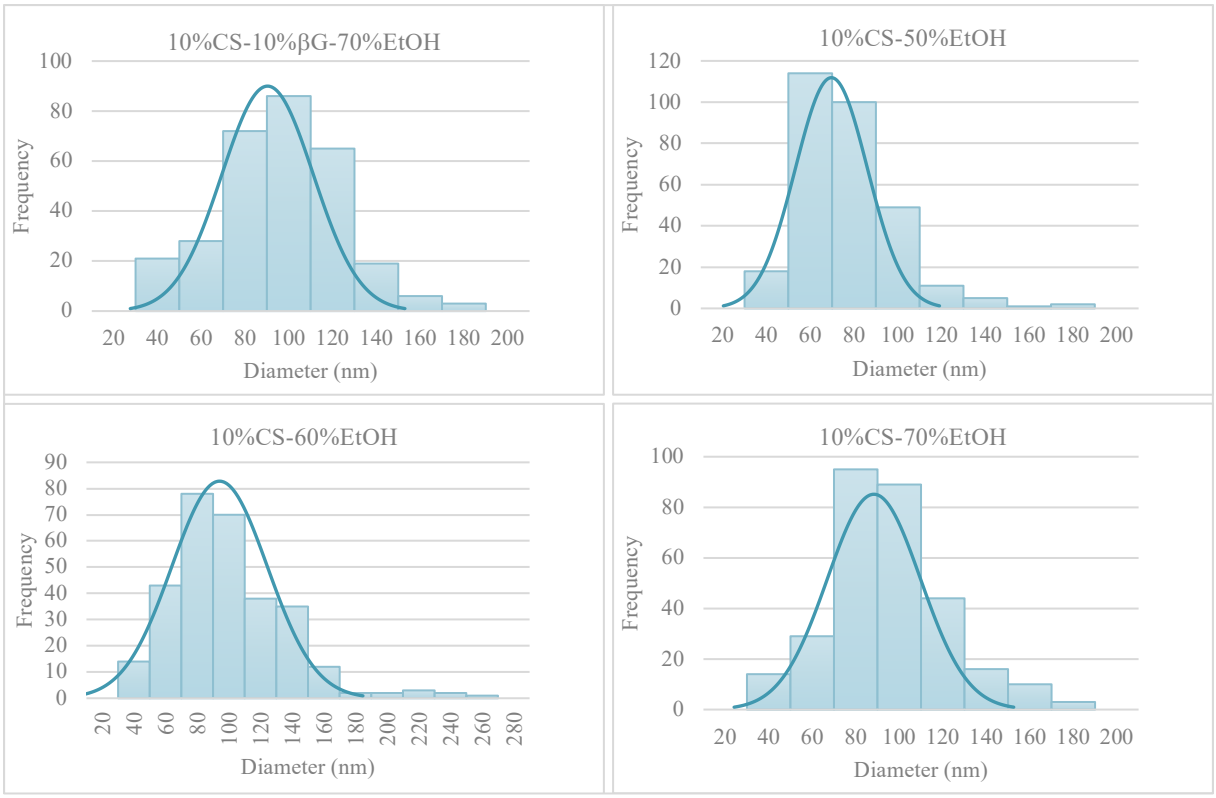

Figure A18: Diameter distribution histograms for fibers produced in the second round of electrospinning.

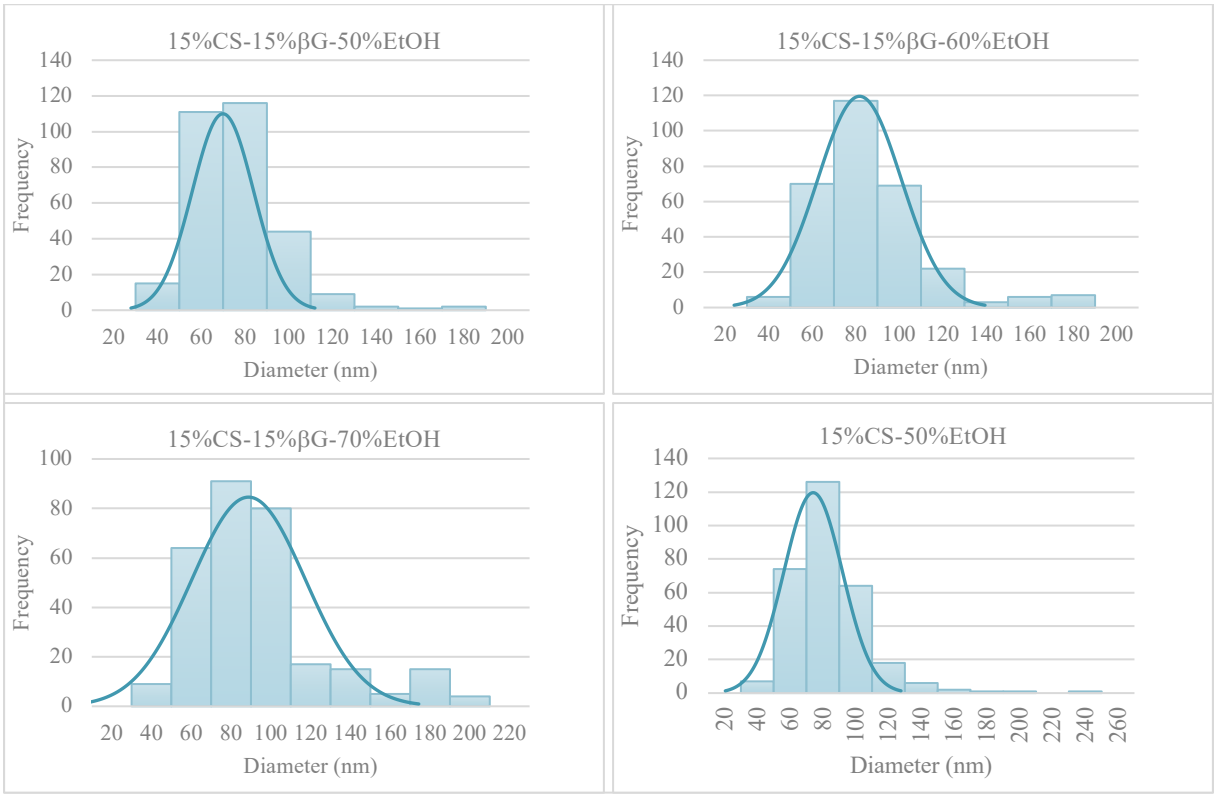

Figure A19: Diameter distribution histograms for fibers produced in the second round of electrospinning.

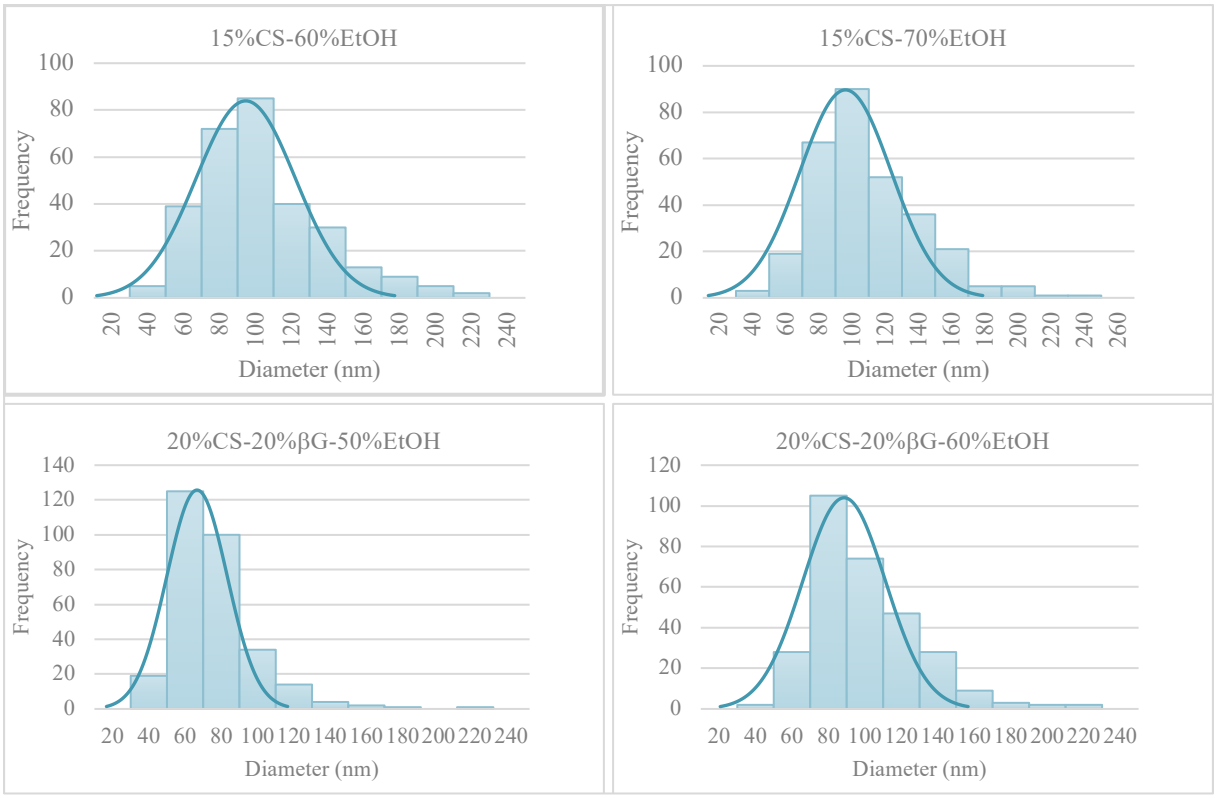

Figure A20: Diameter distribution histograms for fibers produced in the second round of electrospinning.

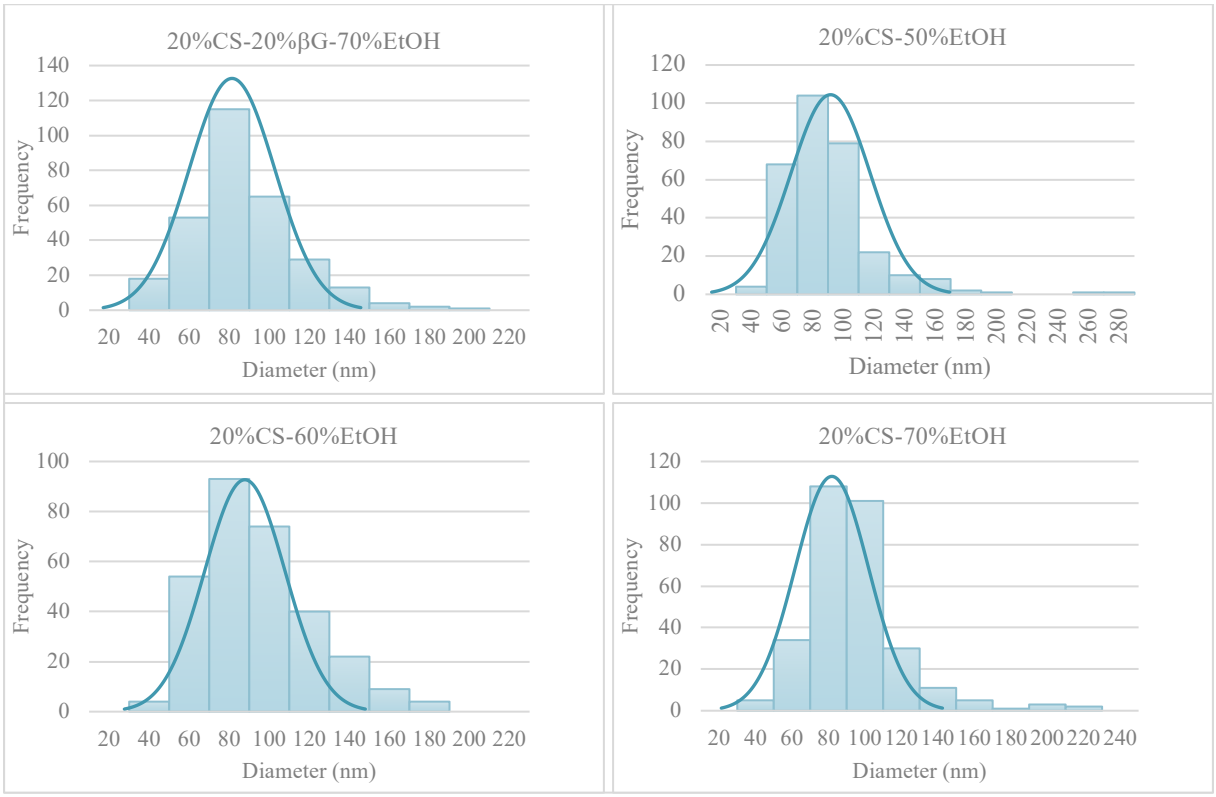

Figure A21: Diameter distribution histograms for fibers produced in the second round of electrospinning.

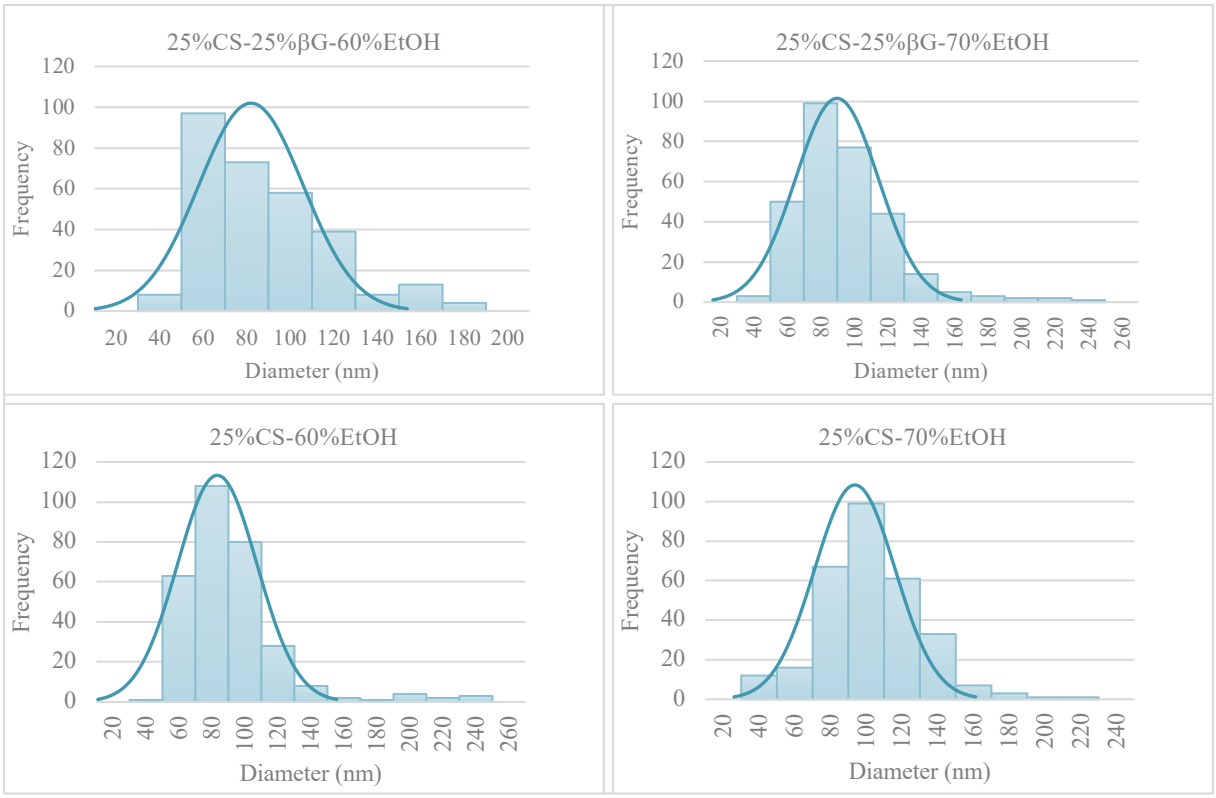

Figure A22: Diameter distribution histograms for fibers produced in the second round of electrospinning.

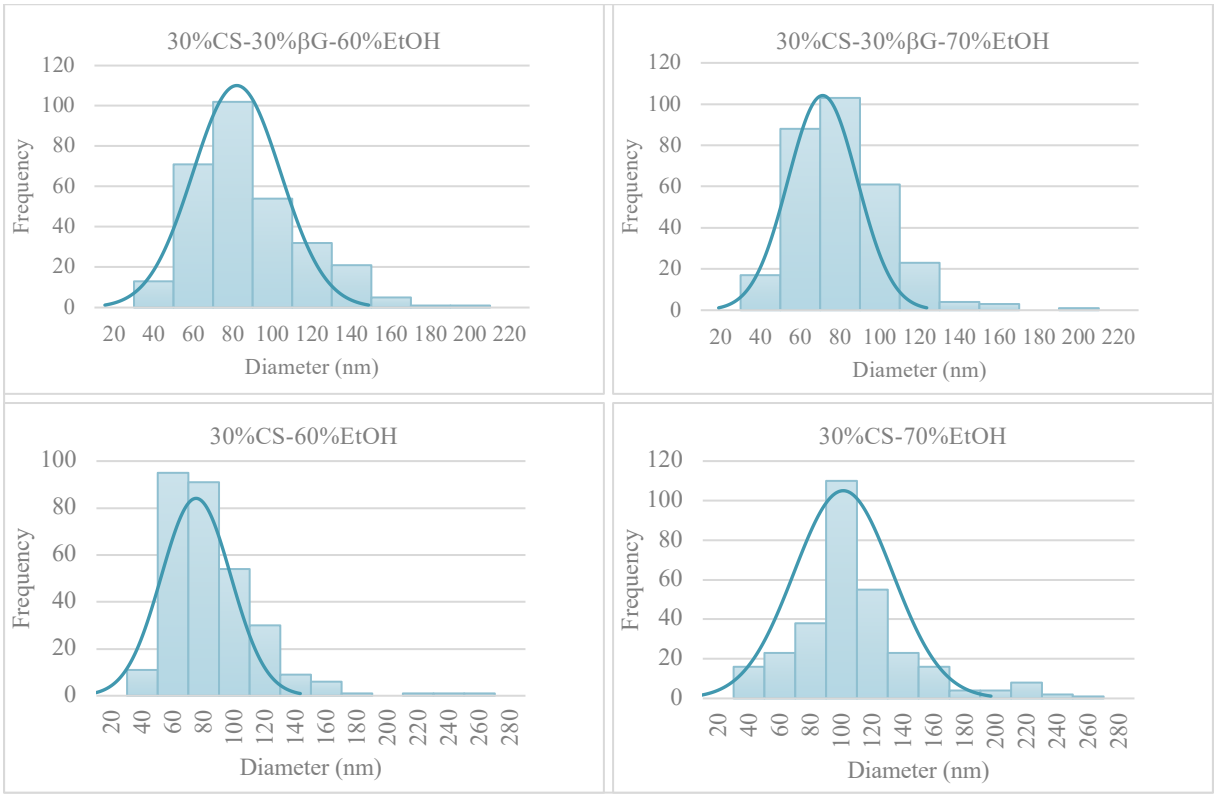

Figure A23: Diameter distribution histograms for fibers produced in the second round of electrospinning.

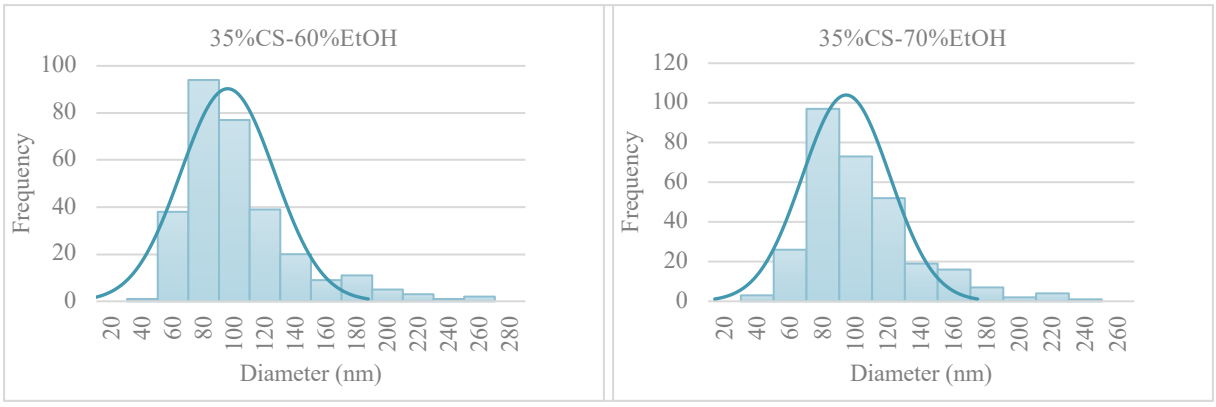

Figure A24: Diameter distribution histograms for fibers produced in the second round of electrospinning.

Absorption capacity

Table A8: Average absorption capacity of the total selection of nanofiber scaffolds. The values are presented as mean ± SD (n = 2).

Polymer concentration	Absorption capacity (%)		
	50% EtOH	**60% EtOH**	**70% EtOH**
5%CS	2058.2 ± 435.6	1909.5 ± 287.6	1923.8 ± 250.6
5%CS-5%βG	2004.4 ± 167.9	2206.6 ± 484.9	1767.3 ± 305.9
10%CS	2212.4 ± 109.5	2089.7 ± 117.6	1758.8 ± 170.8
10%CS-10%βG	1879.7 ± 352.9	2372.9 ± 183.0	1844.6 ± 434.2
15%CS	2178.8 ± 627.7	2047.9 ± 310.8	1944.7 ± 40.9
15%CS-15%βG	3137.4 ± 182.2	2036.5 ± 315.8	2314.2 ± 65.8
20%CS	2571.4 ± 882.9	2073.7 ± 310.0	2040.5 ± 198.8
20%CS-20%βG	2083.0 ± 83.2	2187.0 ± 439.2	2426.8 ± 174.4
25%CS		2612.8 ± 309.2	2262.8 ± 114.0
25%CS-25%βG		2058.5 ± 301.9	2293.2 ± 79.7
30%CS		2627.4 ± 348.2	2259.8 ± 134.9
30%CS-30%βG		1933.3 ± 69.9	2038.6 ± 46.6
35%CS		2752.3 ± 305.5	2409.7 ± 165.2